A Potts Model Investigation of Complexion Transitions and Abnormal Grain Growth

Submitted in partial fulfillment of the requirements for the degree of

Doctor of Philosophy
in
Materials Science and Engineering

William E. Frazier

B.S., Materials Science and Engineering, Drexel University
M.S., Materials Science and Engineering, Carnegie Mellon University

Carnegie Mellon University
Pittsburgh, PA

November 2015

Acknowledgements

This work at Carnegie Mellon University was supported by the Office of Naval Research under grant N00014-11-1-0678. First and foremost, I would like to thank them for their generous support.

My advisors, Professor Tony Rollett and Professor Gregory Rohrer, have encouraged and guided me in my research so that I may reach this point. Without them, none of this work would have been possible. The members of their research groups, which I am incredibly proud to have been amongst the ranks of, have copiously nurtured my love of materials science with countless hours of enlightening discussion. Further, I'd like to specifically mention Brian Lin, Evan Lieberman, Ben Anglin, Sean Donegan, Stephanie Bojarski, and Madeleine Kelly, who all at one point or another went out of their way to help me.

I have many other wonderful people to thank for help and support. The members of Professor Holm's group have been invaluable for their advice. I'd like to very specifically thank Philip Goins, Brian DeCost, and Jonathan Humberson, who have never turned down an opportunity to let me bounce ideas off of them.

I want to thank the entire CMU MSE faculty, who have been one hundred percent helpful to me when I needed them. I would like to especially thank my thesis committee, Professors David Laughlin, Elizabeth Holm, and Jeffrey Rickman for *their* help.

Outside of the CMU, I had several people who were incredibly supportive. My friendships with Meredith Muskovich, David Plecenik, Sarah Ergler, and Shawn Ergler went a long way towards preventing me from going insane over these past four years.

I want to extend a special thank you to Vincent DeGeorge for rushing me downtown the morning after the CMU open house to catch a bus back to Philadelphia when my flight out of Pittsburgh got grounded. It's one of my fondest memories about CMU.

For the past four years, my Mother, Father, Daniel, and Laura, who as I studied in Pittsburgh have had to settle for unconditionally loving me from afar. I assume that they like it that way, but I'd still like to thank them for being nothing but wonderful. Furthermore, and I'm not picking favorites here, I'd like to thank my Dad, who encouraged me to study Materials Science at Drexel and inspired me to pursue a Ph.D.

I want to thank the people who I have forgotten to mention for not taking it personally.

I want to thank my lovely Wife Sarah, who fills my life with nothing but happiness, even when I have to work late nights and pull my hair out. She is my rock.

Last and most importantly, I would like to thank almighty God, who has ordained that I may come to Pittsburgh, pursue the career that I love, and meet all of these exceptional people I have listed. I am truly blessed.

Abstract

The Potts Model of grain growth was adapted for the purpose of simulating abnormal grain growth (AGG) resulting from grain boundary complexion transitions. The transition in grain boundary structure between specific complexion types results in changes in properties. Where the transitions decrease energy and increase the mobility of boundaries, the influence of the processes causing these complexion transitions on the occurrence of AGG was explored. The influence of the processes on the fraction of transitioned boundaries in the material given proximity to an abnormal grain was also explored. AGG occurred provided that such transitions are more likely to occur when adjacent to already transitioned boundaries. AGG was also found to occur provided that transitions were allowed after a predetermined amount of grain boundary motion. The effect of transitions to a high mobility complexion was investigated separately from the effect of changes in energy. The simulations found that when grain boundaries adjacent to transitioned boundaries were more likely to transition to the high mobility complexion themselves, the grain boundaries on the abnormal grains and those immediately adjacent to them were systematically more likely to be in the transitioned state than random chance. However, when grain boundaries were allowed to transition after a predetermined amount of grain boundary motion, only the grain boundaries on the abnormal grains were systematically more likely to be in the transitioned state than random chance. The simulations show how the AGG observed in certain ceramic systems can occur. Simulations and experimental analyses to discriminate the processes causing complexion transitions in such materials are discussed.

Table of Contents

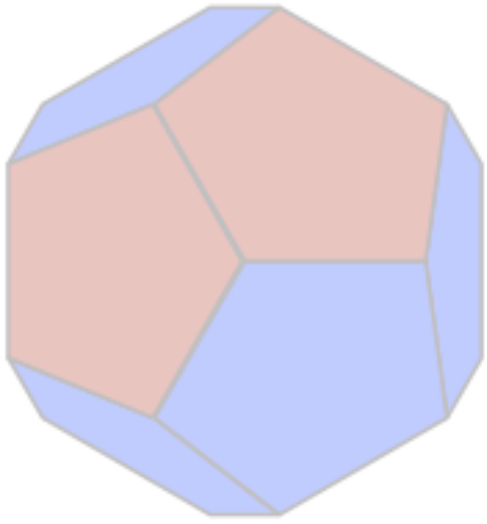

List of Tables

By Page Number

List of Figures

By Page Number:

Chapter One: Introduction

It is generally understood that certain structure sensitive properties of polycrystalline materials depend largely on the properties of grain boundaries. Possibly most famously, the Hall-Petch equation[1,2] relates the yield stress of a polycrystal to average grain size:

$$\sigma_y = \sigma_0 + k/\sqrt{d} \qquad \textbf{(1.1)}$$

Where σ_y is yield stress, d is the average grain diameter, and σ_0 and k are constants. The physical explanation for this relationship in polycrystals is that grain boundaries are significant obstacles to dislocation motion and the total area of the grain boundaries in a polycrystal is inversely proportional to the square root of the average grain diameter. Therefore, as average grain size increases, the amount of resistance to dislocation motion and thus stress required to induce plastic deformation decreases. Other examples are abundant. For example, the voltage across a varistor in semiconducting ceramics is known to be inversely proportional to grain size due to grain boundaries blocking the flow of current[3] .

The goal of grain boundary engineering[4], is to control grain boundary character and improve material properties. Such manipulation is generally performed in polycrystalline materials to increase the population of certain coincidence site lattice (CSL) boundaries, since some of these boundaries typically have improved resistance to detrimental phenomena such as corrosion and stress corrosion cracking[5].

Grain boundaries are understood as two-dimensional defects with five intrinsic parameters: three angles of misorientation between the two abutting grains and two parameters to describe the grain boundary normal vector[6]. This approach to understanding grain boundary properties is often useful: Aust and Rutter[7] notably showed that "special" grain boundaries with higher levels of coherency and (generally) more order were slowed less by Sn impurities in lead. This happens because the higher amount of order on such grain boundaries makes them less likely to accumulate solute, thus slowing them down as predicted by solute drag theory[8]. Solute drag theory also predicts that, with a sufficient amount of solute on a grain boundary and sufficient driving force, a grain boundary can "break away from its solute cloud," which causes the grain boundary to approach its intrinsic mobility, at least for a period of time. Thus, solute drag theory provides a possible explanation for the occurrence of abnormal grain growth (AGG) in some materials, and phase field models conducted by Park[9] have even shown through the use of phase-field grain growth models that AGG can occur through the existence of such behavior. The implication of solute drag theory on preventing an issue such as AGG in materials would be to modify grain boundary character to prevent the occurrence of such break away behavior.

However, many materials systems do not behave consistently with the predictions made by solute drag theory. Harmer[6] notes that while magnesia dopants in alumina do, indeed slow grain growth, dopant with calcia accelerates grain growth[10], and

yttria either increases or decreases grain boundary mobilities, depending upon temperature[11]. Notably, Dillon calculated the effect of solute drag on grain boundary motion in doped aluminas[12] and found that the effects of solute drag could not account for the observed changes in grain boundary motion observed experimentally. Altay and Gülgün[13] found that alumina grains became elongated when a Ca excess of 3-3.5 atoms/nm^2 existed, and further found that abnormal grains appeared when sintering at 1500-1600 °C with an excess of 4.5-8 atoms/nm^2. Dillon and Harmer also made the observation that the size distribution of abnormal grains is not continuous[14]. Instead, there are groups of abnormal grains of approximately similar shape. From this observation, Dillon and Harmer conclude that multiple forms of AGG occur simultaneously in the same, doped material[14]. We would not expect a solute drag effect to have such anisotropy. However, growth morphology in doped aluminas varies with the type of dopant. Abnormal grains in Nd-doped aluminas[52] are roughly equiaxed, as are abnormal grains in Si-doped alumina[47] and Y-doped alumina[52]. Sintering Zr-doped alumina[48] also results in an equiaxed microstructure, as does Mg-doped alumina[5]. Abnormal grains in Ca-doped alumina[13] and La-doped alumina[54], on the other hand, have elongated grain morphologies. Kim found that codoping TiO_2 and SiO_2 in alumina produced plate-like abnormal grains, even though doping with TiO_2 or SiO_2 alone did not[55].

Peculiarities occur in systems other than alumina. It was found by Kasen[15] in 1972 that monolayers of impurities can form on grain boundaries even in ultrapure aluminum provided sufficient grain boundary motion occurs. Fisher[16] notes that

alumina additions to $BaTiO_3$ up to 0.2 mol % increase the nucleation and growth rate of abnormal grains. Further, in the $BaTiO_3$ system, it has been found[17,18] that the addition of more than 0.5 mol % of dopant suppresses abnormal grain growth and the effect has been referred to as the "grain growth anomaly"[17] or the "grain growth inhibition threshold"[18]. Weygand[19] mentions that Ga additions in aluminum increase grain boundary mobility. Work by Cheng[20] and Hibbard[21,22,23] on AGG in electroplated nanonickel finds that AGG occurs in discrete steps that are not spatially or temporally uniform and observes several distinct stages of abnormal grain growth, depending on processing, attributing such growth to the grain boundaries reaching a threshold concentration of sulfur. Lee[24] also observed similar behavior in carburized nickel. Experimentation has shown[25] that grain growth in $SrTiO_3$ abruptly slows at 1400 °C, and does not start to increase again until around 1500 °C.

Harmer, noting similar inconsistencies[6], suggests that in many cases solute content must affect grain boundary structure, thus affecting properties such as grain boundary transport. This implies that the grain boundaries themselves change structure under appropriate conditions in a manner analogous to three-dimensional phases.

This notion, while relatively new, is not an entirely alien concept in materials science. In 1968, Hart[26] noted that absorbed monolayers undergo similar two-dimensional transitions, a phenomena that had been observed experimentally with

molecules of differing complexity[27,28], suggesting that similar "phase" transitions could occur on grain boundaries (Hart suggests that such transitions are the cause for temper brittleness). In 1976, Cahn predicted a pre-wetting transition that could occur before a miscibility gap with the presence of enough solute[29]. Other authors also have suggested that grain boundary wetting occurs due to grain boundary "phase transitions."[30,31,32,33,34] However, while grain boundaries do have thermodynamic properties and can clearly undergo transitions as three dimensional phases do, Cantwell notes that grain boundaries are inhomogeneous, with possible gradients in structure, composition, and order parameter[35], meaning that grain boundaries, and interfaces at equilibrium in general, do not satisfy the Gibbs phase rule. Perhaps the best way to demonstrate this concept is through the repeating polyhedral model of grain boundary structure, seen in Fig. 1.1, as illustrated by Ashby[36].

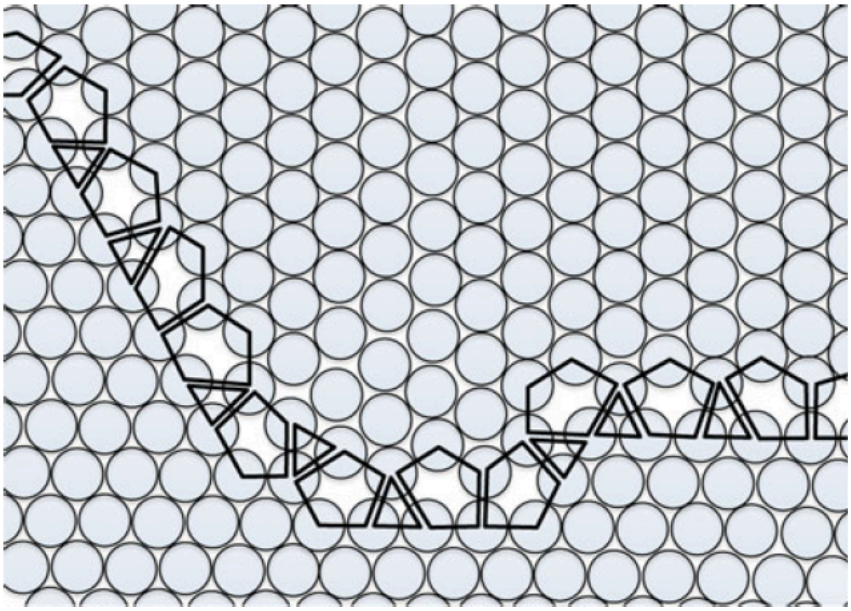

Figure 1.1: Ashby's model of the repeat polyhedral unit model between two close packed hard sphere crystals, composed of pentagons and triangles, as found in Fig. 5 from Rohrer[37]. Apparent structure exists on the grain boundary, but clearly not with a consistent order.

We can see that the equilibrium structure on the grain boundary clearly does not have consistent order. Tang et al.[38] coin the term "complexion" to describe this concept, which he defines as "interfacial material or strata that is in thermodynamic equilibrium with its abutting phases." Hart[39] predicted that such transitions in polycrystalline materials could lead to abrupt changes in material properties, as noted by Cantwell[35], specifically due to changes in non-equilibrium properties like grain boundary mobility and grain boundary diffusivity.

Transitions in grain boundary complexion could also be used to combat grain boundary embrittlement, which occurs when solute segregates to grain boundaries, making them brittle. Among others, cases of grain boundary embrittlement are known to occur in iron, nickel, zirconium[40] and molybdenum[41] systems due to segregation of impurities like sulfur, phosphorous[42], bismuth and antimony[43]. Briant and Messmer[43] made the argument as early as 1984 that impurities electronegative with respect to transition metals such as iron will attract extra electrons and, as a result, weaken nearby metal-metal bonds. As a result, segregation of these impurities to the grain boundaries, whose strength generally dictates the strength of the entire material, weakens the bonds at the grain boundaries and leads to grain boundary embrittlement.

However, Dillon[44,45,46,47] was the first to provide direct evidence that grain boundary complexion transitions cause AGG in a material, identifying six different types of grain boundary complexions in doped aluminas using High Resolution Transmission

Electron Microscopy (HRTEM). Several sources have since provided indirect evidence that these complexions transition by first order mechanisms. Behera showed that the observed grain boundary mobility in Zr-doped alumina increases abruptly between 1550 and 1650 °C, which indicates that complexion transitions occurred, first on the highest energy grain boundaries and then on lower energy boundaries as temperature increased[48]. Behera notes that the variation in grain boundary energy likely accounts for the fact that the increase in mobility was nearly instantaneous with respect to temperature, as would be expected for the nucleation of a bulk phase. Ma found apparent complexion transition "nuclei" in two different systems: first that of a solute bilayer in a Si-Au system observed in HRTEM[49], and then in a CuO-doped TiO_2 bicrystal, observing a monolayer-bilayer transition, a bilayer-trilayer transition, and a trilayer-nanoscale film transition along the grain boundary[50]. In the same paper, Ma observes that a WO_3-doped TiO_2 bicrystal hot pressed at a higher temperature resulted in the formation of precipitates, but no visible complexion transition. Ma points out that these results are consistent with previous experimental observations that doping TiO_2 with WO_3 has no effect on grain growth[51] but that doping with CuO accelerates the process of grain growth and lowers the sintering and densification temperature[51].

In order to better understand complexion transition nucleation behavior, it is our intent to study the effects of these transitions on microstructural evolution, specifically the progress of grain growth and the occurrence of AGG, as will be described in the following chapters.

References

1. Hall EO. The deformation and aging of mild steel. Proc Phys Soc London B 1951;64:747.
2. Petch NJ. The cleavage strength of polycrystals. J Iron Steel Inst 1953;25:174.
3. R.C. Buchanan. Ceramic Materials for Electronics. Third Edition. Published by Marcel Dekker Inc. 2004.
4. G. Palumbo, E.M. Lahockey, P. Lin. Applications for grain boundary engineered materials. J. Mat. 1998;50:40.
5. K.M. Asl, J. Luo. Impurity effects on the intergranular liquid bismuth penetration in polycrystalline nickel. Acta Mater. 2012;60;149.
6. M.P. Harmer. Interfacial kinetic engineering: how far have we come since Kingery's Inaugural Sosman address? J. Amer. Ceram. Soc. 2010;93:301.
7. K. T. Aust, J. M. Rutter. Grain boundary migration in high purity lead and dilute lead-tin alloys. Trans. AIME. 1959;215:119.
8. J.W. Cahn. The impurity-drag effect in grain boundary motion. Act. Met. 1962;10:789.
9. S.G.Kim, Y.B. Park. Grain boundary segregation, solute drag, and abnormal grain growth. Acta. Mat. 2008;56:3739.
10. X.G. Ning, J. Pan, K.Y. Hu, H. Q. Ye. Structural characterization of the β-silicon nitride whisker-aluminide interfaces in a beta-Si_3N_4 whisker-Al alloy 6061 composite material. Philosophical Magazine A: Physics of Condensed Matter: Structure, Defects and Mechanical Properties 1992;66:811.
11. W.H. Tuan, R.J. Brook. Sintering of heterogeneous ceramic compacts. Part 2. Zirconia alumina. J. Mat. Sci. 1989;24:1953.
12. S.J Dillon, S.K. Behara, M.P. Harmer. An experimentally quantifiable solute drag factor. Acta. Mat. 2008;56:1374.
13. A. Altay, M.A. G*ü*lg*ü*n. Microstructural evolution of calcia-doped α-alumina. J. Am. Ceram. Soc. 2003;86:623.
14. G. Palumbo, K.T. Aust. On annealing twins and CSL distributions in FCC materials. Physica Status Solidi A 1992;131:425.
15. M.B. Kasen. Some observations on boundary segregation during grain growth annealing of ultrapurity aluminum. Acta. Met. 1972;20:105.
16. J.G. Fisher, S. Y. Choi, S. J. L. Kang, Abnormal grain growth in barium titanate doped with alumina," J. Amer. Ceram. Soc. 2006;89:2206.
17. J. Daniels, K. H. Hardlt, R. Wernicke, The PTC effect of barium titanate. Philips Tech. Rev. 1978;38:73.
18. M. H. Lin, H. Y. Lu, Densification retardation in the sintering of La2O3-doped barium titanate ceramic. Mater. Sci. Eng. A. 2002;323:167.
19. D. Weygand, Y. Bréchet, E. Rabkin, B. Straumal, W. Gust. Solute drag and wetting of a grain boundary. Phil. Mag. Let. 1997;76:133.
20. L. Cheng, G.D. Hibbard. Abnormal grain growth via the migration of planar growth interfaces," Mat. Sci. Eng. A. 2008;492:128.
21. G.D. Hibbard, V. Radmilovic, K.T. Aust, U. Erb. Grain boundary migration during grain growth in nanocrystalline Ni. Mater. Sci. Eng. A 2008;494:232.

22. G.D. Hibbard, K.T. Aust, U. Erb. On interfacial velocities during abnormal grain growth at ultra-high driving forces. J. Mater. Sci. 2008;43:6441.
23. G.D. Hibbard, J.L. McCrea, G. Palumbo, K.T. Aust, U. Erb. An initial analysis of mechanisms leading to late stage abnormal grain growth in nanocrystalline Ni," Scripta Mater. 2002;47:83.
24. S.B. Lee, N.M. Hwang, D.Y. Yoon, M.F. Henry. Grain boundary facetting and abnormal grain growth in nickel," Metallurgical and Materials Transactions A 2000;31A:985,
25. M. Bäurer, S.-J. Shih, C. Bishop, M.P. Harmer, D. Cockayne, M.J. Hoffman. Abnormal Grain Growth in Doped and Undoped Strontium and Barium Titanate. Acta Mater. 2010;58:290.
26. E.W. Hart. Two-dimensional phase transformations in grain boundaries. Scripta Metal. 1968;2:179.
27. S.J. Gregg. The surface chemistry of solids, 2nd edition. Rheinhold, NY, 1961;62.
28. G.L. Gaines Jr. Insoluble monolayers at liquid-gas interfaces. John Wiley and Sons, Inc, NY. 1966;179.
29. J.W. Cahn. Critical point wetting. J. Chem. Phys. 1977;66:3667.
30. A.P. Sutton, R.W. Balluffi. Interfaces in crystalline materials. Oxford: Oxford Scientific Publications. 1995.
31. E.I. Rabkin, V.N. Semenov, L.S. Shvindlerman, B.B. Straumal. Penetration of Tin and Zinc along tilt grain boundaries 43° [100] in Fe-5 at% Si alloy: premelting phase transition? Acta. Metall. Mater. 1991;39:627.
32. C. Rottman. Theory of phase transitions at internal interfaces. J. Phys. Colleques. 1988;49:313.
33. J.W. Cahn. Transitions and phase equilibria among grain boundary structures. J. Phys. Colloques. 1982;43:199.
34. V. Pontikis. Grain boundary structure and phase transformations: a critical review of computer simulation studies and comparison with experiments. J. Phys. Colleques. 1988:49;327.
35. P.R. Cantwell, M. Tang, S.J. Dillon, J. Luo, G.S. Rohrer, M.P. Harmer. Grain boundary complexions. Acta. Mater. 2014;62:1.
36. M.F. Ashby, F. Spaepen, S. Williams. New model for the structure of grain boundaries: packing of polyhedra. Scr. Metall. 1978;12:193.
37. G.S. Rohrer. Grain boundary anisotropy: a review. J. Mater. Sci. 2011;46:5881.
38. M. Tang, W.C. Carter, R.M. Cannon. Diffuse interface model for structural transitions of grain boundaries. Physical Review B 2006;73:024102.
39. E.W. Hart. The nature and behavior of grain boundaries. New York: Plenum. 1972:155.
40. A.S. Gornakova, B.B Straumal, A.L Petelin, A.B. Straumal. Solid-phase wetting at grain boundaries in the Zr-Nb system. Bulletin of the Russian Academy of Sciences. Physics 2012;76:102.
41. W.T. Geng, A.J. Freeman, G.B. Olson. Influence of alloying additions on impurity induced grain boundary embrittlement. Solid State Communications 2001;119:585.

42. F. Christien, R. Le Gall. Measuring surface and grain boundary segregation using wavelength dispersive x-ray spectroscopy. Surface Science 2008;602:2463.
43. C.L. Briant, R.P. Messmer. An electronic model for the grain boundary embrittlement of Iron, Nickel and Chromium and their alloys by Antimony," Acta Metall 1984;32:2043.
44. S.J. Dillon, M. Tang, W.C. Carter, M.P. Harmer. Complexion: a new concept for kinetic engineering in materials science. Acta. Mater. 2007;55:6208.
45. S.J. Dillon, M.P. Harmer. Demystifying the role of sintering additives with "complexion." J. Euro. Ceram. Soc. 2008;28:1485.
46. S.J. Dillon, M.P. Harmer. Relating grain-boundary complexion to grain-boundary kinetics I: calcia-doped alumina. J. Amer. Ceram. Soc. 2008;91:2304.
47. S.J. Dillon, M.P. Harmer. Relating grain-boundary complexion to grain-boundary kinetics II: silica-doped alumina. J. Amer. Ceram. Soc. 2008;91:2314.
48. S.K. Behera, P.R. Cantwell, M.P. Harmer. A grain boundary mobility discontinuity in reactive element Zr-doped Al_2O_3. Scripta Mater. 2014;90:33.
49. S. Ma, K.L. Asl, C. Tansarawiput, P.R. Cantwell, M. Qi, M.P. Harmer, J. Luo. A grain boundary phase transition in Si-Au. Scripta Mater. 2012;66:203.
50. S. Ma, P.R. Cantwell, T.J. Pennycook, N. Zhou, M.P. Oxley, D.N. Leonard, S.J. Pennycook, J. Luo, M.P. Harmer. Grain boundary complexion transitions in WO_3 – and CuO-doped TiO_2 bicrystals. Acta Mater. 2013;61:1691.
51. Y. Iida, S. Ozaki. Grain growth and phase transformation of titanium oxide during calcination. J. Amer. Ceram. Soc. 1961;44:120.
52. C.M. Wang, J. Cho, H.M. Chan, M.P. Harmer, J.M. Rickman. Influence of dopant concentration on creep properties of Nd_2O_3-doped alumina. J. Amer. Ceram. Soc. 2001;84:1010.
53. I. MacLaren, R.M. Cannon, M.A. G*ü*lg*ü*n, R. Voytovych, N. Popescu-Pogroin, C. Scheu, U. Träffner, M. Rühle. Abnormal grain growth in alumina: synergistic effects of yttria and silica. J. Amer. Ceram. Soc. 2003;86:650.
54. S.A. Bojarski, M. Stuer, Z. Zhou, P. Bowen, G.S. Rohrer. Influence of Y and La additions on grain growth and the grain boundary character distribution of alumina. J. Amer. Ceram. Soc. 2014;97:622.
55. Y.M. Kim, S.H. Hong, D.Y. Kim. Anisotropic Abnormal grain growth in TiO_2/SiO_2-doped alumina. J. Amer. Ceram. Soc. 2000; 83:2809.

Chapter Two: Background

Abnormal grain growth (AGG) is a form of grain growth in which a subset of grains in the microstructure has growth advantages over the others. This results in a microstructure with a multimodal grain size distribution (GSD). The behavior is common and occurs in a host of materials including, but not limited to: alumina[1] , yttria[2], barium titanate[3], boron carbide[4], tungsten carbides[5], nickel alloys[6,25,26], molybdenum alloys[7], and steels[8]. In 1965, Hillert[9] published a quantitative model of grain growth, which suggested that any grain twice the average grain size would grow abnormally. In 1987, however, Thompson[10] predicted that quantitatively this was not the case – abnormal grains could not grow to become abnormal through size advantage alone. Rollett, Srolovitz and Anderson[11] demonstrated this in 1989 using two dimensional Potts Model simulations, further showing that abnormal grains *could* form in the presence of grain boundary mobility anisotropy, with or without grain boundary energy anisotropy, provided that this anisotropy gave certain grains a growth advantage and this growth advantage was sustained. Rollett and Mullins[12] further published a quantitative analysis of the relative grain boundary mobility and energy a grain would need in order to grow to a specific relative grain size, as did Humphreys[13] at around the same time. Other analyses of grain growth have appeared recently, such as those performed by Moroweic[14] based on the curvature around grain vertices and Razzak's[15] analysis of AGG in the case of Zener pinning, which calculated the driving force for a grain to grow based on the assumption that the grain is a sphere growing into a group of smaller spheres. The

analysis of the requirements for a grain to grow abnormally in terms of transitioned boundary coverage, transitioned mobility, and transitioned energy can be found in Chapter Five.

There are multiple physical causes for AGG phenomena. The presence of particles in microstructure is commonly related to the occurrence of AGG. In many cases, such as those demonstrated by Gangulee[16], AGG occurs at around the solvus temperature of the pinned particles. The explanation for the occurrence of AGG in this case is simple. Particles on grain boundaries tend to slow down and stop grain growth such that grain size is limited by the volume fraction of the particles and the size of the particles. However, when the system is heated to near the solvus temperature of the particles, some of the particles shrink or disappear, decreasing both particle volume fraction and particle size. This reduces the pinning effect and allows grain boundaries to move such that some of the grains grow abnormally. Such an effect is not always observed at the solvus temperature, however, as seen by Roberts[17]. Further, similar effects are also seen with pinning of microstructures by voids, which is a notable aftereffect of AGG in many ceramics, and in solute pinned microstructures, as observed by Kim[18]. As discussed in Chapter One, Cahn[19] offered a mathematical explanation for AGG as the result of similar solute drag behavior, where he quantified the velocity of grain boundaries as a function of driving force for grain boundary motion and the concentration of solute on the grain boundary. In this model, Cahn showed that the addition of solute creates a region of instability in which increasing driving force for grain boundary motion *decreases* grain boundary

mobility, resulting in a sudden increase in grain boundary velocity when the driving force is large enough. This reflects the fact that sufficient driving force causes grain boundaries to break free of the "solute cloud" impeding its motion, thus causing them to move close to their intrinsic velocity.

AGG can also occur due to the growth of abnormal subgrains. The Read-Shockley equation approximates the energy of small-angle tilt boundaries from the misorientation between the two grains[20]. These calculations can be made on the basis that the number of dislocations per area of grain boundary increases with increasing misorientation until approximately 15°, at which point dislocation cores begin to overlap and the approximation of a grain boundary as an array of dislocations is no longer valid[21]. The consequence of this is that low angle grain boundaries tend to have low energy and low mobility, while high angle grain boundaries tend to have high energy and high mobility.

In cases in which a material has deformed, recovered and about to recrystallize, the previously undeformed grains have formed a multitude of "subgrains" during deformation. *Most* of these subgrains will have low angle boundaries, and thus low grain boundary mobilities and energies. However, a small minority of the subgrains may have higher angle grain boundaries, resulting in the grains having a copious number of high mobility, high energy grain boundaries[22,49], providing them with a sufficient growth advantage. This means that some rare grains in a textured material may be able to attain a at least somewhat sustained grain boundary

mobility advantage needed for AGG to occur. Work by Holm, Miodownik and Rollett[22] in 2003 demonstrated through use of the Rollett-Mullins equation that such a grain could grow abnormally merely by the virtue of having an advantageous orientation in a textured material, if for example, the grain boundaries were highly mobile when grain boundary misorientation was larger than some threshold angle. Holm suggests that recrystallization nucleates from this abnormal subgrain growth. Similarly, Ko has shown through grain growth simulation that sub-boundary enhanced solid state wetting can explain the so-called "Goss" grain growth in Fe-3% Si Steels[23] and that the resulting abnormal grains in simulations exhibited similar behavior[24]. This claim has a healthy amount of support from experimental observation of recrystallized microstructures. For example, in 2006 Klement[23] found that electrodeposits of nanocrystalline nickel, which has been known[25,26] to grow abnormally above temperatures of 773 K, change preferred orientations from <311>//ND early to a <111>//ND as the abnormal grains form and grow. Similarly, Brons[26] finds that nanotwinned copper when indented and held at cryogenic temperatures experiences AGG in which many of the $\sum 3$ boundaries disappeared and many grains with $\sum 7$ boundaries appeared. Both of these experimental observations suggest that the abnormal grains grew through formation of high energy, high mobility boundaries. Finally, grain boundary complexion transitions cause AGG when a subset of grain boundaries in a system become metastable with respect to a high mobility grain boundary complexion and transition (as seen in Fig. 2.1). This causes a subset of the grain boundaries to obtain a growth advantage large enough to grow abnormally. While evidence of the existence of grain boundary

complexions has been found in a number of different systems, the most compelling work showing the relationship between complexion transitions and increases in grain boundary mobility comes from research performed by Dillon[27,28,29,30] who identified six different grain boundary complexion types in alumina with several different dopants and determined their grain boundary mobilities as a function of temperature.

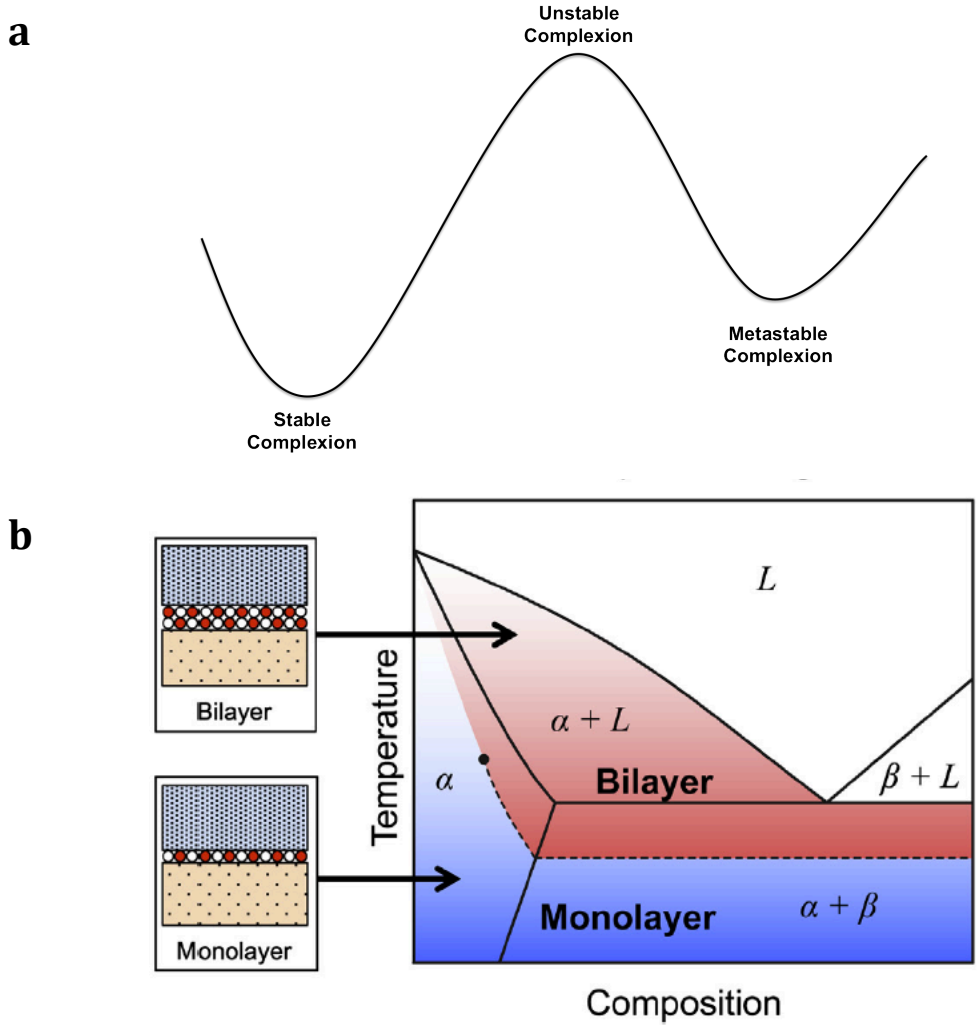

Figure 2.1: a) A complexion is "metastable" if it exists at a local free energy minimum, but not an absolute free energy minimum. Another stable complexion will exist at equilibrium with the abutting phases. b) A schematic complexion diagram from Cantwell et al.[31], which clearly shows that an equilibrium complexion at a lower temperature at a given composition can become metastable with respect to another complexion at an elevated temperature.

These results, shown in Fig. 2.2, demonstrate that changes in complexion towards a macroscale film (complexion VI) increase grain boundary mobility, but the effect of temperature on the reduced grain boundary mobility is roughly the same for all of the different complexions. Harmer[32] explains this behavior in the following way: the grain boundary mobility is dependent on the grain boundary diffusivity, expressed by equation 2.1:

$$D = D_0 e^{-Q/kT} \qquad \textbf{(2.1)}$$

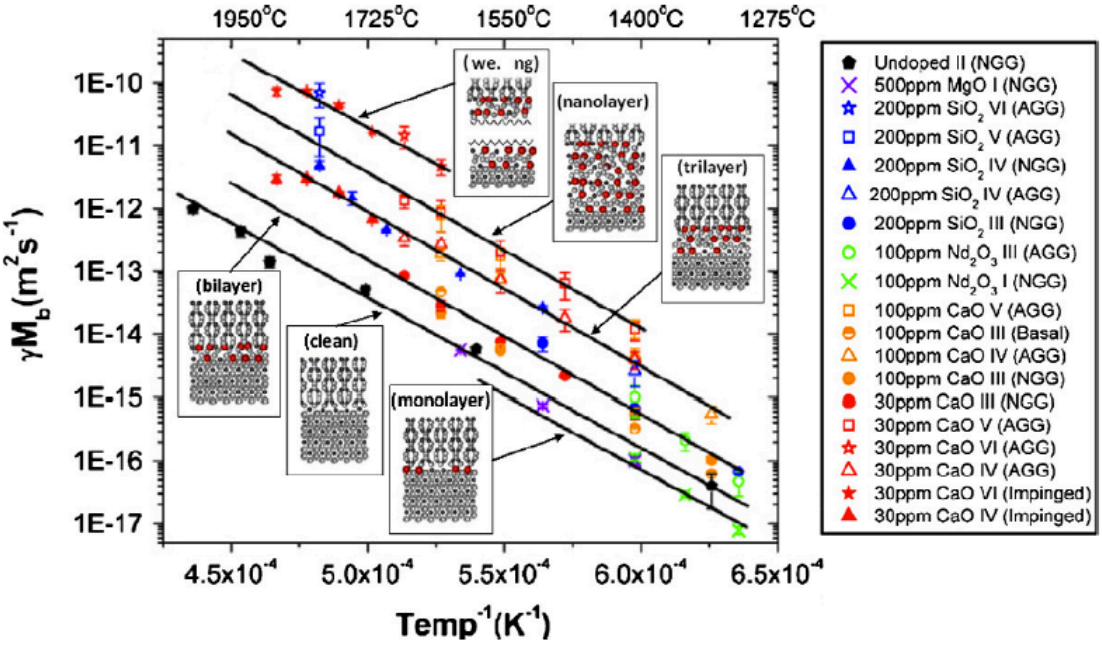

Figure 2.2: The reduced grain boundary mobilities of different grain boundary complexions in aluminas with different dopants, as adapted from Cantwell's[31] adaptation from Dillon[29].

Where k is the Boltzmann constant, T is temperature, D_0 is a constant, and Q is the activation energy of grain boundary diffusion, which can be expressed in terms of the enthalpy and entropy of grain boundary diffusion.

$$D = D_0 e^{\frac{H-TS}{kT}} \quad \textbf{(2.2)}$$

This interpretation suggests that the diffusive mechanism for grain boundary migration does not change when these complexion transitions occur, but that the entropy associated with the grain boundary diffusion does. Hence the slopes of the lines in Fig. 2.2 do not change for different complexions, but the intercepts do. This makes some physical sense, as we can expect a more disordered grain boundary to have more vacancies available for grain boundary diffusion, even if the atomic mechanisms are the same. Harmer[32] mentions that W.D. Kingery, in his 1973 Robert B. Sosman memorial lecture, predicted that such transformations could occur, even though at the time there was no experimental evidence of this ever happening.

Tang et al.[33] notes that disordered grain boundary structures tend to be more stable at higher temperatures and that these structures can progress towards completely liquid films below the melting temperature under appropriate conditions. At the same time, Tang et al.[34,35] also predicted that grain boundaries can undergo order-disorder transitions and demonstrated through calculations on a symmetric grain boundary that first-order grain boundary transitions can be predicted by knowing grain boundary energy and grain boundary energy gradients.

The effects of grain boundary misorientation on the likelihood of grain boundaries to undergo complexion transitions has been studied by Bojarski et al.[36], who found that the grain boundary character distribution (GBCD) in Ca-doped Yttria changes from having large populations of {111} planes to large populations of {001} planes

when abnormal grain growth occurs. She also showed that additions of Y and La in alumina caused the GBCD to favor {0001} and $\{01\bar{1}2\}$ planes, respectively, with *both* planes being favored when both dopants were added[37]. Similar work was also performed by Dillon et al.[38]. Bojarski et al.[36] also performed Atomic Force Microscopy (AFM) measurements which showed that the grain boundary energies in Ca-doped Yttria decreased by a factor of 33% after undergoing AGG. Further work by Bojarski on Ca-doped Yttria showed that the grain boundaries on the abnormal grains had lower energy than the grain boundaries far away from the abnormal grains[39]. Bojarski also showed in experiments with Y-doped Alumina that the distribution of grain boundary energies between a single crystal of sapphire and the alumina depended on the face of the single crystal in contact with the sapphire, observing that abnormal grains far more readily formed on the higher-energy {0001} interface than the low energy $\{01\bar{1}2\}$ interface[40]. Notably, MacLaren et al.[41] had observed amorphous grain boundary films in the same system using HRTEM eleven years prior. Bojarski interpreted this AGG as being the result of complexion transitions occurring on the grain boundaries and Bojarski surmised that the interfaces on which more abnormal growth occurred also more grain boundaries had experienced complexion transitions.

Bojarski's experiments have several different implications: first, that changes in grain boundary complexion in a material can be associated with changes in grain boundary character, second, that high energy grain boundaries are the most likely to make complexion transitions, and third, that grain boundaries near abnormal grains

are roughly as likely to make complexion transitions as the grain boundaries on the abnormal grains themselves. The first two points are intuitive, since we can expect that grain boundaries of specific character will have higher energy and thus be more likely to overcome the activation barrier to make a complexion transition. Unless the distribution of dopant in these experiments was very non-uniform, there is no clear reason why grain boundaries in close proximity to the abnormal growing grains would be more likely than grain boundaries far away to change complexion.

There may be several physical explanations for this phenomena and its connection with AGG. One explanation is that the grain boundaries that move further will accumulate more solute, making them more likely to transition. This would on average give a systematic, persistent growth advantage to the largest grains. However, SIMS micrographs obtained by Wang et al.[42] produced of Nd-doped alumina experiencing AGG show that solute is abundantly present in most grain boundaries, which indicates that most or all grain boundaries in these systems have the requisite solute content in order to transition, just not the activation energy. Further, in several of the cases mentioned, AGG occurred in cases in which solute content was about the solubility limit and no secondary particles appeared. Ma[45] found in his work on CuO-doped TiO_2 that the concentration of solute at which he observed AGG in the titania exceeded the solubility limit of CuO in TiO_2, with no visible precipitation. Similarly, Wang et al.[42] observed AGG in supersaturated Nd-doped alumina at levels below the solubility limit as well. Dillon also observed AGG above the solubility limit in Ca-doped alumina, but observed second phase

particles[29]. This would indicate that, as Dillon[50] predicted, the supersaturation of the grain boundary resulted in a complexion transition, since the interphase energy of a precipitate was too high. More importantly, however, this means that in at least some cases, AGG occurs when grain boundaries that are already supersaturated make complexion transitions. If this is what occurs, then further grain boundary motion should not increase the propensity for grain boundaries to transition.

Another possibility is that when transitioned grain boundaries are eliminated, the excess solute is more likely to diffuse to the adjacent grain boundaries than back into the matrix, making the adjacent boundaries more likely to transition. Hence, as transitioned boundaries are eliminated, nearby boundaries are induced to transition as well. Bojarski's finding that many grain boundaries close to, but not on abnormal grains appear to be transformed appears to be consistent with such a mechanism, and it could be anticipated that the mesoscale effects of such a process on the microstructure would be similar to the effects of transitioned boundaries creating preferential sites for nucleation on triple lines.

We suspect that, on occasion, grain boundary triple lines provide preferential sites for complexion transition nucleation - if a transitioned boundary exists on the triple line. There is some support for this physical explanation in the literature. As previously mentioned in Chapter One, there is some evidence that grain boundary complexions appear in a first order manner, analogous to bulk nucleation[43,44,45]. Notably, liquid metal embrittlement (LME) occurs in some metal alloys when

exposed to liquid metal that wets to the grain boundaries, thereby weakening the material. Luo[46] found not only that liquid Bi penetrates further into a impure Ni (99.5 at% Ni) faster than pure Ni (99.9945 at% Ni), but also that Bi diffusion during LME had led to the formation of Bi bilayers on nearly all of the grain boundaries[47].

In the remainder of this work, we will outline our use of modified versions of the Potts Model, which has a decades-long history of use in modeling grain growth phenomena, to understand how complexion transitions affect microstructural evolution. The simulations described here can be used to determine if the assumed mechanisms lead to results that are consistent with the observations and inspire future experiments to better test the assumptions.

References

1. S. I. Bae, S. Baik. J. Mater. Sci. 1997;28:4197.
2. S. Lartigue-Korinek, C. Carryb, L. Priestera. J. Euro. Ceram. Soc. 2002;22:1525.
3. J. G. Fisher, S. Y. Choi, S. J. L. Kang. J. Amer. Ceram. Soc. 2006; 89: 2206.
4. M. Harmer ,S. Dillon. "Optimizing grain boundary complexions to produce dense pressure-less sintered boron carbide (B_4C)," Internal Report to Air Force Office of Scientific Research 2008.
5. T. Li, Q. Li, J.Y.H. Fuh, P.C. Yuh, L. Luh, C.C. Wu. Materials Science and Engineering A 2007; 445-446: 587.
6. L. Cheng, G.D. Hibbard, Materials Science and Engineering A 2008;492:128.
7. D.L. Worthington, N.A. Predrazas, P.J. Noell, E.M. Taleff. Metallurgical and Materials Transactions A 2013;44:5025.
8. J. Mizera, J.W. Wyrzykowski, K.J Kurzydlowski. Materials Science and Engineering A 1988;104:157.
9. M. Hillert. On the theory of normal and abnormal grain growth. Acta Metall. 1965;13:227.

10. C.V. Thompson, H.J. Frost, F. Spaepen, The relative rates of secondary and normal grain growth. Acta Metall. 1987;33:887.
11. A.D. Rollett, D.J. Srolovitz, M.P. Anderson. Acta Metall 1989;37:1227.
12. A.D. Rollett, W. W. Mullins. Scripta Mater 1997;36:975.
13. Humphreys, F. J. Acta Mater 1997;45:5031.
14. A. Morawiec. Surface area of coarsening cellular structures. Phil. Mag. Letters 2006;86:37.
15. M.A. Razzak, M. Perez, T. Sourmail, S. Cazottes, M. Frotey. A simple model for abnormal grain growth. ISIJ International 2012;12:2278.
16. A. Gangulee, F.M. D'Heurle. Thin Solid Films 1972;12.
17. C. Roberts. PhD Thesis, Carnegie Mellon University, 2007.
18. S.G. Kim, Y.B. Park. Grain boundary segregation, solute drag, and abnormal grain growth," Acta Mater. 2008;56:3739.
19. J.W. Cahn. The impurity-drag effect in grain boundary motion. Act. Met. 1962;10:789.
20. W.T. Read, W. Shockley. Dislocation models of crystal grain boundaries. Physical Review 1950;78:275.
21. G. Gottstein, L.S. Shvindlerman. Grain boundary migration in metals: thermodynamics, kinetics, applications, 2nd Edition. CRC Press 2009.
22. E.A. Holm, M.A. Miodownik, A.D. Rollett. On abnormal subgrain growth and the origin of recrystallization nuclei. Acta Mater. 2003;51:2701.
23. K-J. Ko, A.D.Rollett, N-M. Hwang. Abnormal grain growth of goss grains in Fe 3% Si steel driven by sub-boundary enhanced solid state wetting: analysis by Monte Carlo simulation. Acta Mater. 2010;58:4414.
24. K-J. Ko, J-T. Park, J-K Kim, N-M. Hwang. Morphological evidence that goss abnormally growing grains grow by triple junction wetting during secondary recrystallization of Fe-% Si steel. Scripta Mater. 2008;59:764.
25. G.D. Hibbard, J.L. McCrea, G. Palumbo, K.T. Aust, U. Erb. An initial analysis of mechanisms leading to late stage abnormal grain growth in nanocrystalline Ni," Scripta Mater. 2002;47:83.
26. V. Randle, D. Horton. Grain growth phenomena in Nickel," Scripta Metallurgica et Materialia 1994;31:891.
27. S.J. Dillon, M. Tang, W.C. Carter, M.P. Harmer. Complexion: a new concept for kinetic engineering in materials science. Acta. Mater. 2007;55:6208.
28. S.J. Dillon, M.P. Harmer. Demystifying the role of sintering additives with "complexion." J. Euro. Ceram. Soc. 2008;28:1485.
29. S.J. Dillon, M.P. Harmer. Relating grain-boundary complexion to grain-boundary kinetics I: calcia-doped alumina. J. Amer. Ceram. Soc. 2008;91:2304.
30. S.J. Dillon, M.P. Harmer. Relating grain-boundary complexion to grain-boundary kinetics II: silica-doped alumina. J. Amer. Ceram. Soc. 2008;91:2314.
31. P.R. Cantwell, M. Tang, S.J. Dillon, J. Luo, G.S. Rohrer, M.P. Harmer. Grain boundary complexions. Acta. Mater. 2014;62:1.
32. M.P. Harmer. Interfacial kinetic engineering: how far have we come since

Kingery's Inaugural Sosman address? J. Amer. Ceram. Soc. 2010;93:301.
33. M. Tang, W.C. Carter, R.M. Cannon. Diffuse interface model for structural transitions of grain boundaries. Physical Review B 2006;73:024102.
34. M. Tang, W.C. Carter, R.M. Cannon. Grain boundary transitions in binary alloys. Physical Review Letters 2006;97:075502.
35. M. Tang, W.C.Carter, R.M. Cannon. Grain boundary order-disorder transitions. J. Mater. Sci. 2006;41:7691.
36. S.A. Bojarski, S. Ma, W Lenthe, M.P. Harmer, G.S. Rohrer. Changes in the grain boundary character and energy distributions resulting from a complexion transition in Ca-doped yttria. Metall. and Mater. Trans. A. 2012;43:3532.
37. S.A. Bojarski, M. Stuer, Z. Zhou, P. Bowen, G.S. Rohrer. Influence of Y and La additions on grain growth and the grain boundary character distribution of alumina. J. Amer. Ceram. Soc. 2014;97:622.
38. S.J. Dillon, H. Miller, M.P. Harmer, G.S. Rohrer. Grain boundary plane distributions in aluminas evolving by normal and abnormal grain growth and displaying different complexions. Int. J. Mat. Res. 2010;101:50.
39. S.A. Bojarski, J. Knighting, S. Ma, W. Lenthe, M.P. Harmer, G.S. Rohrer. The relationship between grain boundary energy, grain boundary complexion transitions, and grain size in Ca-doped yttria. Mater. Sci. Forum 2013;753:87.
40. S.A. Bojarski, M.P. Harmer, G.S. Rohrer. Influence of grain boundary energy on the nucleation of complexion transitions. Scripta Mater. 2014;88:1.
41. I. MacLaren, R.M. Cannon, M.A. G*ülgü*n, R. Voytovych, N. Popescu-Pogroin, C. Scheu, U. Träffner, M. Rühle. Abnormal grain growth in alumina: synergistic effects of yttria and silica. J. Amer. Ceram. Soc. 2003;86:650.
42. C.M. Wang, J. Cho, H.M. Chan, M.P. Harmer, J.M. Rickman. Influence of dopant concentration on creep properties of Nd_2O_3-doped alumina. J. Amer. Ceram. Soc. 2001;84:1010.
43. S.K. Behera, P.R. Cantwell, M.P. Harmer. A grain boundary mobility discontinuity in reactive element Zr-doped Al_2O_3. Scripta Mater. 2014;90:33.
44. S. Ma, K.L. Asl, C. Tansarawiput, P.R. Cantwell, M. Qi, M.P. Harmer, J. Luo. A grain boundary phase transition in Si-Au. Scripta Mater. 2012;66:203.
45. S. Ma, P.R. Cantwell, T.J. Pennycook, N. Zhou, M.P. Oxley, D.N. Leonard, S.J. Pennycook, J. Luo, M.P. Harmer. Grain boundary complexion transitions in WO_3 – and CuO-doped TiO_2 bicrystals. Acta Mater. 2013;61:1691.
46. K.M. Asl, J. Luo. Inpurity effects on the intergranular liquid bismuth penetration in polycrystalline nickel. Acta Mater. 2012;60:149.
47. J. Luo, H. Cheng, K.M. Asl, C.J. Kiely, M.P. Harmer. The role of a bilayer interfacial phase on liquid metal embrittlement. Science 2011;333:1730.
48. W.C. Carter, M. Baram, M. Drozdov, W.D. Kaplan. Four questions about triple lines. Scripta Mater. 2010;62:894.
49. R.W. Cahn. A new theory of recrystallization nuclei. Proc. Phys. Soc. London A 1950;63:323.
50. S.J. Dillon, M.P. Harmer, G.S. Rohrer. Influence of interface energies on solute partitioning mechanisms in doped aluminas. Acta Mater. 2010;58:5097.

Chapter Three: Hypotheses

It has been shown that AGG can occur due to the formation of low energy, high mobility grain boundary complexions at the expense of high-energy, low mobility grain boundary complexions. It has also been shown that such transitions appear to occur on individual grain boundaries in first-order, nucleation and growth processes. We will further show that AGG does not occur when the probability of a grain boundary undergoing a complexion transition is independent of whether or not its neighbors are transitioned. The origin of this bias is not entirely clear, but the mechanism should change the extent of AGG and the features of the evolved microstructure. Instead of attempting experimentally to accept or reject a single proposed mechanism, we quantitatively interrogated the microstructural evolution resulting from two possible scenarios:

1. The probability of a grain boundary nucleating a complexion transition increases when it is adjacent to one or multiple transitioned grain boundaries.
2. The probability of a grain boundary nucleating a complexion transition increases with grain boundary motion that sweeps up solute.

We hypothesized that quantitative correlations exist between the process of complexion transition nucleation and the nature of microstructural evolution that occurs, specifically the following:

1. Abnormal grains that form in the Potts Model will have a higher fraction of transitioned boundaries than random chance.
2. If the probability of a transition to a high mobility complexion is dependent on adjacency to transitioned boundaries, then grain boundaries adjacent to abnormal grains will have a higher fraction of transitioned boundaries than random chance in the Potts Model.
3. Abnormal grain growth will not occur in the Potts Model in number fractions more than one in ten thousand grains when the probability of transitioning is dependent on grain boundary motion. The occurrence of abnormal grains will be established by the appearance of a grain larger than ten times the average volume in simulation. If Abnormal grain growth occurs when the probability of a transitioning is dependent on grain boundary motion, then grain boundaries adjacent to abnormal grains will have a higher fraction of transitioned boundaries than random chance in the Potts Model.

These hypotheses were tested using the Potts Model of grain growth, as discussed in the following chapters.

Chapter Four: The Potts Model of Grain Growth

4.1 Basic Method

The work described primarily uses the Potts model of grain growth, which has been used by Rollett et al[1]. (and many others) to study abnormal grain growth starting in the mid and late 1980s, which in turn was based on the pioneering work of Anderson et al[2]. A regular grid of random grain IDs is assembled, and randomly selected IDs can change ID to that of a neighbor with a probability dependent on the energy change, ΔE, associated with the change of ID and the "mobility" of the boundary between the neighbors. The total energy of the grid is defined by the equation:

$$E = -\frac{J}{2} * \sum_i^N \sum_j^{NN} (\boldsymbol{\delta}_{S_i S_j} - 1) \qquad \textbf{(4.1)}$$

Here, J is the grain boundary energy between two cells of grains i and j, S_i and S_j denote ID, δ is the Kronecker delta function[3], N is the number of voxels and NN is the number of nearest neighbor voxels, and the factor of two accounts for double counting in the summations. Thus, the probability of ID reorientation can be expressed by the piecewise-defined function:

$$p = \begin{cases} M * J & , \ \Delta E < 0 \\ M * J * e^{\frac{-\Delta E}{J * kT}} & , \ \Delta E \geq 0 \end{cases} \qquad \textbf{(4.2)}$$

Here, M is the grain boundary mobility, ΔE is change in energy associated with the reorientation, T is temperature and k is the Boltzmann constant. The presence of J

in the denominator ensures that boundaries with different energies have similar roughness since the main effect of finite lattice temperature is to allow the boundary to increase its local arc length by adding kinks or steps. Some implementations of this method assign a fifty percent probability of reorientation when $\Delta E = 0$. Note that in the basic (isotropic) Potts model, J and M are constant. Grain boundary energy and mobility anisotropy are applied by making them a function of the two IDs i and j, so in these cases $J = J(i,j)$ and $M = M(i,j)$, as will be discussed in the next section. In addition to grain growth, this model is used for recrystallization[4] and particle coarsening[5].

4.2 Modeling Abnormal Grain Growth

Methods implemented for AGG in the Potts model largely vary considerably. For example, Rollett et al.[1] in their 1988 work declare "Type I" and "Type II" grains, for which boundaries between same-types had low grain boundary mobility and high grain boundary energy, while boundaries between dissimilar-types had high grain boundary mobility and low grain boundary energy (some variations of this approach give only Type II – Type II grain boundaries high mobility and low energy).

Other methods determine M and J based on grain boundary misorientation, which Holm[6] and a number of others use to model abnormal subgrain growth. The Read-Shockley equation of grain boundary energy as it depends on grain boundary misorientation can be seen in equation 4.3:

$$\gamma(\theta) = \begin{cases} \frac{\theta}{\theta_1}[1 - \ln\frac{\theta}{\theta_1}], & \theta < \theta_1 \\ 1 & , \theta \geq \theta_1 \end{cases} \quad \textbf{(4.3)}$$

Further, the grain boundary mobility can be approximated as the following, which is intended to provide a smooth transition between the low mobilities of low angle boundaries and the much higher mobilities of high angle grain boundaries[7]:

$$M(\theta) = \begin{cases} 1 - e^{[-n(\frac{\theta}{\theta_m})^d]}, & \theta < \theta_m \\ 1 & , \theta \geq \theta_m \end{cases} \quad \textbf{(4.4)}$$

Here, θ is misorientation between two grains, $\theta_1 = \theta_m = 15^o$, and m and d are constants. By these equations, both grain boundary energy and mobility increase with increasing misorientation, which means that typical high angle grain boundaries will have high grain boundary mobility, but also high grain boundary energy. Meanwhile, low angle grain boundaries will have low grain boundary energy, but also low grain boundary mobility. Holm adapts the Read-Shockley equation slightly to determine the grain boundary energy and mobility between grain IDs i and j:

$$\gamma(\theta_{i,j}) = \begin{cases} .6, & ,\theta < \theta_1 \\ \frac{\theta}{15^0}[1 - \ln\frac{\theta}{15^0}] & ,\theta_1 < \theta < 15^0 \\ 1 & ,\theta > 15^0 \end{cases} \quad \textbf{(4.5)}$$

The lower bound of θ_1 is a limit placed to prevent grain boundary wetting, which occurs when grain boundaries have relative energies below half the normal grain

boundary energy. Holm also uses the following misorientation-dependent formula for grain boundary mobility:

$$M(\theta_{i,j}) = k\theta_{i,j}^{5}\exp\left(\frac{-Q}{RT}\right) \quad \textbf{(4.6)}$$

The misorientation angle itself, $\theta_{i,j}$ is calculated from the matrix typically used to describe the misorientation between two orientations, commonly parameterized with Bunge Euler angles. Variations of these modifications to the Potts Model have been used, some of which impose no variation in grain boundary mobility, and others not imposing the floor in grain boundary energy. These formulations were originally used to show how abnormal subgrain growth nucleates recrystallization phenomena, but many variations of the Potts Model today incorporate grain boundary anisotropy using similar operations.

Many versions of the Potts Model simply evaluate *M* and *J* on the basis of the grain IDs i and j without any crystallographic orientations assigned to the grains. In the most basic, isotropic case, mobility and grain boundary energy are described as:

$$M(i,j) = 1 \quad \textbf{(4.7)}$$

$$J(i,j) = 1 \quad \textbf{(4.8)}$$

This alone, does not, of course, create the grain boundary mobility or energy anisotropy needed to facilitate the growth of abnormal grains. In the case of a model incorporating abnormal grain growth due to changes in grain boundary complexion, these equations must be modified.

$$M(i,j) = \begin{cases} 1\ , & T(i,j) = 1 \\ M_{Min}\ , & T(i,j) = 0 \end{cases} \quad \textbf{(4.9)}$$

$$J\ (i,j) = \begin{cases} J_{Min}\ , & T(i,j) = 1 \\ 1\ , & T(i,j) = 0 \end{cases} \quad \textbf{(4.10)}$$

The function *T(i,j)* is an indicator that returns one when the grain boundary is in the high mobility complexion and zero when the grain boundary is in the default low mobility complexion not transitioned. *T(i,j)* is entirely dependent on experimental design. For example, we can choose to transition all of the boundaries of a grain with ID i_{Ab} by defining *T(i,j)* in the following way:

$$T(i,j) = \begin{cases} 1, & i = i_{Ab}\ or\ j = i_{Ab} \\ 0, & otherwise \end{cases} \quad \textbf{(4.11)}$$

This simulation setup allows us to simulate grain growth in a simple, one-component material, making only structural changes to the grain boundaries. We will outline in Chapter 6 how the version of the Potts Model used in this work updates the function *T(i,j)* as the simulation progresses, transitioning grain boundaries to high mobility, low energy complexions in order to induce AGG in the simulation.

References

1. A.D. Rollett, D.J. Srolovitz, M.P. Anderson, Simulation and theory of abnormal grain growth – anisotropic grain goundary energies and mobilities. Acta Metall. 1989;37:1227.
2. P.S. Sahni, G.S. Grest, M.P. Anderson, D.J. Srolovitz. Kinetics of the Q-State Potts Model in two dimensions. Physical Review Letters 1983;50:263.

3. C.S. Park, T.W. Na, H.K. Park, B.J. Lee, C.H. Han, N.M. Hwang. Three-dimensional Monte Carlo simulation for the effect of precipitates and sub-boundaries on abnormal grain growth. Scripta Mater. 2012;66:398.
4. P. Peczak, M.J. Luton. A Monte Carlo study of the influence of dynamic recovery on dynamic recrystallization. Acta Metall. Mater. 1993;41:59.
5. S.B. Lee, J.M. Rickman, A.D. Rollett. Three dimensional simulation of isotropic coarsening in liquid phase sintering I: a model," Acta Mater. 2007;55:615.
6. E.A. Holm, M.A. Miodownik, A.D. Rollett. On abnormal subgrain growth and the origin of recrystallization nuclei. Acta Mater. 2003;51:2701.
7. G. Gottstein, L.S. Shvindlerman. Grain boundary migration in metals," CRC Press 1999.

Chapter Five: Establishing Criteria for the Growth of an Abnormal Grain

5.1 The Rollett-Mullins Equation of Grain Growth

We recall that the Rollett-Mullins[1] equation of grain growth:

$$\left\langle \dot{\rho} \middle| R_A \right\rangle = \frac{M_{BB}\gamma_{BB}}{2\left\langle R_B \right\rangle^2} G(\rho,\mu,\Gamma) \qquad \textbf{(5.1)}$$

Where $\left\langle \dot{\rho} \middle| R_A \right\rangle$ is the average rate of change of the radius of a "A" grains normalized to the average grain size given the average A grain radius R_A. M_{BB} and γ_{BB} are the grain boundary mobility and energy of "normal" grain boundaries, or in this case grain boundaries that are not transitioned. $\left\langle R_B \right\rangle$ is the average radius of the normal "B" grains, and G(ρ, μ, Γ) is described in equation 5.2:

$$G(\rho,\mu,\Gamma) = \mu\Gamma(a + (a-2)\frac{1}{\rho}) - \frac{\rho}{4} \qquad \textbf{(5.2)}$$

Here, ρ is normalized size of A grains relative to the B grains, μ is the mobility of a grain boundary on an A grain with respect to the mobility on B grains, Γ is the energy of a grain boundary on a B grain with respect to the energy on B grains, and a is:

$$a = \frac{6}{\pi}\arcsin\left(\frac{1}{2\Gamma}\right) \qquad \textbf{(5.3)}$$

Clearly, $\left\langle \dot{\rho} \middle| R_A \right\rangle$ will only be positive when G(ρ, μ, Γ) is positive, so any and all abnormal grains that appear and remain will have to have grain boundary mobility and energy advantages, as well as a starting grain size such that G(ρ, μ, Γ) is positive.

We can estimate whether or not grains will grow with a certain fraction of transitioned boundaries by calculating an "effective" relative grain boundary mobility and energy of the grain at large:

$$\mu_{Eff} = f_T + (1 - f_T)\frac{1}{M_{Min}} \quad \textbf{(5.4)}$$

$$\Gamma_{Eff} = f_T J_{Min} + (1 - f_T) \quad \textbf{(5.5)}$$

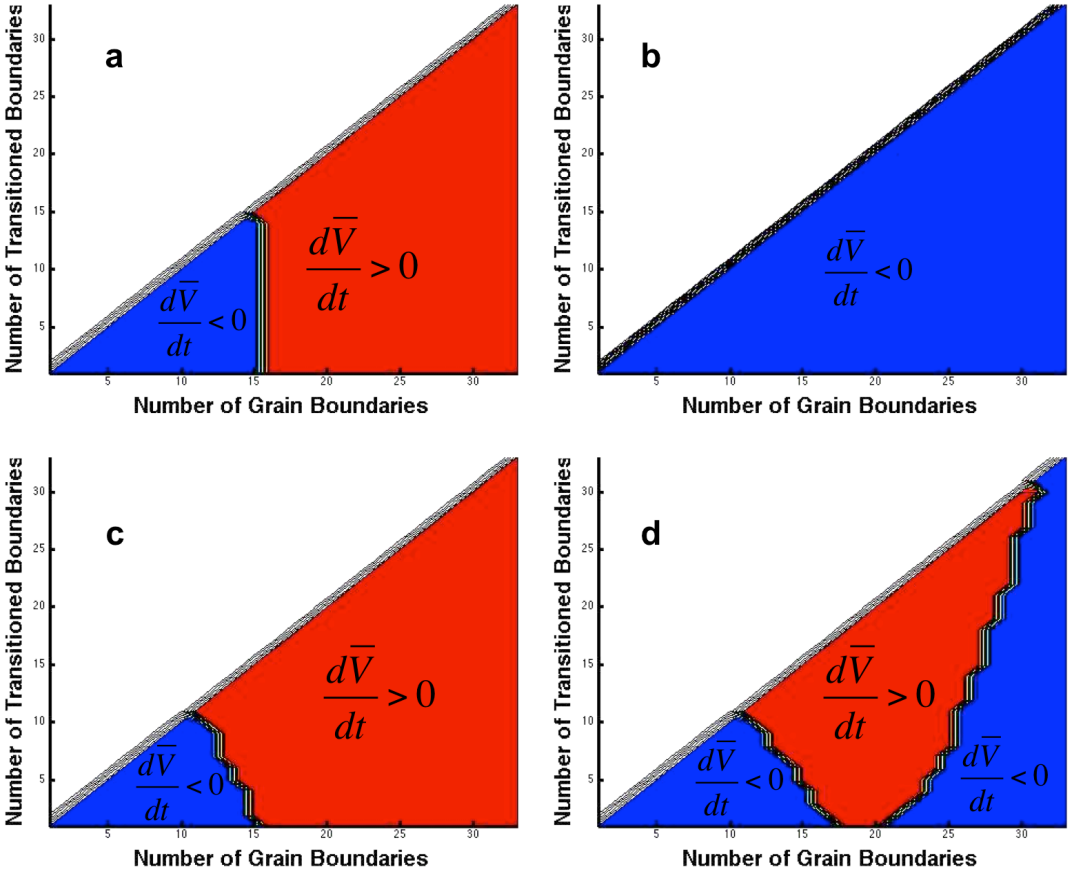

Figure 5.1: Criteria of the number of transitioned grain boundaries required for a grain to grow given the number of boundaries the grain has, as predicted by the Rollett-Mullins equation, for M_{min} and J_{min} of a) M_{min} = 0.05, J_{min} = 1.0, b) M_{min} = 1.0, J_{min} = 1.0, c) M_{min} = 0.05, J_{min} = 0.6, and d) M_{min} = 1.0, J_{min} = 0.6.

The number of boundaries on a grain is linearly related to ρ, and we can determine coefficients for the relationship by plotting the relative sizes of grains in a

microstructure against their topological class. We can easily estimate a number of transitioned boundaries based on ρ and f_T. This allows us assess the sign of $G(\rho, \mu, \Gamma)$ ($dV/dt < 0$ when G is negative and $dV/dt > 0$ when G is positive) for a given number of grain boundaries and transitioned boundaries. A few of these results for several levels of M_{min} and J_{min} can be seen in Fig. 5.1, in which we predict growth or shrinkage of a grain for its given topological class and number of transitioned boundaries:

We see several expected trends, the first of which being that the Rollett-Mullins equation predicts that no grains will grow with respect to the average grain size when $M_{min} = 1.0$ and $J_{min} = 1.0$ (5.1b) , a situation with no grain boundary mobility or energy anisotropy. Second, when only grain boundary mobility anisotropy exists (5.1c), the growth of the grain with respect to the average grain size is virtually unaffected by the number of transitioned boundaries on the grain, with grains growing when they have more than 15 grain boundaries. This is a reasonable prediction, as increasing transitioned grain boundary mobility should not change dihedral angles at triple junctions, but should increase the swiftness in which grain boundaries move towards their centers of curvature. In the opposite way, decreasing J_{min} and introducing grain boundary energy anisotropy causes the growth of a grain to be largely dependent on the number of transitioned grain boundaries, as seen in Fig. 5.1c and 5.1d. This, of course, happens because the introduced grain boundary energy anisotropy changes the dihedral angles of grain boundary triple junctions, thus change the grain boundaries' curvatures.

5.2 Comparison to Potts Model Results

We used a version of the Potts Model that transitioned selected grain boundaries to determine the fraction of transitioned boundaries a specific grain i_{Ab} needs to grow. Each of these simulations used the same 641-grain microstructure on a 100 by 100 by 100 grid and ran for 100 MCS, recording whether or not the grain had grown volumetrically (as opposed to relative to the average grain size). For these simulations, T(i,j) is expressed as:

$$T(i,j) = \begin{cases} 1, \ i = i_{Ab} \ or \ j = \ i_{Ab} \ , \ t = 0 \ \exists \ \sum_{j=0}^{Q} T(i_{Ab}, j) * B(i_{Ab}, j) = C \\ 0, \ \ otherwise \end{cases} \quad \textbf{(5.6)}$$

Here, Q is the total number of grain IDs in the simulation (For this microstructure, Q = 641), C is a number between 1 and $NN(i_{Ab})$, and B(i,j) is a function that determines whether or not the grain boundary between grains i and j exists. Simulations were performed on the microstructure for each of the 641 grains for combinations of M_{min} = 0.05 and 1.0 with J_{min} = 0.6, 0.8, 0.9, 0.95, and 1.0. Though the Potts Model simulations described by equation 5.6 only search for growth in volumetric terms and not growth relative to the growth of the microstructure, the results of the simulations appear consistent with those predicted by Rollett-Mullins. We see these results below in Fig. 5.2.

Despite only measuring the likelihood of volumetric growth, the Potts Model shows a dependence of grain growth on grain boundary energy anisotropy similar to that predicted by the Rollett-Mullins equation.

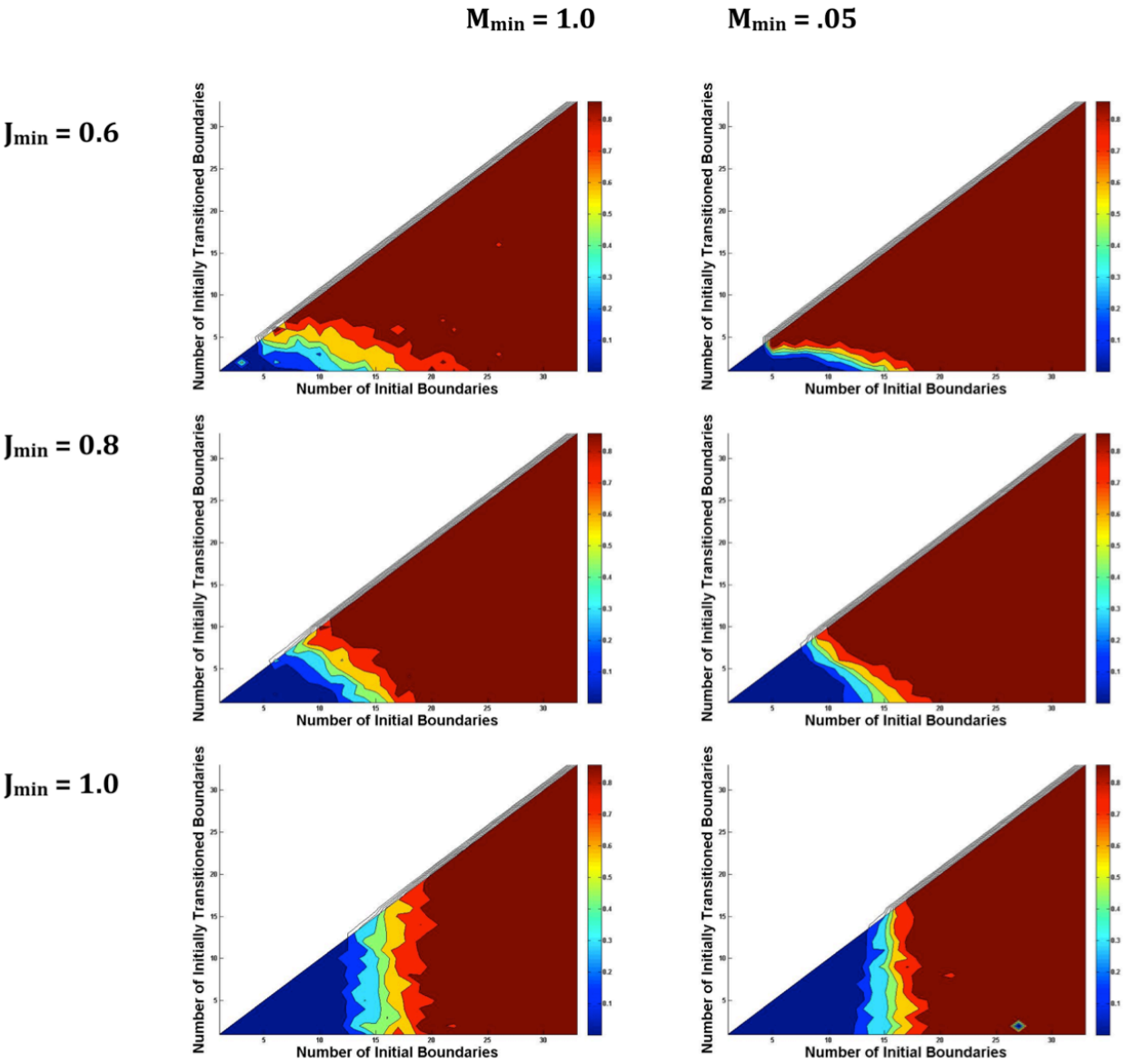

Figure 5.2: Likelihood of grain growth in Potts Model over 100 MCS given the initial number of grain boundaries and the initial number of transitioned grain boundaries, with varying grain boundary energy and grain boundary mobility advantages.

Volumetric growth of grains is relatively unaffected by the number of transitioned boundaries in cases where there is only grain boundary mobility anisotropy. Decreasing M_{min}, thus increasing the grain boundary mobility anisotropy for transitioned boundaries, decreases the width of the frontier between volumetric

grain growth and grain shrinkage. This is all consistent with the predictions made by the Rollett-Mullins equation, which suggest that adding grain boundary mobility anisotropy only accelerates the process of grain growth or shrinkage. Justifiably, the Potts Model predicts that the frontier between the grains that will grow volumetrically and those that will shrink is past the predictions made by Rollett-Mullins for relative grain growth. The slope of this frontier is clearly more affected by changes in J_{min}; we can see that the frontier for volumetric growth as predicted by the Potts Model for $J_{min} = 0.8$ is roughly the same as the frontier for relative growth predicted by Rollett-Mullins for $J_{min} = 0.6$.

Perhaps most conveniently, the frontier between volumetric grain growth and grain shrinkage for cases of grain boundary mobility anisotropy and no grain boundary energy anisotropy is almost identical to the analogous frontier predicted by Rollett-Mullins for relative grain growth. In this case, there is one major discrepancy between the two models: a large enough grain will shrink relative to the average grain size, but will not cease to grow volumetrically. A first order calculation shows that in order for this to become an influential factor in relative grain growth for an $M_{min} = 0.05$, the grain must be considerably larger – on the order of ten to eighty times average grain diameter! In this special case, when a grain grows volumetrically, unless it is extremely large, it is reasonable to assume that it is growing relative to the average grain size.

The introduction of grain boundary energy anisotropy, however, underscores how necessary it really is for an abnormal grain to maintain a certain number of transitioned boundaries at its given topological class. If a grain with transitioned boundaries grows and loses those transitioned boundaries as it grows, the grain will lose much of its growth advantage even when the transitioned boundary is replaced with a normal grain boundary.

These simulations provide some insight as to which grains can grow and how many transitioned grain boundaries they need to grow, but not how quickly they grow, or whether the growth occurring will be enough for the grains to become "abnormal."

5.3 The Razzak Equation of Grain Growth

Srolovitz[2,3,4] and Morawiec[5] have derived models of grin growth based on models of the coarsening of cellular structures and predict grain growth behaviors of the entirety of the microstructure over time based on grain boundary curvature, which is a computationally expensive calculation. Razzak[6], in a newer quantitative approach to AGG for use in cases of grain growth as the result of particle pinning, models abnormal grains large spheres growing into a matrix of smaller spheres. Razzak simply calculates that the rate of a grain's growth is proportional to the driving force for its growth by a factor of the grain boundary mobility:

$$\frac{dD_{Ab}}{dt} = M_{Eff}\left(P_{D_{Ab}} - P_Z\right) \qquad \textbf{(5.7)}$$

For our purposes, we do not have to consider Zener Pinning, so equation 5.7 simplifies to equation 5.8.

$$\frac{dD_{Ab}}{dt} = M_{Eff} P_{D_{Ab}} \tag{5.8}$$

Razzak derives the term for the driving force for the grain to grow as:

$$P_{D_{Ab}} = \frac{2\gamma}{D_n}\left[\mu - (1-\mu)\left(\frac{D_n}{D_{Ab}}\right)^2 + (2\mu - 1)\frac{D_n}{D_{Ab}}\right] \tag{5.9}$$

Here, $\gamma = \Gamma$ in the Rollett-Mullins equation, D_n is the average diameter of normal grains. If we assume that grains are spherical, then μ, is as described in equation 5.10:

$$\mu = \frac{n_n}{4}\left(\frac{D_n}{D_n + D_{Ab}}\right)^2 \tag{5.10}$$

The term n_n very simply describes the number of neighbors bordering the growing "sphere." Potts Model simulations were run on the 100x100x100, 641 grain microstructure for 1000 MCS to demonstrate that grain growth could be predicted by using the Razzak model. Grain Boundaries were transitioned in the following manner:

$$T(i,j) = \begin{cases} 1, & i = i_{Ab} \; or \; j = \; i_{Ab} \; , B(i_{Ab}, j) = 1, t = 0 \\ 0, & otherwise \end{cases} \tag{5.11}$$

For each execution of the simulation for a grain i_{Ab}, the growth of the grain over the next Monte Carlo step was predicted by the Razzak model in the following manner.

At the beginning of each step, we calculated the diameter of grain i_{Ab}, $D_{Ab}(t)$ and the average diameter of the neighboring grains $D_n(t)$. We initially set $D_{Est}(t)$, our estimation of $D_{Ab}(t)$ by the Razzak Model, so that $D_{Est}(0) = D_{Ab}(0)$. We then determined the number of neighboring grains to i_{Ab} and calculated $\mu(i)$:

$$\mu(t) = \frac{n_n(t)}{4}\left(\frac{D_n(t)}{D_n(t) + D_{Ab}(t)}\right)^2 \quad \textbf{(5.12)}$$

We can determine f_T for grain i_{Ab} by simply checking all of i_{Ab}'s neighbors for transitioned boundaries:

$$f_T(t) = \frac{\sum_{i=1}^{n_n} \begin{cases} 1, T(i_{Ab}, i) = 1 \\ 0, otherwise \end{cases}}{n_n} \quad \textbf{(5.13)}$$

We then determined $M_{Eff}(t)$ and $\gamma(t)$ using equations 5.5 and 5.6, respectively. Then we find dD_{Ab}/dt by combining equations 5.8 and 5.9, which we use to predict the radius of i_{Ab} at the next step:

$$D_{Est}(t+1) = D_{Est}(t) + \frac{dD_{Ab}}{dt} \quad \textbf{(5.14)}$$

We can see that in Fig. 5.3 that this method overall is fairly effective at predicting the rate of a grain's growth.Obviously there are several sources of error in such calculations, such as the fact that grains are certainly not spherical, though in many structures we can regard them as equiaxed. The grain observed sees quick, dramatic changes in D_{Ab}/D_n, which is clearly the result of neighboring grains disappearing. Less visibly, this also affects M_{Eff} and γ_{Eff}, which are both dependent on the transitioned state of the grain boundaries. This being said, our implementation of the Razzak model appears to be accommodating to these abrupt changes. We can

see in each of the cases in Fig. 5.3 that the grain grows under conditions of grain boundary mobility and energy anisotropy, as predicted by the Rollett-Mullins equation. However, the magnitude and duration of the growth is clearly dependent on the grain boundary energy anisotropy. In later simulations, we will generally regard a grain ten times the volume – or approximately 2.15 times the diameter of the average grain to be abnormal. If we regard D_{Ab}/D_n as a rough estimate of the normalized grain size, then we see that with only grain boundary mobility anisotropy (M_{mn} = .05), the grain in question does not become abnormal over the entire course of the 1000 MCS simulation.

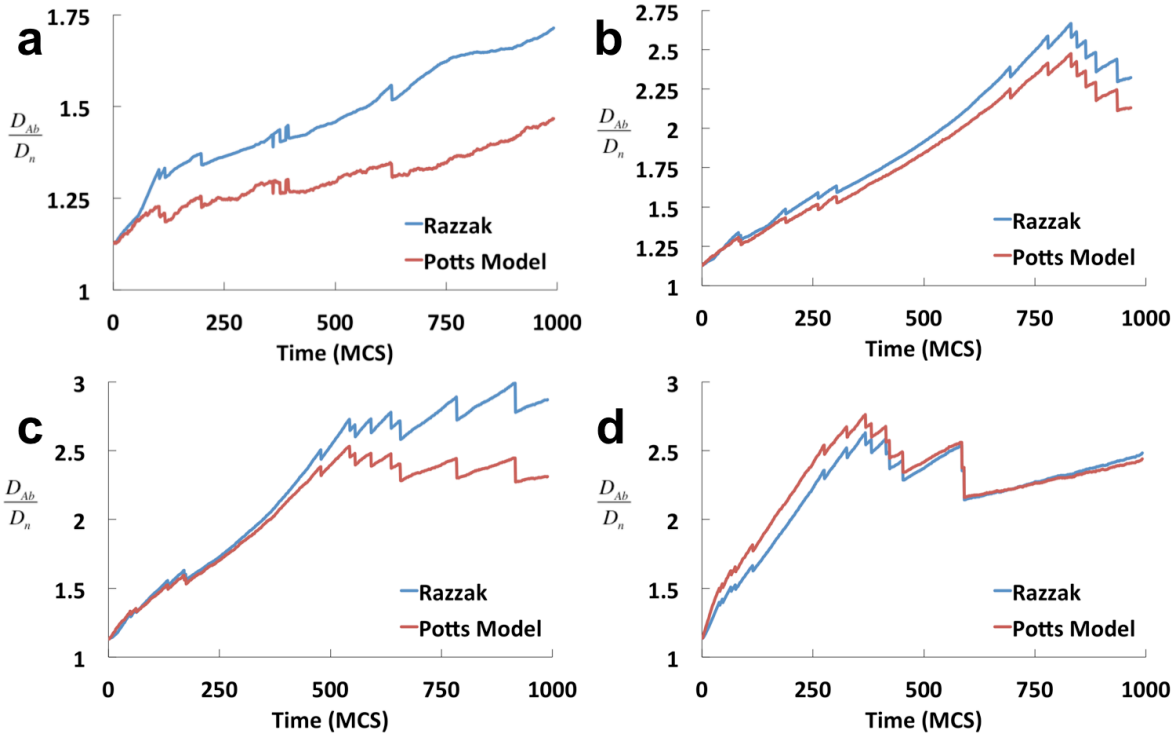

Figure 5.3: Growth of a 17-sided grain with grain boundary mobility and energy advantages of 20x mobility and a) 100 % energy, b) 90 % energy, c) 80 % energy, and d) 60 % energy in the Potts Model, compared with our predictions using the Razzak equation.

The other three simulations shown introduce grain boundary energy anisotropy, causing the grain to grow abnormally, but the grain begins to shrink after a period of

time. This period of time appears to decrease as J_{min} decreases. This happens because as the grain grows, some of the transitioned boundaries the grain started with disappear, and this process is happening faster as J_{min} goes down.

While this work demonstrates the qualifications for the growth of a single grain in a microstructure, It appears, then, that we have demonstrated fairly generous qualifications in terms of transitioned grain boundaries that are necessary to become abnormal, but have not yet provided more conservative estimates of the fraction of grains that can become abnormal, or taken in to account the existence of other transitioned boundaries in the microstructure, which would make determining which grains will become abnormal more complex. The following chapters examine grain growth behavior in such situations.

References

1. A.D. Rollett, W.W. Mullins, On the growth of abnormal grains. Scripta Mater. 1997;36:975.
2. D.J. Srolovitz, M.P. Anderson, G. S. Grest, P.S. Sahni. Grain growth in two dimensions. Scripta Metall. 1983;17:241.
3. R.D. MacPherson, D.J. Srolovitz, The Von Neumann relation generalized to coarsening of three-dimensional microstructures. Nature 2007;246:1053.
4. E.A. Lazar, J.K. Mason, R.D. MacPherson, D.J. Srolovitz. A more accurate three-dimensional grain growth algorithm. Acta Mater. 2011;59:6837.
5. A. Morawiec. Surface area of coarsening cellular structures. Philosophical Magazine Letters 2006;86:37.
6. M.A. Razzak, M. Perez, T. Sourmail, S. Cazottes, M. Frotey. A simple model for abnormal grain growth. ISIJ International 2012;52:2278.

Chapter Six: Boundary-Based Transition Mechanisms in the Potts Model

6.1 Adjacency-Based Complexion Transitions

In this chapter, we will provide a detailed description of our methodology for transitioning grain boundaries in the Potts Model to the high mobility complexion.

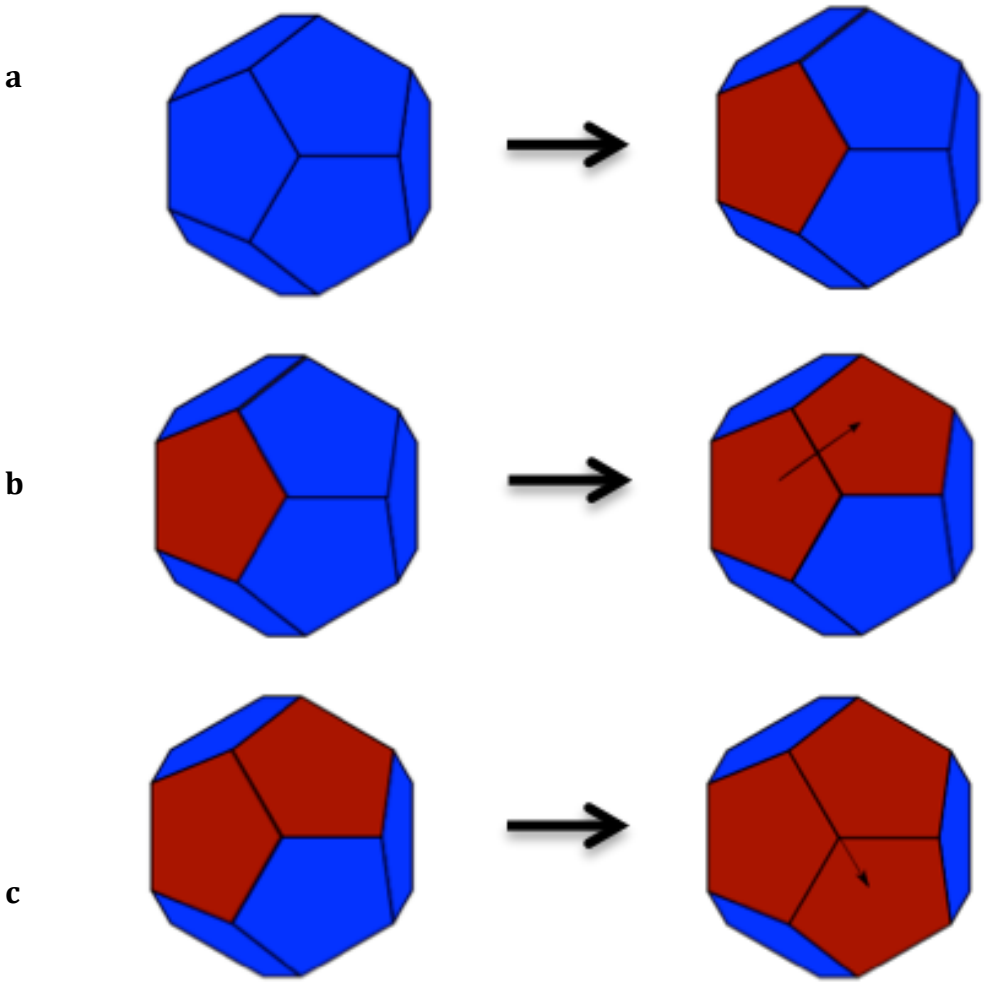

Figure 6.1: (a) The "independent" grain boundary transition, (b) the "adjacent" grain boundary transition, and (c) the "Double Adjacent" grain boundary transition. Here the blue surfaces represent not-transitioned grain boundaries and the red surfaces represent the transitioned grain boundaries. Note that in the case of the adjacency transition, mechanism is not a simple "enveloping" step, as the transition can occur for any grain boundary bordering the transitioned boundary by a triple line.

As described in Frazier et al[1], boundaries were selected to transition ($T(i,j) = 1$) periodically over time during each simulation. Fig. 6.1 shows three hypothetical mechanisms by which these transitions were allowed to occur in the Potts Model. First and most obviously, the "N_0," or "Independent" rule specifies that some fraction of grain boundaries will be able to transition to the high mobility, low energy complexion without any neighboring transitioned boundaries. This condition ensures that at least some of the grain boundaries are transitioned in the simulation.

The second rule, the "N_1," or "Adjacency" rule, allows grain boundaries that border at least one already transitioned grain boundary to transition. Any boundary connected to an already transitioned grain boundary through a triple line should be able to transition by this rule when selected. The adjacency transition is not a simple "enveloping" step, since the transition can occur for any grain boundary bordering the transitioned boundary by a triple line. This means that any three transitioned boundaries produced by this mechanism do not necessarily have to share one grain.

The third and final rule, the "N_2," or "Double Adjacency" rule, allows grain boundaries to transition if they border two transitioned grain boundaries which are themselves adjacent.

In Table 1, B(i,j) is an indicator function that returns one when the grain boundary exists and zero when it does not. The total number of sites available for each type of transition, that is, the number of grain boundaries which can undergo a transition to

the high mobility grain boundary complexion by a given mechanism, can be described with the following equations:

$$N_I = \sum_I^{N_{IDs}} \sum_j^{N_{IDs}} \frac{(1-T(i,j))*B(i,j)}{2} \quad \textbf{(6.1)}$$

$$N_{Adj} = \sum_i^{N_{IDs}} \sum_j^{N_{IDs}} \left(\left[\begin{cases} 1/2, & \sum_k^{NN_i} T(i,k) + \sum_l^{NN_j} T(j,l) > 0 \\ 0, & else \end{cases} \right] * \left(1 - T(i,j)\right) * B(i,j) \right) \quad \textbf{(6.2)}$$

$$N_{DAdj} = \sum_i^{N_{IDs}} \sum_j^{N_{IDs}} \left[\begin{matrix} 1/2 & \sum_k^{NN_i} \sum_l^{NN_i} T(i,k)*T(i,l)*B(l,k) + \sum_m^{NN_j} \sum_n^{NN_j} T(j,m)*T(j,n)*B(m,n) > 0 \\ 0 & else \end{matrix} \right] * (1-T(i,j))*B(i,j) \quad \textbf{(6.3)}$$

The number of sites that can be transitioned by each rule on a given step, N_T, is simply the minimum between the preset limit, R, which defines the rate of complexion transitions allowed per step, and the number of sites available. Now, the fraction of transitioned grain boundaries, f_T, is the number of transitioned boundaries divided by the total number of grain boundaries:

$$f_T = \frac{\sum_i^{N_{IDs}} \sum_j^{N_{IDs}} T(i,j)*B(i,j)}{\sum_i^{N_{IDs}} \sum_j^{N_{IDs}} B(i,j)} \quad \textbf{(6.4)}$$

Here N_{IDs} is the number of grain IDs in the microstructure. In the model, these sites are only allowed to transition, however, if the fraction of transitioned boundaries is below the preset limits N_0 for independent transitions, N_1 for adjacency transitions, and N_2 for double adjacency transitions. These preset limits are put in place to reflect the assumption that most grain boundaries are not transitioned.

We stress that each transition made is characterized only by the mechanism that was initially used to transition the boundary. For example, a grain boundary may meet the criteria to perform an adjacency transition, but make an independent transition instead. Thus sometimes, by chance, some grain boundaries that made independent transitions will appear to have made adjacency transitions. In the same way, some grain boundaries that made adjacency transitions will become disconnected from their neighboring transitioned boundaries over time, and appear to have made independent transitions.

$$N_{T,I} = \begin{cases} \min(N_I, R_I), & f_T < N_0 \\ 0 \quad , & f_T \geq N_0 \end{cases} \tag{6.5}$$

$$N_{T,Adj} = \begin{cases} \min\left(N_{Adj}, R_{Adj}\right), & f_T < N_1 \\ 0 \quad , & f_T \geq N_1 \end{cases} \tag{6.6}$$

$$N_{T,DAdj} = \begin{cases} \min\left(N_{DAdj}, R_{DAdj}\right), & f_T < N_2 \\ 0 \quad , & f_T \geq N_2 \end{cases} \tag{6.7}$$

In each round of transitions, the model first makes Independent (N_0) transitions, then adjacency (N_1) transitions, and finally double adjacency (N_2) transitions. An illustration of how the fraction of transitioned boundaries should change with time can therefore be seen in Fig. 6.2. Amended with these rules, the Potts model was used with a 100x100x100 grid, starting with a microstructure composed of 2,687 grains. Simulations ran for 10^7 time steps at kT = 1.0, which is generally regarded as large enough to avoid lattice pinning effects from the square grid[2,3]. It is possible to simulate microstructures with more grains or with a higher level of resolution, but

this simulation size was found to be sufficient to show the occurrence of AGG. transitioning grain boundaries at a rate of $R_I = R_{Adj} = R_{DAdj} = 50$ every 5000 time steps. The simulation was repeated several hundred times, using different set values of N_0, N_1, and N_2. Among the different variations of the three parameters that can exist, certain combinations were singled out for scrutiny.

The condition $N_0 > N_2 = N_1 = 0$ ensures that the only grain boundaries ever transitioned will be independent transitions. The condition of $N_1 > N_0 > N_2 = 0$ ensures that the only grain boundaries ever transitioned will be either independent or adjacent transitions. This scenario improves the probability of a given grain boundary transitioning if it borders one already transitioned grain boundary, but does not further improve the chances of grain boundaries transitioning in the event that the boundary is a double adjacency site. The propagation of transitioned boundaries through the microstructure is completely random with adjacency transitions, but transitioned boundaries will be more likely to share a common grain. The condition $N_2 > N_1 > N_0 > 0$ allows for independent, adjacency, and double adjacency grain boundary transitions. Preferential sites created by the independent and adjacent transitions should provide many sites for double adjacency transitions and grains transitioned in this way will always share a grain with at least two other transitioned boundaries. Finally, the condition of $N_2 > N_0 > N_1 = 0$ allows for independent and double adjacency transitions, but *disallows* adjacency transitions. This means that sites for double adjacency transitions will only appear once two

neighboring grain boundaries undergo independent transitions. Descriptions for each of these conditions can be found in Table 6.2.

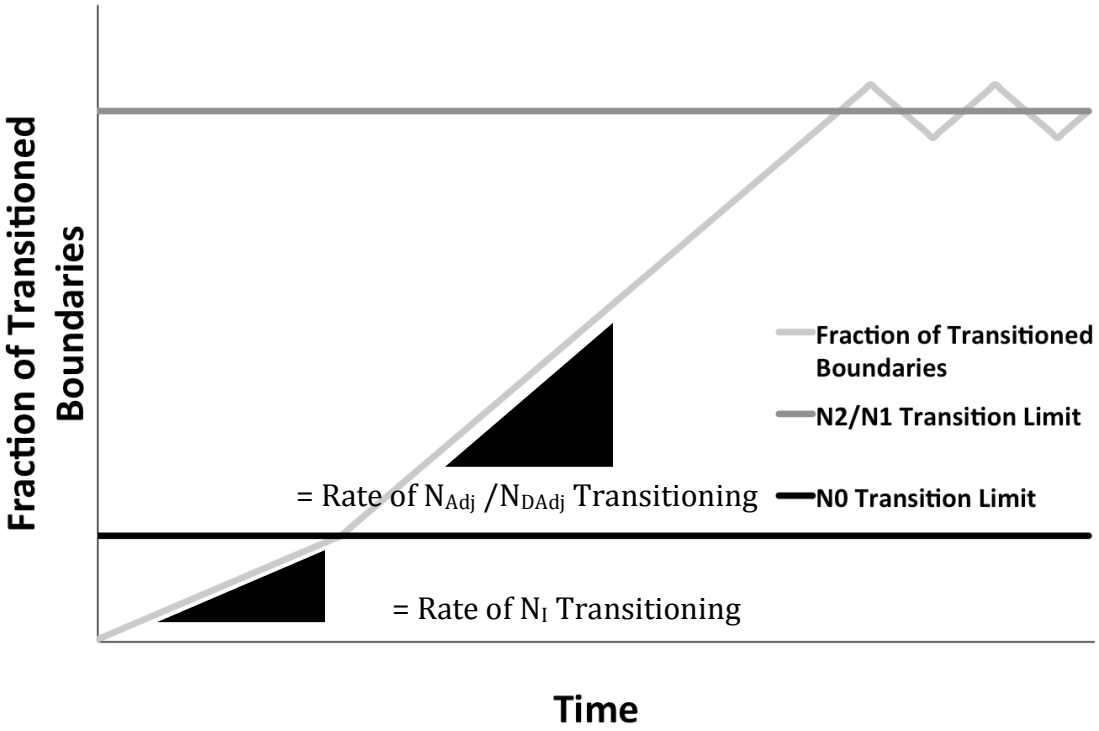

Figure 6.2: A plot of the fraction of transitioned boundaries as it should change with time as the modified Potts model runs. The model transitions boundaries at a constant rate until the fraction of boundaries transitioned reaches a preset threshold, at which point the model stops transitioning boundaries and some grain boundaries are eliminated. The oscillations at long times indicates that, in the event that the fraction of transitioned boundaries falls below the preset limit, transitions are added at the same rate until the fraction of transitioned boundaries is once again above the threshold.

Table 6.1: The different grain boundary transitioning mechanisms and their conditions.

Type of Transition	Explanation	Transitioning Condition
The "N_I" or "Independent" Transition	Grain boundary transitions without preferential site	$T(i,j) = 0, B(i,j) = 1$ Not-yet-transitioned grain boundary needs to exist
The "N_{Adj}" or "Adjacency" Transition	Preferential site for grain boundary transition provided by one previously transitioned grain boundary	$T(i,j) = 0, B(i,j) = 1$ Not-yet-transitioned grain boundary needs to exist $\sum_{k}^{NN_{i,}} T(i,k) * B(i,k) + \sum_{l}^{NN_j} T(j,l) * B(j,l) > 0$ At least one grain boundary that borders the grain boundary in question must be transitioned
The "N_{DAdj}" or "Double Adjacency" Transition	Preferential site for grain boundary transition provided by two adjacent, previously existing transitioned Grain Boundaries	$\mathrm{T(i,j)} = 0, \mathrm{B(i,j)} = 1$ Not-yet-transitioned grain boundary needs to exist $\sum_{k}^{NN_{i,}} \sum_{l}^{NN_i} T(i,k) * T(i,l) * B(l,k) + \sum_{m}^{NN_{i,}} \sum_{n}^{NN_i} T(j,m) * T(j,n) * B(m,n) > 0$ At least two adjacent transitioned grain boundaries must neighbor the grain boundary in question

Table 6.2: A table showing the expected grain boundary transitioning behavior that will come from different variations in the independent, random branching and percolated transition limits.

Scenario	Expected Behavior
$N_0 > N_2 = N_1 = 0$	Only Independent Transitions Appear.
$N_1 > N_0 > N_2 = 0$	Independent transitions and adjacency transitions appear.
$N_2 > N_1 > N_0 > 0$	Independent transitions, adjacency transitions, and double adjacency transitions appear.
$N_2 > N_0 > N_1 = 0$	Independent transitions appear, and double adjacency transitions may appear.

For this work, special attention was given to the region in which the total number of independent, adjacency, and double adjacency boundaries consisted of less than one percent of the boundaries because preliminary simulations suggested that this region contained a frontier that, once crossed, AGG goes from being highly unlikely to highly likely. In an effort to determine how the likelihood of AGG changed with the changing parameters and gain insight into what features of a grain may be conducive to AGG besides the formation of grain boundary complexions, an additional three sets of simulations were run: one with a pair of inserted independent transitions allowing for varying fractions of adjacency transitions, one with an independent transition bordering an adjacency transition allowing for varying fractions of double adjacency transitions, and finally one with a varying fraction of independent transitions allowing for a high number of double adjacency transitions.

6.2 Grain Boundary Motion-Induced Complexion Transitions

In another separate set of simulations, Which will be described in Frazier et al.[4], the occurrence of grain boundary complexion transitions was instead made to be

dependent on a function, F(i,j), for each boundary that changes as grain IDs reorient. This function provides a measure of the total volume that a single grain boundary "sweeps out" in either direction.

$$F(i,j) = F(i,j) + 1 \quad \textbf{(6.8)}$$

$$F(j,i) = F(j,i) - 1 \quad \textbf{(6.9)}$$

Initially, F(i,j) = 0 for all i and j. In these simulations, we periodically updated T to make it dependent on F by allowing grain boundary transitions to occur when F exceeded a predetermined threshold, C. Note that the transitioned state is unique for each grain boundary, meaning that when a transitioned grain boundary disappears it will have not effect on the transitioned state of its neighbors afterwards:

$$Tr(i,j) = \begin{cases} 1, & F(i,j) \geq C \\ 0, & F(i,j) < C \end{cases} \quad \textbf{(6.10)}$$

These simulations were performed based on the assumption that grain boundaries become metastable with respect to the high mobility complexion after accumulating solute, and that the solute accumulates on the grain boundaries through grain boundary motion. For the purpose of these simulations, we do not take into account factors such as the area of the grain boundary. Accordingly, the effect of the change in C on the grain growth behavior was of particular interest. For this purpose, the value of C was varied between 5 (less than five percent of the initial average grain volume) and 2,000 (about seven times the initial average grain volume). To validate the efficacy of the model, a grain growth simulation was run on a grain growing into a columnar microstructure, setting C = 20,000. Fig. 6.3 and Fig. 6.4 show the

microstructure and the changes in F(i,j) over the course of this test simulation. It can be clearly seen that F(i,j) increases monotonically until it reaches approximately the set threshold for transitioning at 20,000, at which point F(i,j) increases monotonically at a faster rate. Each simulation was ran for $t = 10^7$ and checked for the presence of abnormal grains over the course of the simulation, with an abnormal grain being defined as having a volume ten times that of the average grain, as well as the visual representation of the entire simulation as it progressed. This may not capture subtler results of the simulation, such as the connectivity of transitioned boundaries through triple lines, but was deemed sufficient to define the conditions under which abnormal grains can grow. Chapter Seven will examine and discuss the results of these simulations.

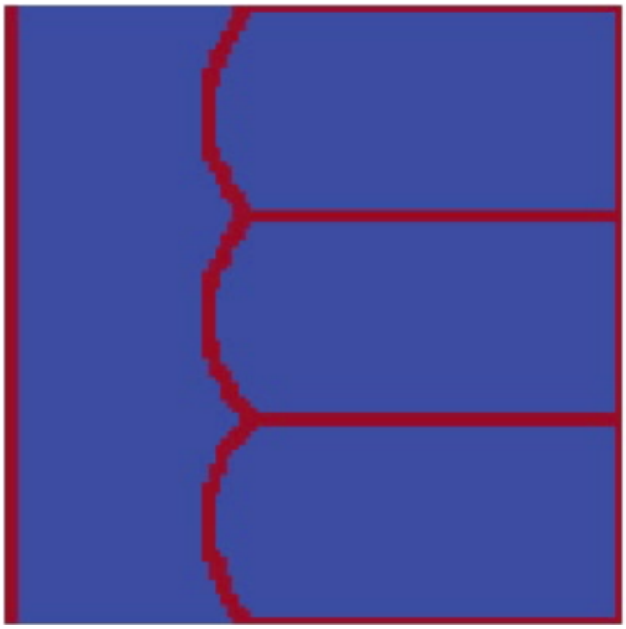

Figure 6.3: The columnar microstructure during the "test" simulation, with C = 20,000 and transitioned grain boundary mobility twenty times normal.

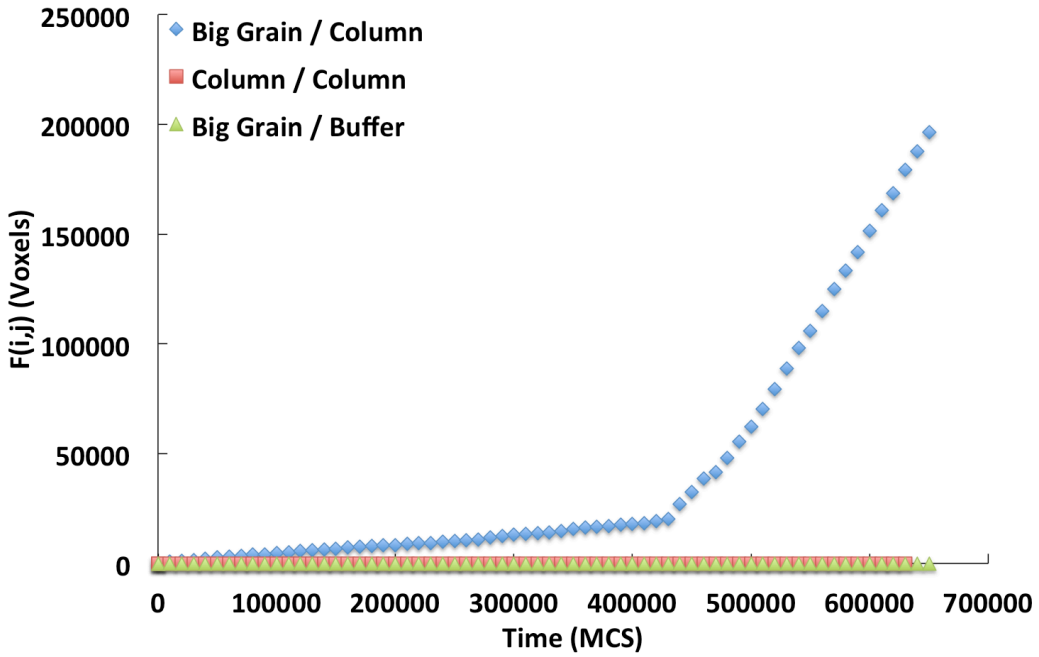

Figure 6.4: F(i,j) for grain boundaries between the big grain and one of the columnar grains, compared with the volumetric grain boundary motion between two of the columnar grains and with an immobile "buffer" layer.

6.3 Grain Boundary Distance Analysis

The relative likelihood of the abnormal grains' boundaries, the nearest-neighbor grain boundaries, and the next-nearest-neighbor grain boundaries to be in the transitioned state was calculated periodically over the course of each simulation. A schematic representation of this analysis is shown in Fig. 6.5: The analysis was performed to in order to assess how the likelihood of a grain boundary to be in the transitioned state varied as a function of distance from the abnormal grains and the rules that allowed for the transitions.

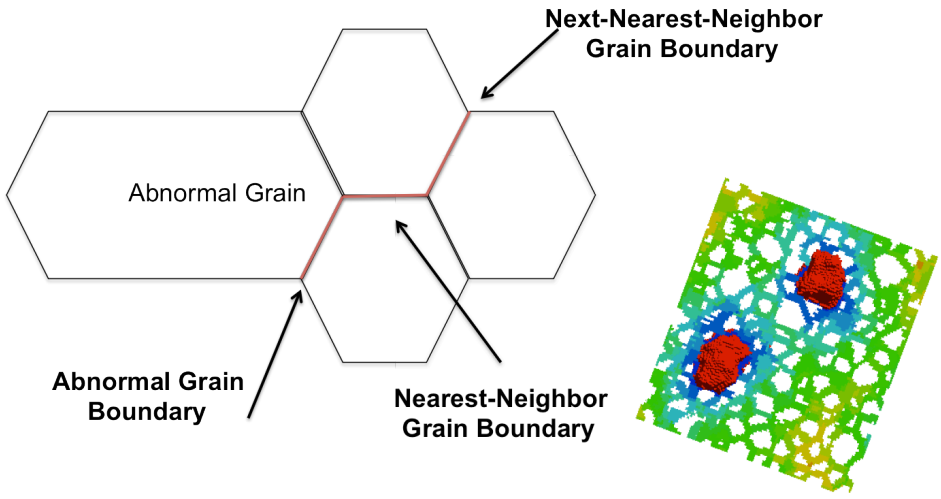

Figure 6.5: A schematic representation of the grain boundary distance analysis. Abnormal grain boundaries are regarded as the grain boundaries *on* an abnormal grain, while nearest-neighbor grain boundaries share a triple line with abnormal grain boundaries. Next-nearest-neighbor grain boundaries share triple lines with nearest-neighbor grain boundaries, but expressly *not* abnormal grain boundaries. This classification algorithm produced the image on the right, in which the boundaries closest to the abnormal grains (red) are colored in blue, with the furthest away colored in yellow.

6.4 Grain Boundary Motion Analysis

Grain boundary motion was tracked over the course of the simulations performed by establishing a metric very similar to the one used to assign complexion transitions in this work earlier in the chapter; for each instance of the microstructure that was collected at time *t*, for each point in the microstructure, when a voxel of grain *i* was previously in grain *j* at time *t-1*, increment *F(i,j,t)*. This method thus describes all net grain boundary motion in the microstructure. While this method will not accurately reflect the grain boundary motion associated with a grain boundary rotating, it was selected for its ability to measure net grain boundary motion towards a center of curvature.

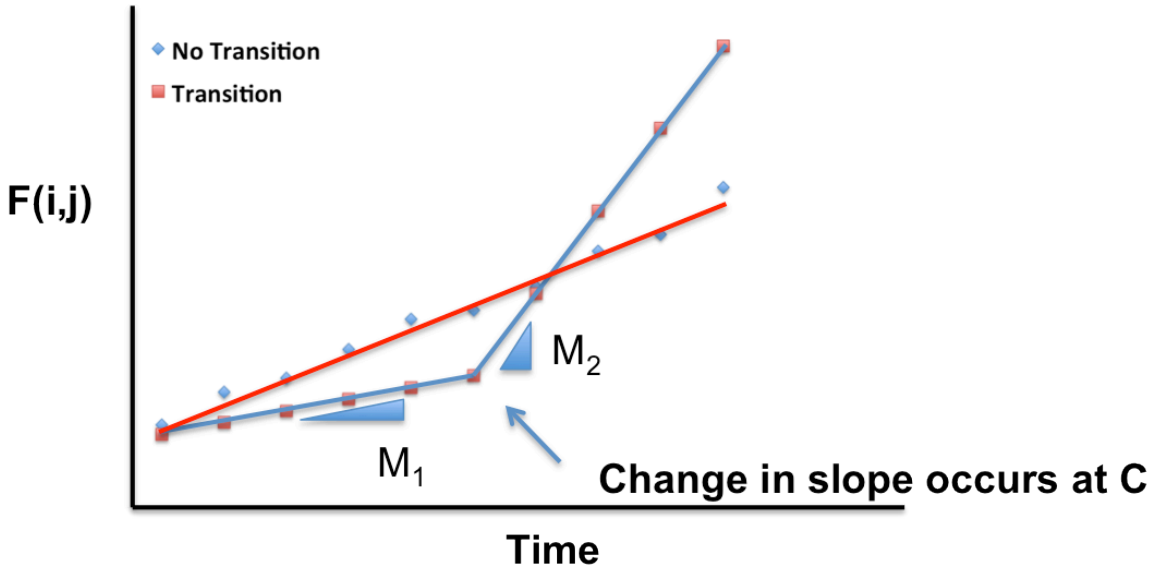

Fig 6.6: Schematic representation of algorithm used to determine volumetric grain boundary motion before a grain boundary complexion transition. Finding the best two-line fit for volumetric grain boundary motion over time can identify C and t_{trans}. When no fit is possible such that $M_2/M_1 > 1/M_{min}$, a single linear fit is used instead, which implies a very earlier complexion transition has occurred, or no complexion transition at all.

It was assumed that the occurrence of a grain boundary complexion transitions should be closely associated with a relative increase in the slope of *F(i,j)* with respect to *t*, as is shown through the example in Fig. 6.6. Thus we inferred when the complexion transitions happened and after how much grain boundary motion. This was done via a simple linear regression of *F(i,j,t)* with respect to *t*, using an algorithm that fits *F(i,j,t)* to two lines with the constraint that the slope of the second line must be larger than the first by a factor of the mobility advantage $1/M_{min}$. A schematic of such an algorithm can be seen in Fig 6.6. This algorithm was performed on simulation data in which grain boundary complexion transitions were

motion controlled and simulation data in which adjacency transitions were allowed. The results of these analyses can be found in Chapter 7.

References

1. W. E. Frazier, G.S. Rohrer, A.D. Rollett, Abnormal Grain Growth in the Potts Model Incorporating Grain Boundary Complexion Transitions that Increase the Mobility of Individual Boundaries. Acta Mater. 2015;96:390.
2. D. Zöllner, A New Point of View to Determine the Simulation Temperature for the Potts Model Simulation of Grain Growth, Computational Materials Science 86 (2014) 99-107.
3. M.A. Miodownik, K.G.F. Janssens, D. Raabe, E. Kozeschnik, B. Nestler, Computational Materials Engineering, Elsevier Academic Press (2007).
4. W. E. Frazier, G. S. Rohrer, A. D. Rollett, A Potts Model of Grain Growth Incorporating Grain Boundary Motion-Induced Complexion Transitions. TBA

Chapter Seven: Boundary-Based Transition Mechanisms in the Potts Model and AGG

7.1 Abnormal Grain Growth and Adjacency Transitions

Results of the simulations performed in Chapter 6 were analyzed for two key pieces of information: the occurrence of abnormal grain growth and the fraction of transitioned grain boundaries on abnormal grains. In this respect, our first goal was to determine the combinations of independent and adjacency transitions in the microstructure that would lead to AGG. We performed simulations allowing for between 0 and 100 adjacency transitions to appear in the microstructure (Fewer than 0.6 % of all boundaries in the microstructure) with a N_1:N_0 ratio of at most 60, setting M_{min} = 0.05 (A mobility advantage of twenty).

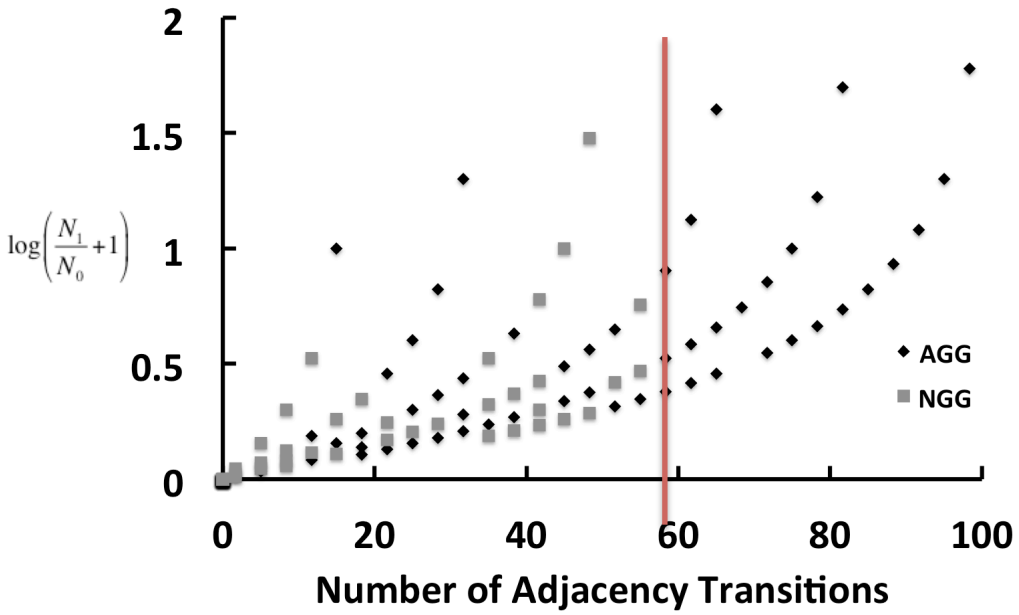

Figure 7.1: A plot of the occurrence of AGG with varying numbers of adjacency transitions and N_1:N_0 ratios in a microstructure initially containing 19,629 boundaries. AGG occurred in all simulations performed with over 60 adjacency transitions allowed.

The results that appear in Fig 7.1 clearly show the dependence of the occurrence of AGG on the number of adjacency transitions allowed in simulations. Note that the curves apparent in the figure are a consequence of the controls on transition rates in the code and have no significance per se.

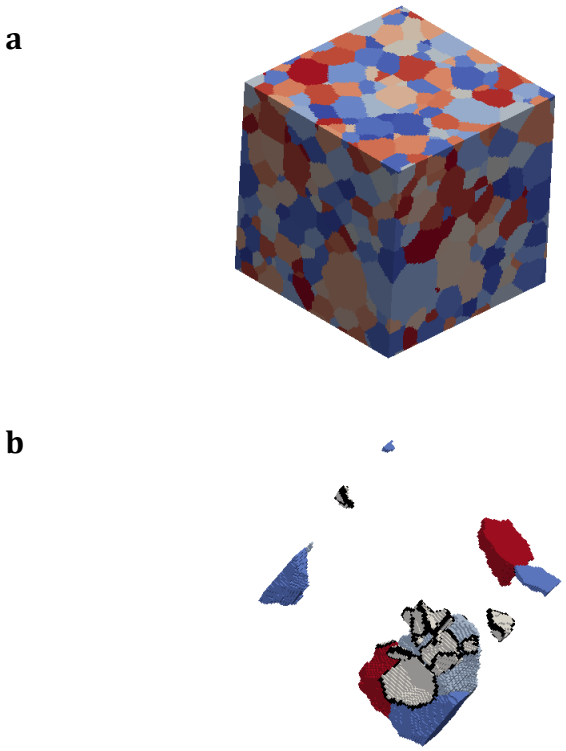

Figure 7.2: a.) The microstructure and b.) the transitioned boundaries (Filtered for M > .5) seen in white, outlined in black, and abnormal grains in blue, light blue, and red formed due to adjacency and independent transitions in the modified Potts model after 10^7 MCS, with the limiting fractions for independent and adjacency transitions set at .0001 (~3 boundaries) and .005 (~85 boundaries), respectively.

It is obvious from this plot that the occurrence of AGG becomes more likely as more adjacency boundaries are allowed to appear in the simulation, and becomes close to certain after around .3 % of all boundaries (roughly 60 boundaries in the simulation) are allowed to make the adjacency transition. These changes can be

seen in Fig 7.2. Here, an abnormal grain with multiple transitioned boundaries has clearly appeared, which demonstrates that AGG can occur with a simple "random branching" method of complexion transition propagation over triple lines, as some grains gain enough transitioned boundaries to grow abnormally simply by chance.

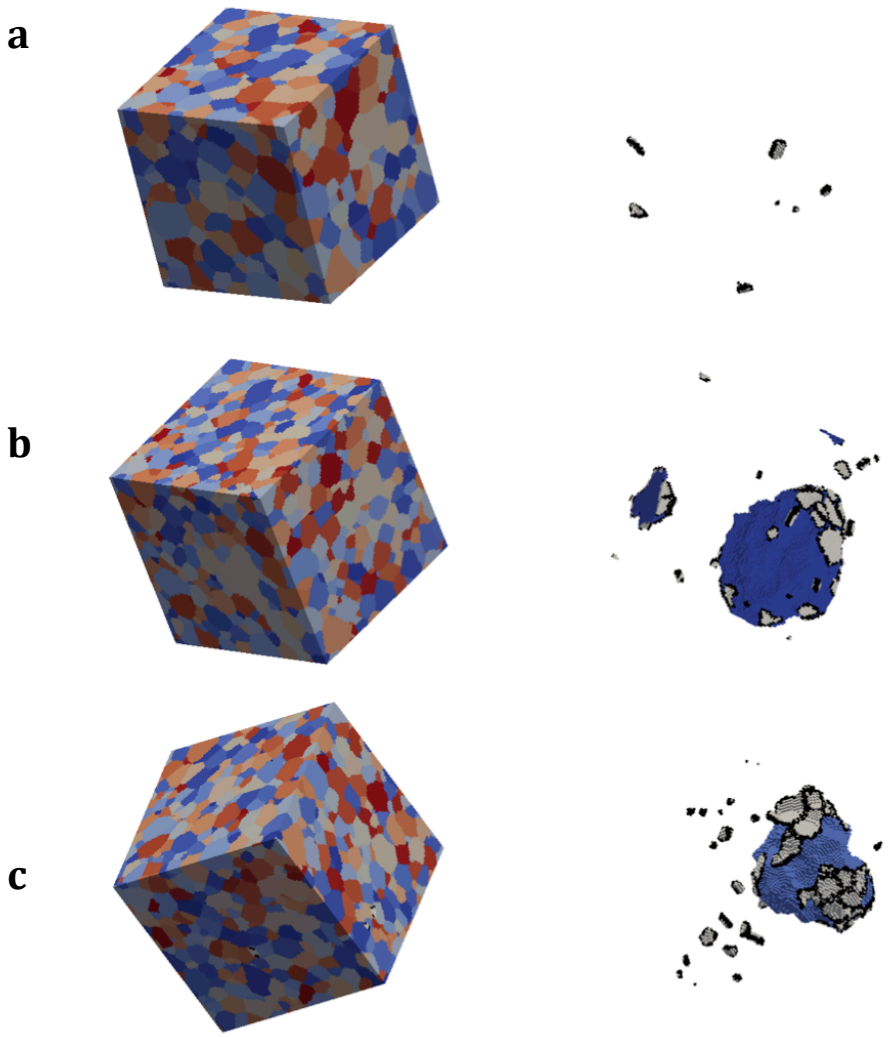

Figure 7.3: Grain growth over 10^7 steps for N_2 = .9 % and N_0 = 0.114 % after 10^7 steps (a), N_2 = 0.9 % and N_0 = 0.276 % after $3*10^6$ steps (b), and N_2 = 0.9 % and N_0 = 0.816 % after $3*10^6$ steps. Resulting microstructures are shown on the left and transitioned grain boundaries in the microstructures are shown on the right (filtered for M > .5) in white and outlined in black, as well as the present abnormal grains, which are blue. AGG is clearly present in (b) and (c), with connectivity between transitioned grain boundaries obviously high.

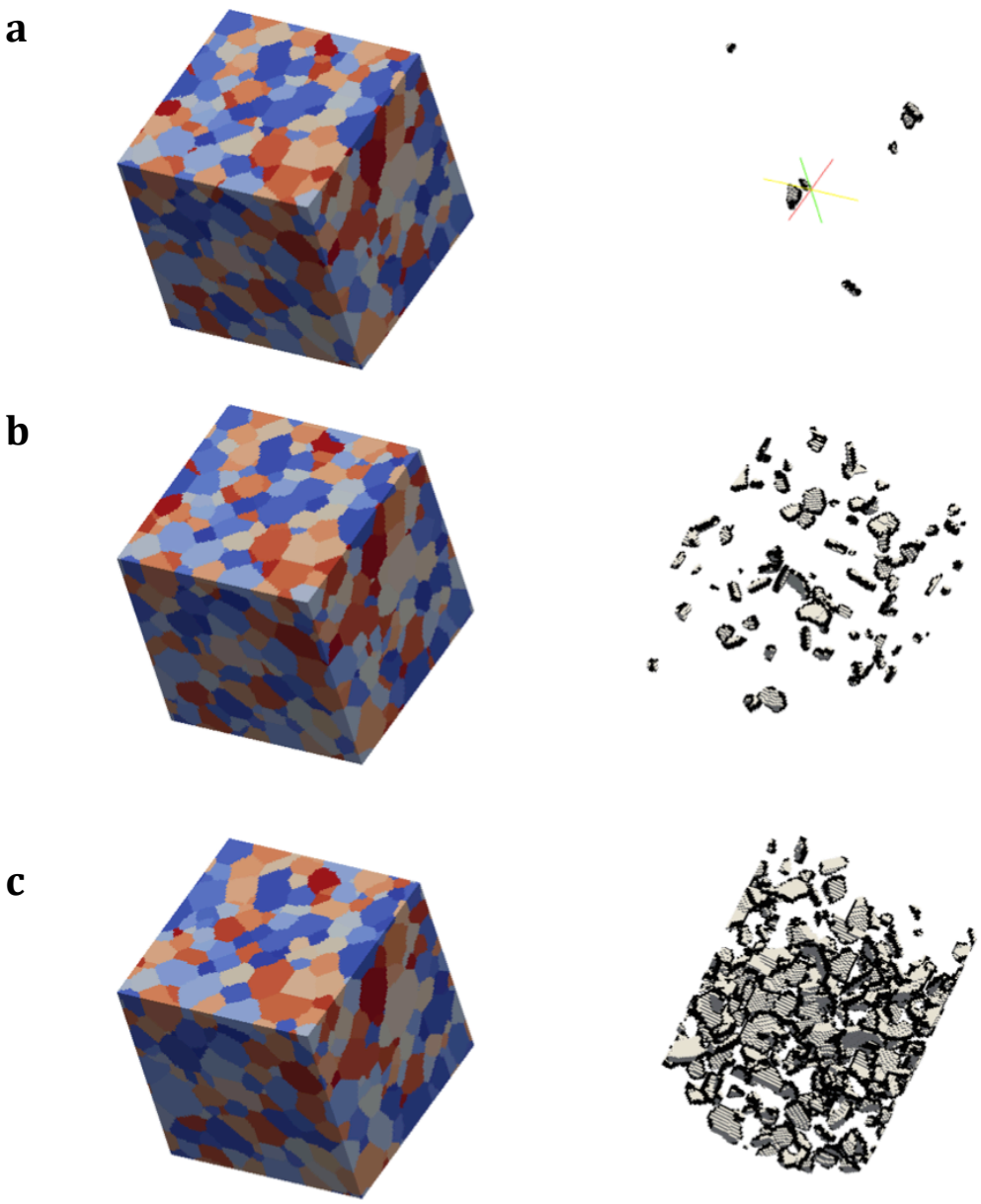

Figure 7.4: Grain growth over 10^7 steps for N_0 thresholds of 0.1 %(a), 1 % (b), and 10 % (c) of all grain boundaries, with no N_1 or N_2 transitions allowed to occur. Resulting microstructures are shown on the left and transitioned grain boundaries in the microstructures are shown on the right (filtered for M > .5) in white, outlined in black. No AGG is present and no networks of transitioned boundaries are present.

Further, AGG can also occur when transitions are only allowed to spread by the double adjacency rule, as shown in Fig 7.3. With enough independent transitions allowed in the simulation, occasionally some of them come into contact, allowing the transitions to spread by the double adjacency rule. Thus, as when only adjacency

and independent boundary transitions were allowed, some grains gained enough transitioned boundaries to grow abnormally. However, if only independent grain boundary transitions are allowed, the same kind of growth does not appear to be possible, as Fig 7.4 demonstrates.

There is a relatively simple probabilistic explanation for why AGG occurs in the simulations where the transitioned boundaries with high mobility are added in clusters and why AGG does not occur when the grain boundary transitions are independent. If we assume that the probability of any grain boundary transitioning over a period of time is one percent and that a typical fourteen sided grain needs half of its boundaries to transition to become abnormal, this suggests that the probability of a single one of these grains growing is $p = (0.01)^7 = 10^{-14}$. At most only one in a trillion grains could possibly be abnormal and this would never be observed.

However, we can find that by assuming that a boundary neighboring a transitioned boundary is more likely to transition by a factor of fifty, then the chances of *one grain* accumulating enough transitioned boundaries to grow abnormally is roughly $p = (0.01)(0.5)^6 = 0.000156$. Dillon and Harmer[1] estimate similar abnormal grain number fractions in their observations of AGG in Ca-doped Alumina, and speculate that the fraction of abnormal grains in a "typical" microstructure is on the order of 1 in 10,000 to 1 in 1,000,000.

We can see this effect in action in Fig 7.5, which shows that if you provide a single seed for adjacency or double adjacency transitions, then AGG becomes possible after 23 adjacency or 3 double adjacency transitions. When only adjacency transitions were allowed to occur from the independent transition, AGG became close to certain after roughly 0.3 % of boundaries (roughly 60 boundaries) were allowed to make adjacency transitions, which can be inferred from Fig 7.5 as the cumulative probability of AGG in the set of such simulations becomes roughly linear at this point. When only double adjacency transitions were allowed to occur from the independent-adjacency junction, the occurrence of AGG became close to certain after a much smaller fraction of boundaries were transitioned – the cumulative probability plot becomes linear with only 0.05 % of grain boundaries allowed to transition (~10 boundaries).

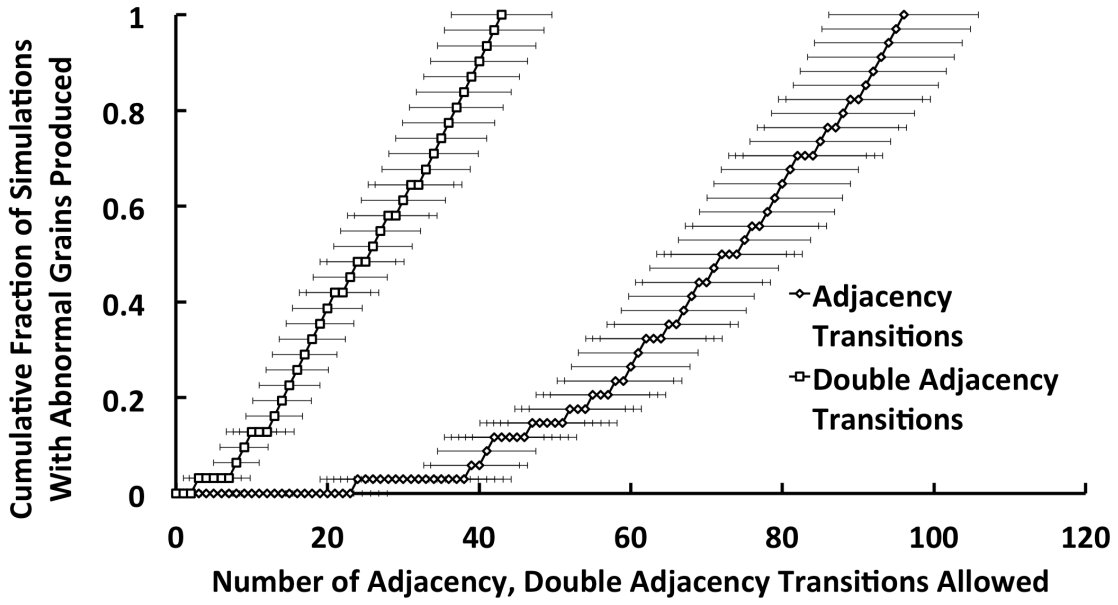

Figure 7.5: The cumulative probability of AGG in the set of simulations upon allowing for a set number of adjacency transitions and a set number of double adjacency transitions.

The reason for the observed behavior is clear: logically, grain boundary transitions that transition by the double adjacency mechanism must exist on the same grain with two other grain boundaries that are also transitioned. This means that any preferential sites that these transitioned grain boundaries create must *also* exist on the same grain. If these are the only transitions that exist in the simulation, then all of the transitioned grain boundaries will share one grain, essentially making the double adjacency mechanism an enveloping mechanism. This basically means that we are measuring roughly how many transitioned boundaries grains should, on average need to become abnormal with an $M_{min} = 0.05$. Plausibly, this number seems to be roughly ten, roughly have the number of boundaries on an above-average sized grain.

In the case only allowing for adjacency transitions, we have a much more complex interplay between grain growth and grain boundary transitions; as they occur, some grains by chance accumulate enough transitioned boundaries to grow abnormally. As the number of adjacency transitions increases, the probability of this happening becomes close to certain. It is clear that eventually the addition of more transitioned boundaries will stifle AGG rather than promote it, but preliminary simulations show that the number of transitioned grain boundaries required to do this would constitute a large fraction of the grain boundaries in the microstructure.

Finally, when double adjacency transitions were essentially free to occur, but constrained by the presence of randomly touching independent transitions, the

cumulative probability of AGG becomes linear after the fraction of transitioned boundaries allowed to occur by independent transitions is roughly 0.1 %.

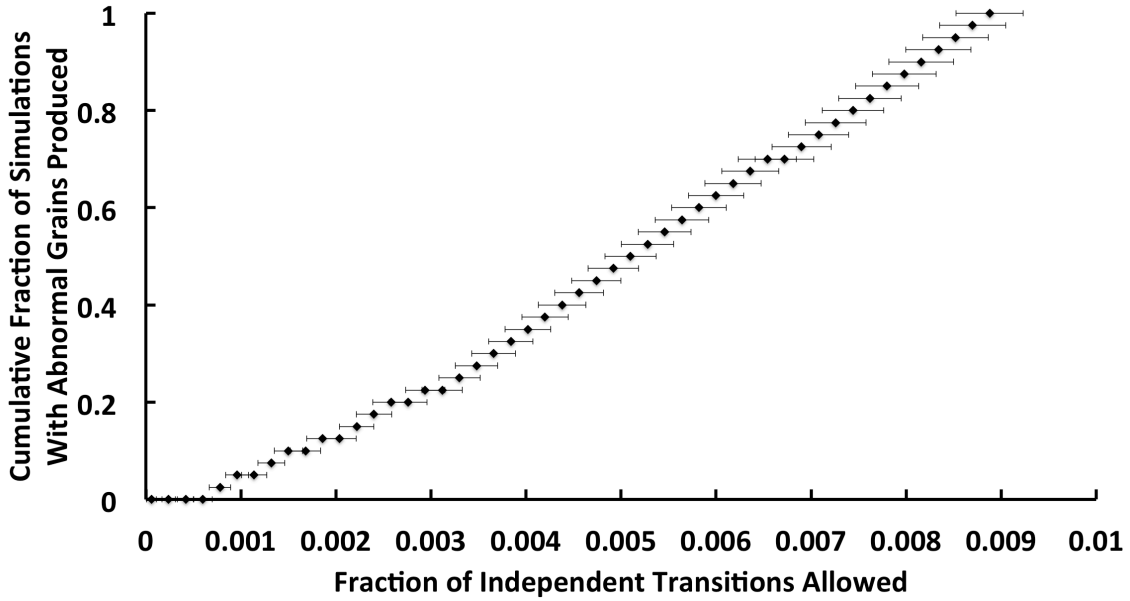

Figure 7.6: The cumulative probability of AGG in the set of simulations upon allowing for a set fraction of independent transitions and a set fraction of double adjacency transitions.

How is it possible that AGG can still occur when the probability of an independent transition is so small? It seems highly unlikely that a site for a double adjacency transition could even exist, but we can show through simple probabilistic estimates that the probability of two transitioned boundaries in the microstructure sharing a triple line, the requirement in our simulations for a double adjacency transition, is quite high. We calculate this in an analogous fashion to estimating the probability that two individuals in a room share a common birthday. If we assume that grains have on average fourteen grain boundaries[2], then the total number of boundaries in the system is about seven times the number of grains, Q. We assume that each grain boundary on average is enclosed by five triple lines[3], so transitioning one grain

boundary in the microstructure means that on average eleven grain boundaries (five neighboring boundaries from each grain, plus the transitioned grain boundary itself) cannot transition in order to avoid forming a double adjacency site. Therefore, the total number of "people" in the room is N_T, the number of transitioned boundaries, the total number of possible "birthdays" is 7Q, and every additional "person" eliminates eleven birthdays. We can then estimate the probability that at least two transitioned grain boundaries in the system will come into contact as:

$$P_{Site} \approx 1 - \prod_{i=1}^{N_T} \left(1 - \frac{11i}{7Q}\right) \quad \textbf{(7.1)}$$

When Q = 3,000 (~21,000 grain boundaries) and N_T = 100 (~0.5 % of all boundaries transitioned), the probability of at least two of these boundaries being in contact, thus creating a double adjacency site is approximately 93 %. With less than one in one hundred boundaries in the system transitioned, a double adjacency transition site could be expected to appear readily.

In addition, the fraction of transitioned boundaries on abnormal grains was tracked over time in three different scenarios, as seen in Fig 7.7: first, in which independent and adjacency transitions occurred, second, in which independent and double adjacency transitions occurred, and finally in which all three types of transitions were allowed to occur. This result can be seen in Fig 7.7. Simulations in which adjacency transitions induce AGG should on average have a smaller fraction of

transitioned boundaries on abnormal grains than simulations in which a combination of adjacency and double adjacency transitions induce AGG.

The number of abnormal grains was also tracked in these simulations. In each of the three scenarios abnormal grains appeared with only one percent of all boundaries transitioned, but using all three transition rules in combination resulted in an over twofold increase in the number of abnormal grains per volume.

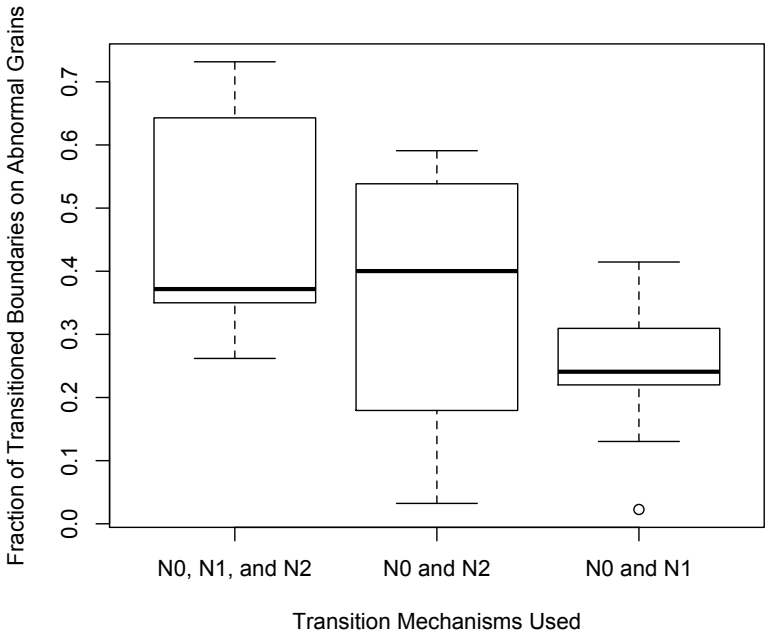

Figure 7.7: The fraction of transitioned boundaries on abnormal grains after 10^7 MCS in simulations allowing for either the independent and double adjacency propagation mechanisms, the independent and adjacency propagation mechanisms, or the independent, adjacency, and double adjacency propagation mechanisms. Ten simulations were performed for each scenario.

These results all demonstrate that complexion transitions on a subset of grain boundaries to a higher mobility and lower energy state can lead to abnormal grain growth, but if such transitioned boundaries are randomly dispersed in the

microstructure, they are unlikely to initiate abnormal grain growth. When the nucleation of transitioned boundaries is biased, clusters of transitioned boundaries form resulting in the formation of a few abnormal grains. While experimental evidence appears to indicate a bias resembling the one simulated – increased likelihood of transitioning due to adjacency to transitioned boundaries, the physical explanation for this bias remains unclear. One possible explanation for the bias is that when a grain boundary transitions, sometimes this creates a preferential site on triple lines that reduces the nucleation barrier for a complexion transition. A voxel-by-voxel simulation of grain boundary transitions and grain growth that reflects this hypothetical effect will be discussed in the following chapter.

7.2 Motion-Induced Complexion Transitions and AGG

AGG was found to occur depending on the mobility advantage of the transitioned boundaries and the amount of grain boundary motion required for the transitions to occur, as delineated in Chapter 6, Section 2. Fig. 7.8 clearly shows a case in which an abnormal grain formed. This shows that abnormal grains can indeed form when grain boundary complexion transitions nucleate as the result of grain boundary motion.

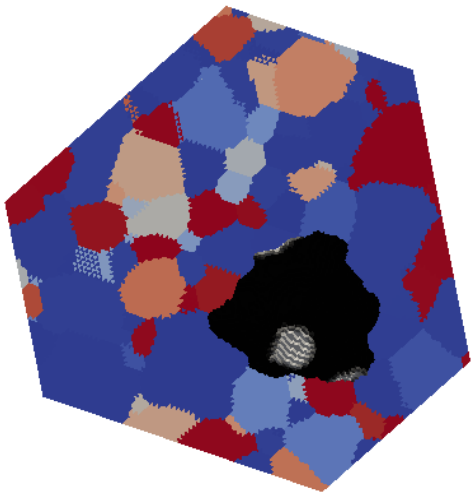

Figure 7.8: An abnormal grain (black) at the end of a Potts Model simulation lasting 50,000,000 MCS with C = 200 with transitioned grain boundary mobility one hundred times larger than normal (M_{min} = 0.01). Transitioned boundaries (white) can be seen on the surface of the abnormal grain. Only a two-dimensional slice of the simulation is shown.

Several transitioned boundaries are clearly visible on the surface of the abnormal grain. Fig. 7.9 shows that the transitioned grain boundaries appear roughly evenly spaced. It is noticeable through visual examination of the microstructure that the connectivity of the grain boundaries is low, a feature of the microstructure that will be explored later in the section. The amount of grain boundary motion required to induce a transition can vary over a wide range and still produce abnormal grains. Fig 7.10 shows that AGG continues to be possible when C, the amount of volumetric grain boundary motion required for a grain boundary transition to occur, is nearly ten times the initial average grain volume V_i (a grain boundary would have to sweep out ten times the initial average grain volume in order to transition) or close to one

hundredth the initial average grain volume (the grain boundary transition is almost instantaneous).

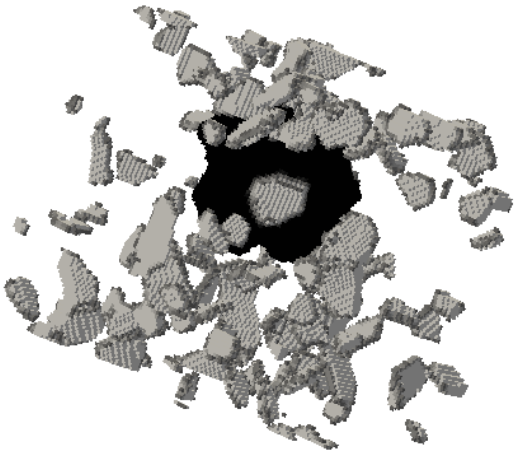

Figure 7.9: An abnormal grain (black) at the end of a Potts Model simulation lasting 50,000,000 MCS with C = 200 with transitioned grain boundary mobility one hundred times larger than normal (M_{min} = 0.01). All features of the microstructure have been filtered out of the image, except for the abnormal grain and the transitioned boundaries, which are shown in white.

The amount of grain growth necessary for AGG as it depends on C and the transitioned grain boundary mobility was studied by comparing the average grain volume when the first abnormal grain appeared, V_f, to V_i. This analysis was performed to provide a unit-less quantification of the "incubation" time required for an abnormal grain to form. The occurrence of AGG in the simulations was relatively insensitive to change in grain boundary mobility, but had a logarithmic relationship with V_i/C, as shown in Fig. 7.11.

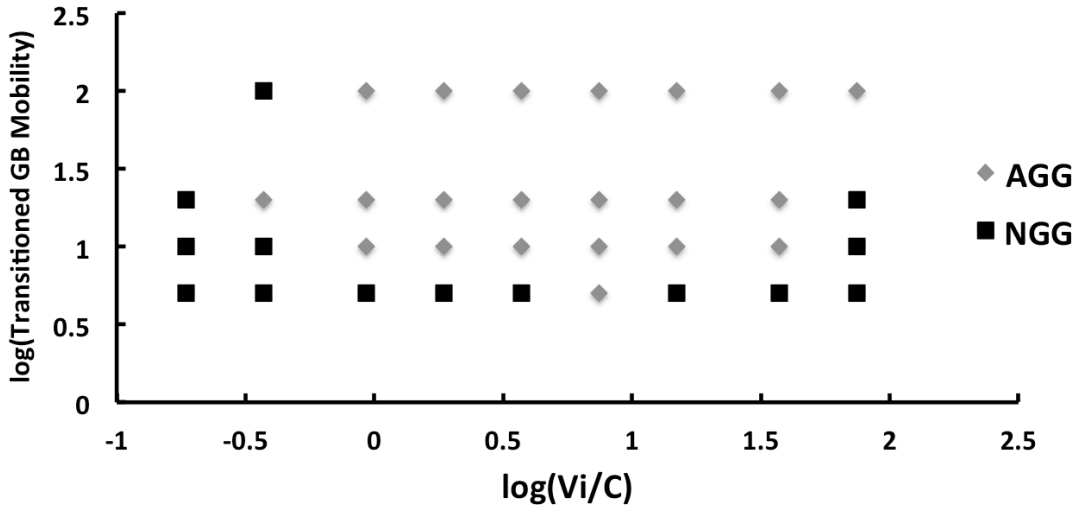

Figure 7.10: The occurrence of AGG as dependent on the transitioned grain boundary mobility and the initial average grain volume in comparison to the parameter C.

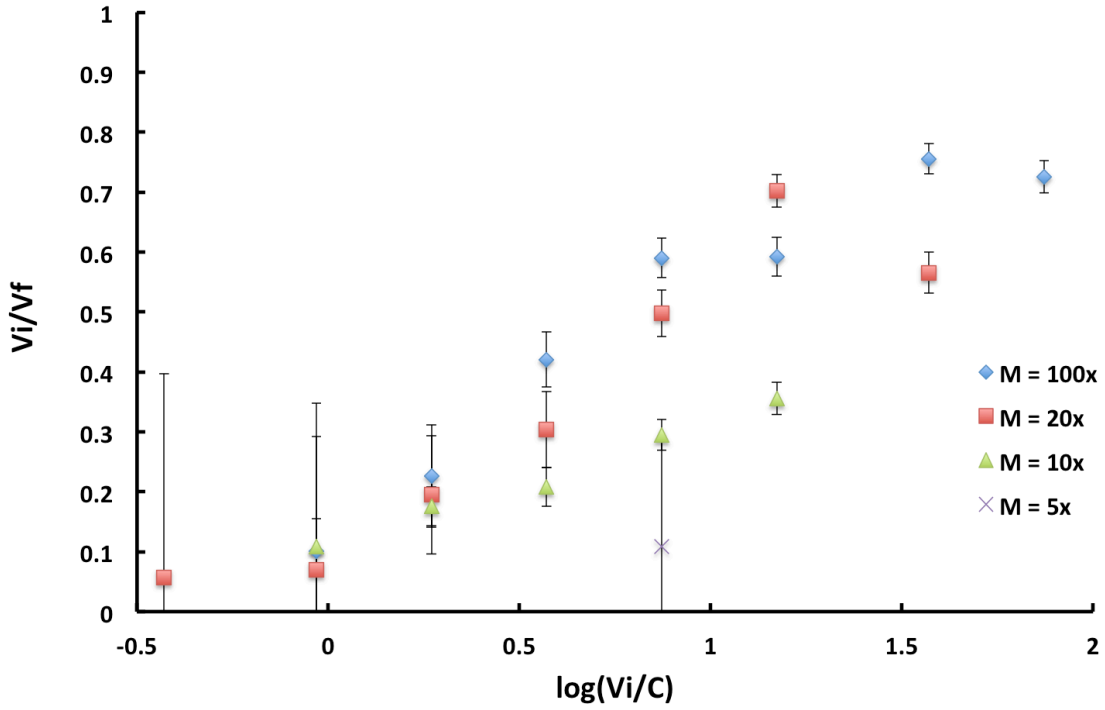

Figure 7.11: The average grain volume at the start of each simulation (each simulation is a single data point) in comparison to the average volume at the beginning of AGG, as dependent on the initial average grain volume in comparison to the parameter C.

This shows that V_i/V_f does not indicate the amount of time required for the first abnormal grain to appear, only the amount of coarsening before the first abnormal

grain appeared. The amount of coarsening before the first grain boundary transition appears will be entirely dependent on C, since the grain growth up until the first grain boundary transition is entirely isotropic. Therefore, any variance in V_i/V_f due to changes in the transitioned grain boundary mobility results from grain growth over the period between the first grain boundary transition and the appearance of the first abnormal grain. This provides a small window of time in which the transitioned grain boundary mobility can significantly change V_i/V_f. Consequently, V_i/V_f varies weakly as a function of the transitioned grain boundary mobility, unless that mobility is sufficiently low. Note that in Fig. 7.11, the microstructure coarsens far less before AGG when the transitioned grain boundary mobility is only five times the initial mobility.

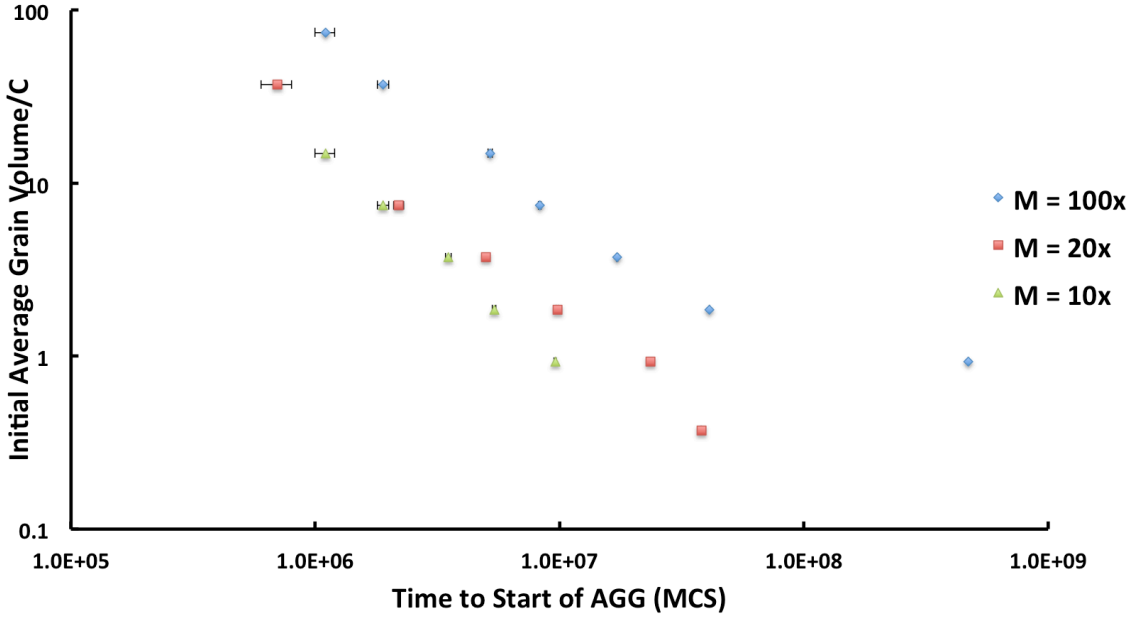

Figure 7.12: The amount of time required for the AGG to start (determined by the existence of one grain or more in the microstructure with greater than ten times the average volume) as dependent on the initial average grain volume in comparison to the parameter C.

Fig. 7.12 shows that the amount of simulation time before the first abnormal grain appears increases with the increase in the transitioned grain boundary mobility. This makes sense, since the transitioned grain boundary mobility is a constant 1.0 and M_{min}, the default grain boundary mobility, is the actual variable that changes. As discussed previously, when the relative mobility of the transitioned grain boundaries is high, the amount of time between the appearance of the first transitioned grain boundary and the first abnormal grain decreases. The log of the time required for the first abnormal grain to appear follows an inverse-normal relationship with the log of V_i/C. This reflects that when the amount of grain boundary motion required for grain boundaries to transition is small, grain boundaries transition faster, causing abnormal grains to appear faster.

7.3 Analysis of Transitioned Grain Boundary Fractions

Tracking the fraction of the abnormal grains' boundaries that are transitioned, as well as their nearest neighbors, reveals that the grain boundaries on the abnormal grains are significantly more likely to be transitioned over the period of time during which the abnormal grain is detectable (a volume greater than three times the $\bar{V}$). The fraction of boundaries that are transitioned on the abnormal grains' boundaries, nearest neighbor grain boundaries and next-nearest neighbor grain boundaries can be seen in Fig. 7.13. A more complete list of these simulation results can be found in Appendix C.

The same fraction of nearest neighbor and next-nearest neighbor grain boundaries are transitioned over the course of the abnormal grain growth. The simulation illustrated by Fig. 7.13 does not portray then entire progression of AGG, e.g., from the appearance of the first abnormal grains until the grain size distribution once again becomes "normal". Fig. 7.14 shows this progression more clearly. While the threshold grain boundary motion C for the transition to occur is four times smaller than the simulation results shown in Fig. 7.8, the early segment of the simulation shows the same trend: the grain boundaries on the abnormal grains are more likely to be transitioned than the nearest neighbor grain boundaries, and those are roughly as likely to be transitioned as the next-nearest neighbor grain boundaries. However, as AGG progresses further, the nearest and next-nearest neighbor boundaries "catch up", until at the end of AGG the fractions of transitions on all three classes of boundaries are close to equivalent. The growth advantage that the abnormal grains had diminishes as additional boundaries transition over the course of the simulation. We can see this more clearly when we normalize these fractions by the fraction of transitioned boundaries over the microstructure as a whole, as seen in Fig. 7.13: At the beginning of abnormal grain growth for the simulation, an abnormal grain's boundary is close to seven times more likely to be in the transitioned state than the average grain boundary. This relative likelihood decays as more grain boundaries transition, causing the abnormal grains to lose their growth advantage. The boundaries on the abnormal grains remain more likely to have been transitioned for less than half of the period in which abnormal grains appear.

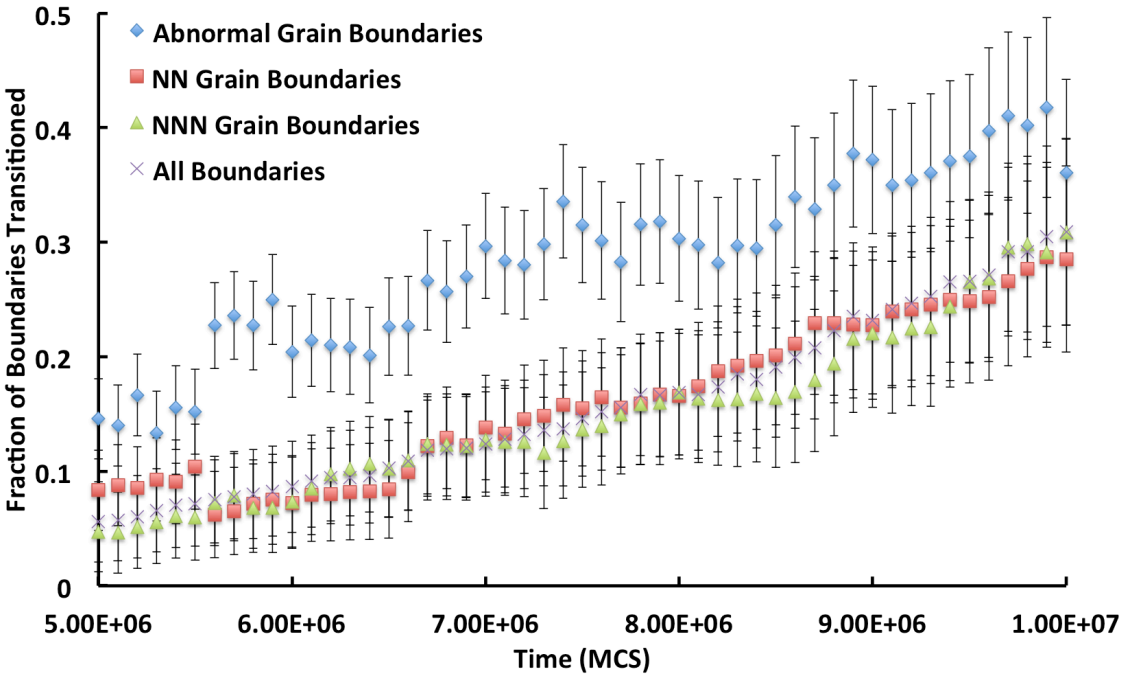

Figure 7.13: The fraction of transitioned grain boundaries on the abnormal grain boundaries, their nearest neighbor grain boundaries, and their next-nearest neighbor grain boundaries over the course of a single simulation where C = 100 and transitioned grain boundaries had twenty times the normal grain boundary mobility (M_{min} = .05).

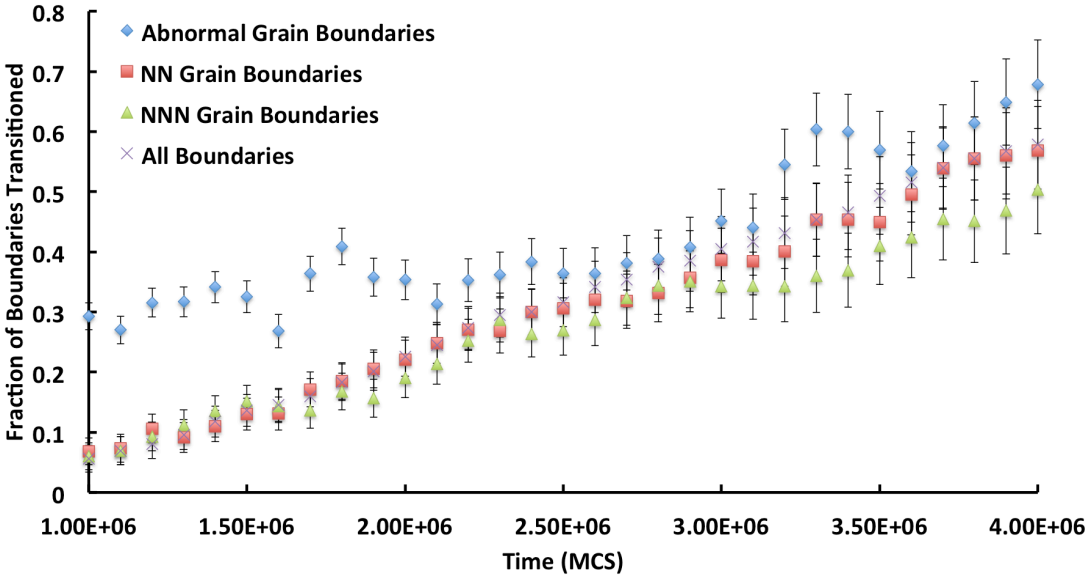

Figure 7.14: The fraction of transitioned grain boundaries on the abnormal grain boundaries, their nearest neighbor grain boundaries, and their next-nearest neighbor grain boundaries over the course of a single simulation where C = 25 and transitioned grain boundaries had twenty times the normal grain boundary mobility (M_{min} = .05).

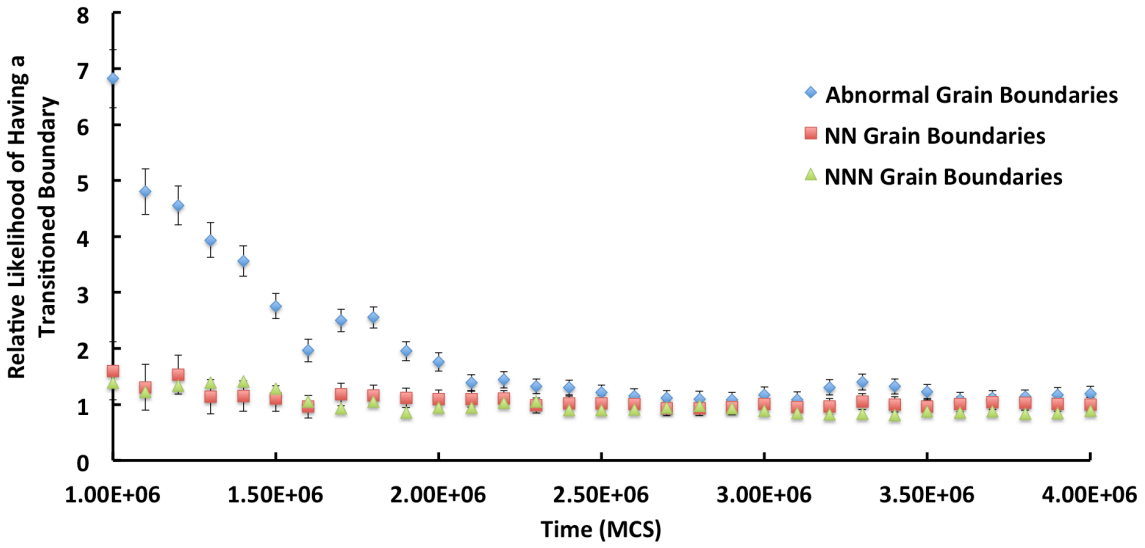

Figure 7.15: The relative likelihood of grain boundaries being transitioned to the high mobility complexion for abnormal grain boundaries, their nearest neighbor grain boundaries, and their next-nearest neighbor grain boundaries over the course of a single simulation, where C = 25 and transitioned grain boundaries had twenty times the normal grain boundary mobility (M_{min} = .05).

It is demonstrably clear the abnormal grains will initially be more likely to have transitioned boundaries, but this is not the case with the nearest and next-nearest neighbor grain boundaries. We see this by examining the probability that the abnormal grain boundaries are transitioned in comparison to the probability that the nearest-neighbor grain boundaries are transitioned. This contradicts our hypothesis that the nearest-neighbor grain boundaries should be more likely than random chance to be in the transitioned state. Fig. 7.16 a-c shows that the increased relative likelihood of an abnormal grain's boundaries being in the transitioned state disappears quickly, especially when the increase in grain boundary mobility is large. Increasing the grain boundary mobility advantage of the transitioned state decreases the amount of grain growth that must occur in order for an abnormal

grain to appear. When the mobility advantage was only a factor a ten, abnormal grains appeared after sixty percent of all grains had been eliminated. Increasing the transitioned grain boundary mobility by a factor of one hundred allowed for AGG to occur after twenty percent of the grains had been eliminated. Increasing the grain boundary transition threshold, C, also increases the fraction of grains that must be eliminated before an abnormal grain appears. We can see that increasing transitioned grain boundary mobility appears to increase the relative likelihood of an abnormal grain's boundaries being transitioned when they first appear, but this effect decays rapidly as more grains disappear. Meanwhile, changing the transition threshold C appears to have little effect. Fig. 7.17 further quantifies this growth advantage early in AGG. One detail we can see is that the time span of AGG in terms of the number of grains eliminated decreases a C increases. For example in Fig. 7.17.c, we see that close to seventy-five percent of the abnormal grains are eliminated over the course of AGG when C is ten, or roughly three percent of the initial average volume. When C is 200 voxels, or roughly two-thirds the initial average volume, ten percent of grains are eliminated over the course of AGG. The plots in Fig. 7.17 exhibit similar trends as those in Fig. 7.16. More importantly, we see that the factor by which abnormal grains are more likely to be transitioned than random boundaries rises comparably to the factor by which abnormal grains are more likely to be transitioned than neighboring boundaries, which confirms the observation that any increase in likelihood of being transitioned nearest neighbor grain boundaries receive from bordering abnormal grains is small.

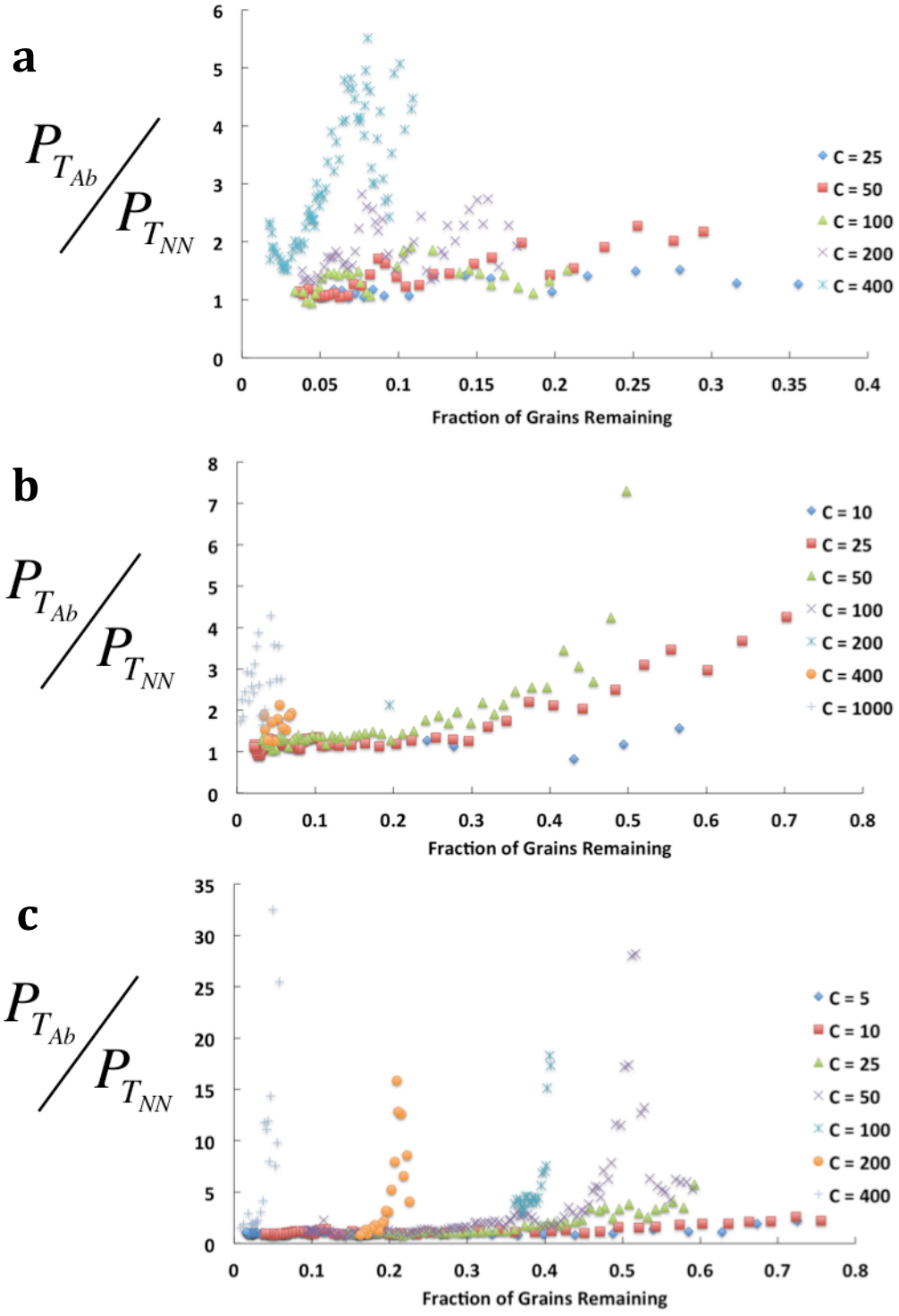

Figure 7.16: The probability that abnormal grain boundaries are in the transitioned state divided by the probability that the nearest neighbor grain boundaries are in the transitioned state, given the transition threshold C and the fraction of grains remaining for a transitioned grain boundary mobility ten times (a), twenty times (b), and one hundred times (c) the normal grain boundary mobility.

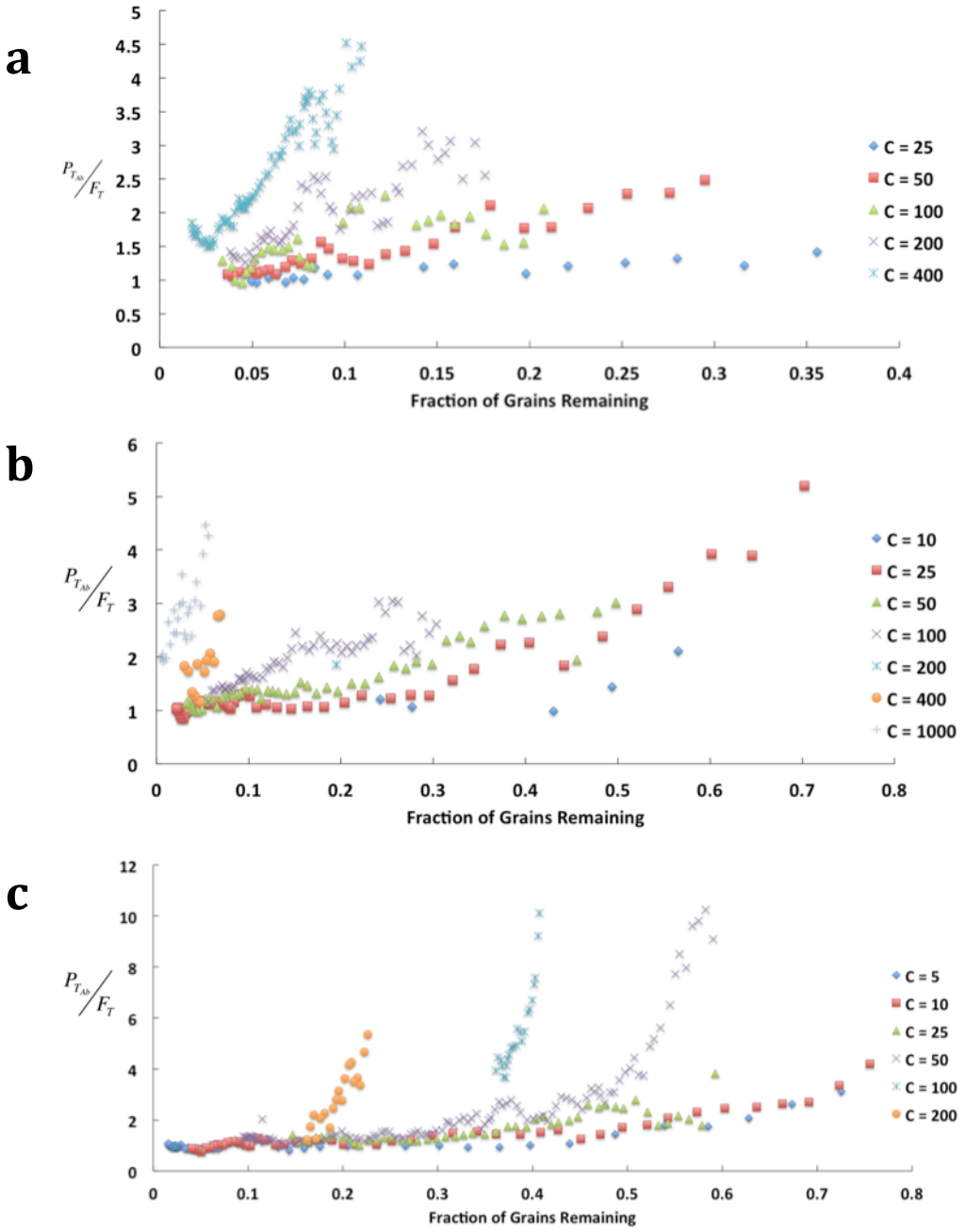

Figure 7.17: The probability that abnormal grain boundaries are in the transitioned state divided by fraction of grain boundaries in the microstructure that are transitioned, given the transition threshold C and the fraction of grains remaining for a transitioned grain boundary mobility ten times (a), twenty times (b), and one hundred times (c) the normal grain boundary mobility.

The difference observed between the relative likelihood of abnormal grain boundaries and nearest neighbor grain boundaries to be transitioned appears to

vary depending on the process used to introduce the complexion transitions. Fig 7.18 shows the same analysis performed on a simulation allowing only adjacency transitions:

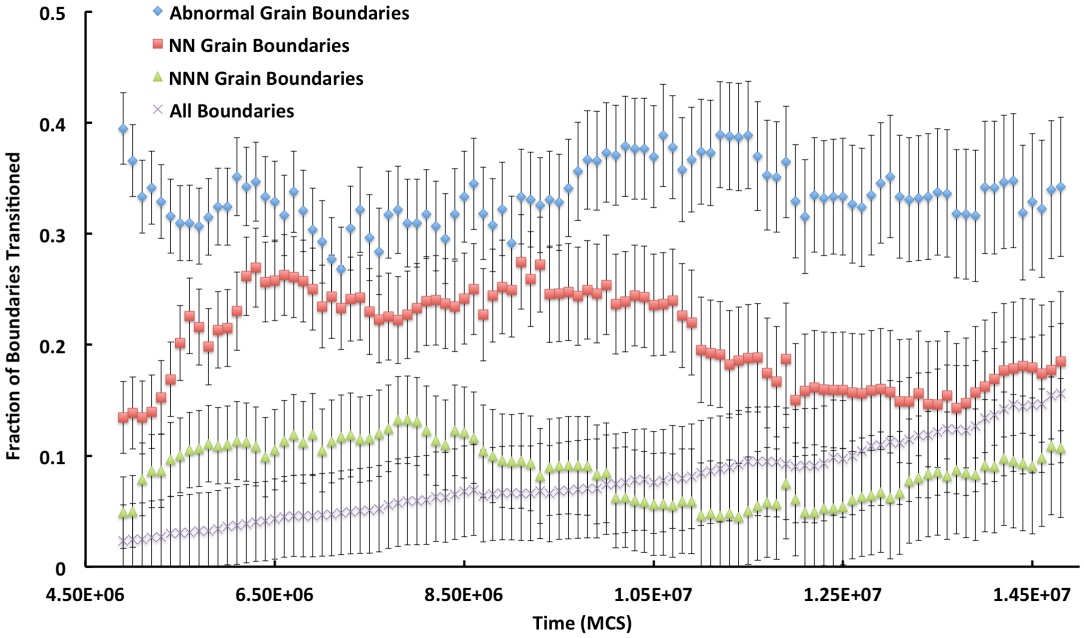

Figure 7.18: The likelihood of grain boundaries being transitioned to the high mobility complexion for abnormal grain boundaries, their nearest neighbor grain boundaries, and their next-nearest neighbor grain boundaries over the course of a single simulation allowing for adjacency transitions at a rate of one per ten thousand MCS, where transitioned grain boundaries had twenty times the normal grain boundary mobility (M_{min} = .05).

Here, both the nearest-neighbor and next-nearest-neighbor grain boundaries are more likely than random chance to be in the transitioned state at the beginning of AGG. Fig. 7.19 shows the relative likelihoods that each class of boundary is transitioned with respect to random chance. The effect still decays as it did in the simulations in which transitioning occurred after grain boundary motion, but the decay is slower than that seen in Fig 7.15. This confirms the hypothesis that nearest-neighbor grain boundaries will be more likely to be transitioned than random

chance when boundaries bordering transitioned boundaries are more likely to nucleate complexion transitions.

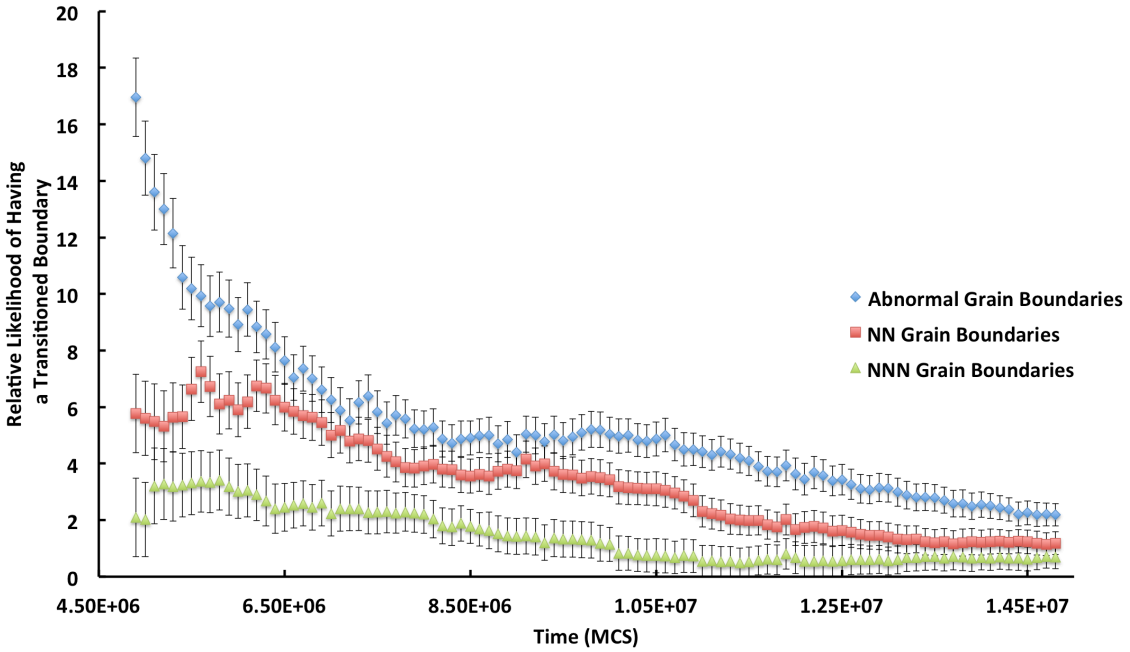

Figure 7.19: The relative likelihood of grain boundaries being transitioned to the high mobility complexion for abnormal grain boundaries, their nearest neighbor grain boundaries, and their next-nearest neighbor grain boundaries over the course of a single simulation allowing for adjacency transitions at a rate of one per ten thousand MCS, where transitioned grain boundaries had twenty times the normal grain boundary mobility (M_{min} = .05).

7.4 Grain Boundary Motion Analysis

The results of the grain boundary motion analysis described in Chapter 6 for a simulated microstructure with an M_{min} = 0.05 and C = 100 can be seen in Fig. 7.20. It is very clear that there is a central tendency, or in this case, a mode in the distribution of calculated grain boundary motion before transitions occur, at around approximately C = 100 voxels. This is consistent with simulation parameters that force transitions to the high mobility complexion when $F(i,j)$ = 100. This means that the grain boundaries that experienced a dramatic increase in grain boundary

motion by at least a factor of twenty did so after an average of roughly 100 voxels of net grain boundary motion. This mode in the distribution does not appear in the same way when the grain boundary transitions are adjacency transitions, as is shown via an analogous histogram in Fig. 7.21, which allowed one adjacency transition every 10,000 MCS and approximately 20 independent transitions over $1.5*10^7$ MCS. The distribution in this case is skewed, indicating that whether or not the grain boundaries transitioned was dependent on factors other than grain boundary motion.

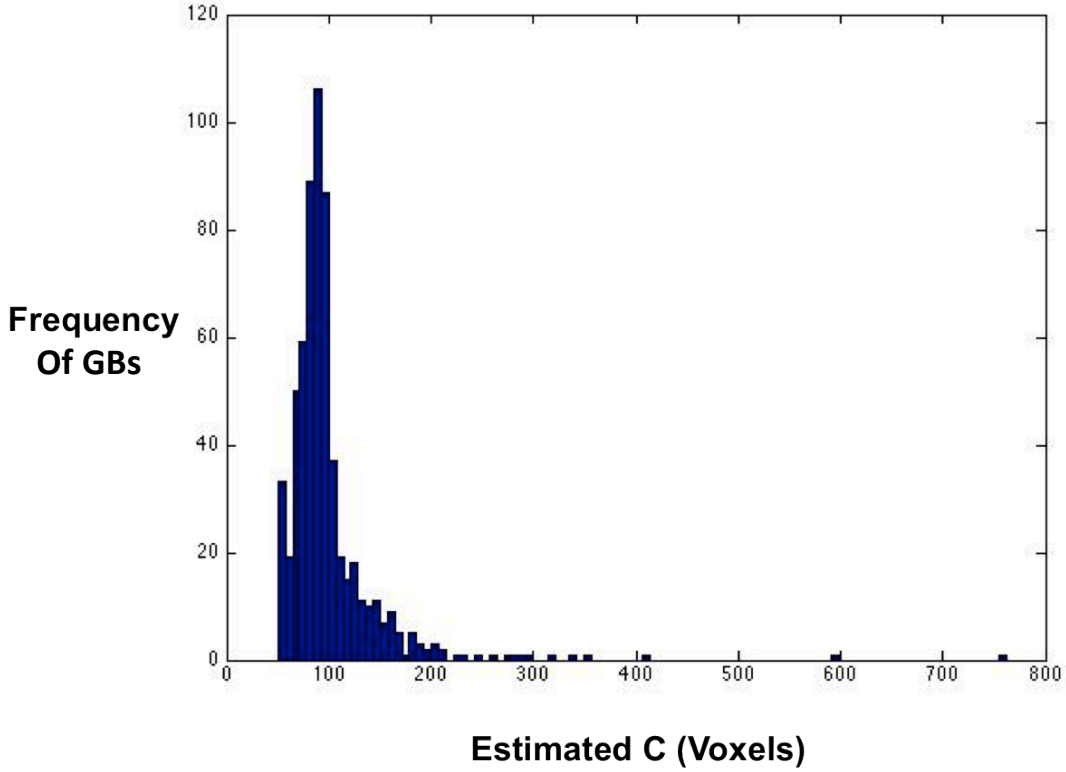

Figure 7.20: A histogram of the estimated volumetric grain boundary motion before complexion transitions occurred in a simulation in which C = 100 and the mobility advantage was $1/M_{min}$ = 20. Events for which "C" were estimated to have been smaller than 50 voxels have been removed to emphasize the central tendency at around 100 voxels.

The physical explanation for the lack of central tendency seen in Fig 7.21 is simple – whether or not a grain boundary transitions in aforementioned simulation is only dependent on its proximity to a transitioned boundary, not its own motion. Therefore, we expect the grain boundaries that experience an abrupt increase in motion by a factor or twenty do so in a manner that doesn't appear closely linked to grain boundary motion.

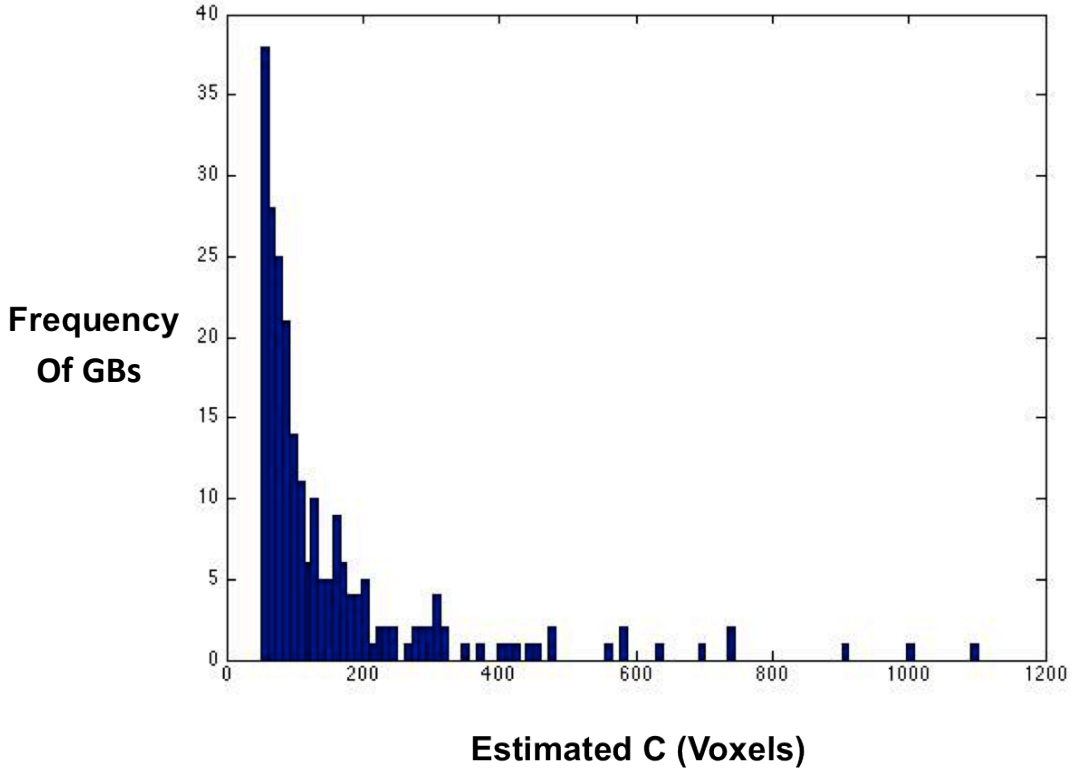

Figure 7.21: A histogram of the estimated volumetric grain boundary motion before complexion transitions occurred in a simulation allowing for twenty independent transitions and one adjacency transition every 10,000 MCS, with a mobility advantage of $1/M_{min}$ = 20. Events for which "C" were estimated to have been smaller than 50 voxels have been removed to emphasize any visible central tendency.

As a result, the volumetric grain boundary motion before transitions when only adjacency transitions are allowed roughly follows the distribution we would expect

for the simple volumetric motion of grain boundaries over their lifetimes. This analysis has useful applications in experiment, which we will discuss in Chapter 12.

References

1. S.J. Dillon, M.P. Harmer, J. Eur. Ceram. Soc. 2008;28:1485.
2. K.A. Newhall, L.L. Pontani, I. Jorjadze, S. Hilgenfeldt, J. Brujic. Size-topology relations in packings of grains, emulsions, foams, and biological cells," Physical Review Letters 2012;108:268001.
3. P.R. Rios, M. E. Glicksman, Topological theory of abnormal grain growth. Acta Mater. 2006;54:5313

Chapter Eight: A Potts Model With Voxel-Based Complexion Growth

8.1 Modifications to Potts Model Calculations

This chapter will described modifications to the Potts Model to simulate grain growth with segments of grain boundary transitioned to the high mobility complexion that grow via a cellular automata. The boundary-based model of grain boundary transitions simplifies the process of nucleation and growth that must be occurring for a transitioning boundary. Therefore, a Potts Model that transitioned grain boundaries on a voxel-by-voxel basis was devised. First, the model tracked whether or not each voxel was on a grain boundary or not through the parameter *a(i)*, as shown in equation 8.1:

$$a(i) = \sum_{j}^{NN_i}(1 - \delta_{ij}) \tag{8.1}$$

A parameter *Cp(i)* to track the transitioned status of each voxel was also assigned, with a default assignment:

$$Cp(i) = \begin{cases} 1, & a(i) > 0 \\ 0, & a(i) = 0 \end{cases} \tag{8.2}$$

A voxel inside of a grain has *Cp(i)* = 0 and a voxel on the boundary has *Cp(i)* = 1. When *Cp(i)* = 2, the that section of grain boundary is said to be in the transitioned state. Thus, no voxels are assigned *Cp(i)* = 2 by default. Next, we will assign a

function that determines the grain boundary mobility and grain boundary energy of each voxel:

$$J_{Pre}(i) = \begin{cases} J_{min}, & Cp(i) = 2 \\ 1.0, & otherwise \end{cases} \quad \textbf{(8.3)}$$

$$M_{Pre}(i) = \begin{cases} 1.0, & Cp(i) = 2 \\ M_{Min}, & otherwise \end{cases} \quad \textbf{(8.4)}$$

These functions determine the values of pre-factors that we will use to determine the grain boundary energy and mobility between grains *i* and *j*:

$$J(i,j) = \begin{cases} \min\left(J(i), J(j)\right), & ID(i) \neq ID(j) \\ 0, & ID(i) = ID(j) \end{cases} \quad \textbf{(8.5)}$$

$$M(i,j) = \begin{cases} \max\left(M(i), M(j)\right), & ID(i) \neq ID(j) \\ 0, & ID(i) = ID(j) \end{cases} \quad \textbf{(8.6)}$$

Note that in this case *i* and *j* are two voxels in the simulation grid, not two grain IDs. The grain IDs are simply determined by *ID(i),* which tracks the grain ID of each voxel in the grid. No other modifications are made to the Potts Model's algorithm to determine voxel reorientations.

8.2 Nucleation and Growth Algorithm

For this model, we will assume that the formation of stable transitioned nuclei are exceedingly rare, to the point that only one may form homogeneously on the surface of several thousand grains. For this purpose, we will establish a function that

determines the fraction of grain boundary area that is transitioned in a given step in the simulation:

$$f_T = \frac{\sum_{i=0}^{N} \begin{cases} 1, Cp(i)=2 \\ 0, otherwise \end{cases}}{\sum_{i=0}^{N} f(x) = \begin{cases} 1, Cp(i)>0 \\ 0, otherwise \end{cases}} \quad \textbf{(8.7)}$$

Then, we will set a condition for the "nucleation" of new transitioned voxels, for which every step the simulation will pick voxels on grain boundaries at random and set *Cp(i)* = 2 until f_T meets the following condition:

$$f_T \geq f_T^* = 0.0001 \quad \textbf{(8.8)}$$

We choose the parameter f_T^* = 0.0001 in order to insure the formation of viable transitioned nuclei, but also limit the number of boundaries transitioning without a propagation mechanism. The boundary-based Potts Model of grain growth has demonstrated that grain boundary transitions occurring independently of each other does not lead to AGG on its own, so we cannot expect to see useful results by increasing f_T^*.

We defined two functions to determine whether or not grain boundary complexions can spread across grain boundaries and triple lines - *Tr(i,j)* and *Pr(i,j,k)*, respectively. Both functions take the grains on the boundary or triple line as input, returning 1 when spreading is possible and returning zero otherwise. In the simulations described, *Tr(i,j)* and *Pr(i,j,k)* for all possible combinations of *i, j,* and *k* were determined at random at the beginning of the simulation.

Two cases were considered for simulation – the first, where few grain boundaries can transition and transitions can spread across triple lines easily ("grain boundary limited), and the second, where all grain boundaries can transition and transitions can only spread across a few triple lines (triple line limited). We can simulate both scenarios in the voxel-based Potts Model using two different conditions:

$$P(\Pr(i,j,k)=1)=P_{Tl}<1, \quad P_{GB}=1 \tag{8.9}$$

$$P(Tr(i,j)=1)=\ P_{Gb}<1, \quad P_{Tl}=1 \tag{8.10}$$

The first condition allows for propagation of grain boundary complexions to all grain boundaries, but only across some triple lines, while the second condition allows grain boundary complexions to spread across all triple lines, but only to some grain boundaries. It is reasonable to expect that the grain growth behavior exhibited in both scenarios will be noticeably different; we can expect very few grain boundaries to be completely "closed" to transitioning in the first case, since this would require each of a grain boundary's triple lines to have $Pr(i,j,k) = 0$. Since each grain boundary on average has five edges, we can estimate that the probability of such an event happening to be roughly $(1-P_{Tl})^5$. Even if only five percent of triple lines allow for propagation, only about seventy-seven percent of grain boundaries will be entirely closed at any given point in time. Further, this status is an ever-evolving one, changing as a grain boundary gains new edges and loses old ones. Grain boundaries in the second case, however are either "open" or "closed," and once all open boundaries have been transitioned, the only new boundaries that can

transition will be the new boundaries that appear as a consequence of growth for which *Tr(i,j) = 1*. It is intuitively obvious that we can expect a much larger fraction of grain boundaries to have transitioned in the condition of this triple junction limited behavior.

The algorithm for "growth" of the grain boundary transitions itself iterates every step in the following way (A schematic illustration of this process can be found in Appendix A):

1. First, we count the number of voxels on grain boundaries ($a(i) > 0$), N_{Act}.
2. For N_{Act} iterations, we select a point on a grain boundary at random and inspect its neighbors. None of the neighboring voxels can transition if:
   - $Cp(i) \neq 2$ (The voxel is not transitioned).
   - There are three different neighbors of IDs i, j, and k such that $Pr(i,j,k) = 0$. This would mean the voxel is on a closed triple line.
   - The grain boundary that the voxel is on of IDs i and j has $Tr(i,j) = 0$. This would mean that the voxel lies on a closed grain boundary.
3. If none of the conditions mentioned in step 2 are met, then set $Cp(j) = 2$ for all neighboring voxels for each $ID_j \neq ID_i$. This rule prevents transitioned voxels from simply "enveloping" a grain.

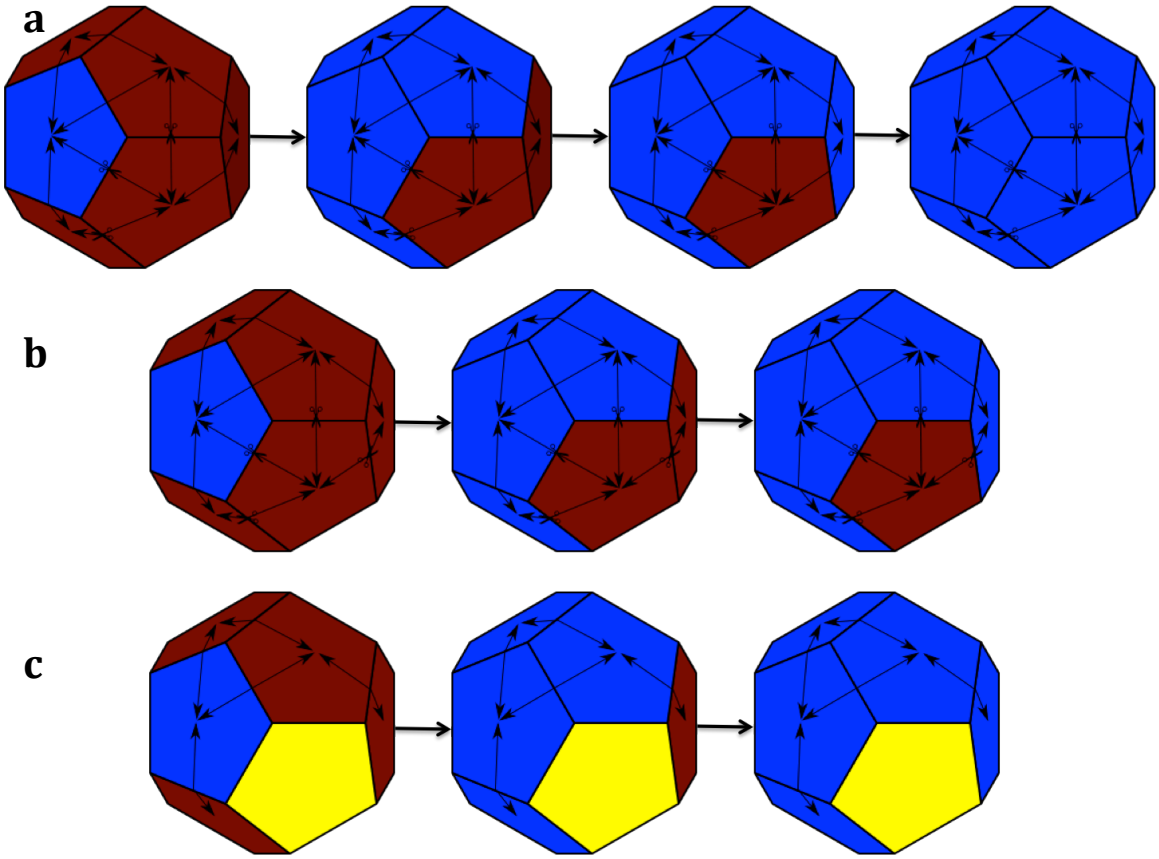

Figure 8.1: A transition spreads across "open" triple lines (a), a transition cannot spread to a grain boundary because there is no open pathway for it to spread (b), and a case where the transition cannot spread to a grain boundary because the grain boundary is not capable of transitioning(c). Here, transitioned boundaries are shown in blue, untransitioned boundaries are shown in red, and grain boundaries incapable of making transitions are shown in yellow.

The choice to make the number of growth step iterations equal to the number of voxels on grain boundaries, N_{Act}, is done to keep the process of complexion growth related to grain boundary area as opposed to the simulation's constant volume. For example, we could set the number of iterations to be the same as the number of voxels in the simulation, but this would mean complexion growth would speed up as the simulation progressed and grain boundaries were eliminated.

There are also two conditions for which a transitioned voxel will "revert" to a not-transitioned state, occurring when:

1. Grain ID reorientations happen such that a transitioned voxel i is no longer on a grain boundary ($a(i) = 0$).
2. Grain ID reorientations happen such that an ID on a transitioned voxel i changes to the grain ID on a not-transitioned voxel j.

This ensures that grain boundaries on which the high mobility complexion is forbidden do not make the transition. A schematic illustration of how this happens can be found in Appendix A:

8.3 Experimental Design

A series of Potts Model simulations were run on a 100x100x100 grid for 10000 MCS each, with $kT = 1.0$ on a microstructure with microstructures of between 2500 grains and 8000 grains. For all simulations, the minimum grain boundary mobility, M_{min} was set as 0.01, with varying transitioned grain boundary energy (J_{min}), fractions of grain boundaries that can transition (P_{Gb}) and fractions of triple lines that can be spread through (P_{Tr}). To minimize effects of the impingement of abnormal grains, collection of simulation data ceased when the abnormal grains stopped growing with respect to the average grain size. Further, verification that a 100x100x100 simulation size is large enough can be found in Appendix B. The

simulation space can be seen in Fig. 8.1**.** In addition to the tracking the simple occurrence of AGG in these simulations, we measured the extent of abnormal grain growth in the two cases by tracking the abnormal volume fractions over time. When AGG occurred, we also determined the fraction of transitioned boundaries on the abnormal grains, the nearest-neighbor grain boundaries, and the next-nearest-neighbor grain boundaries in a manner analogous to the analysis performed in Chapter 7.

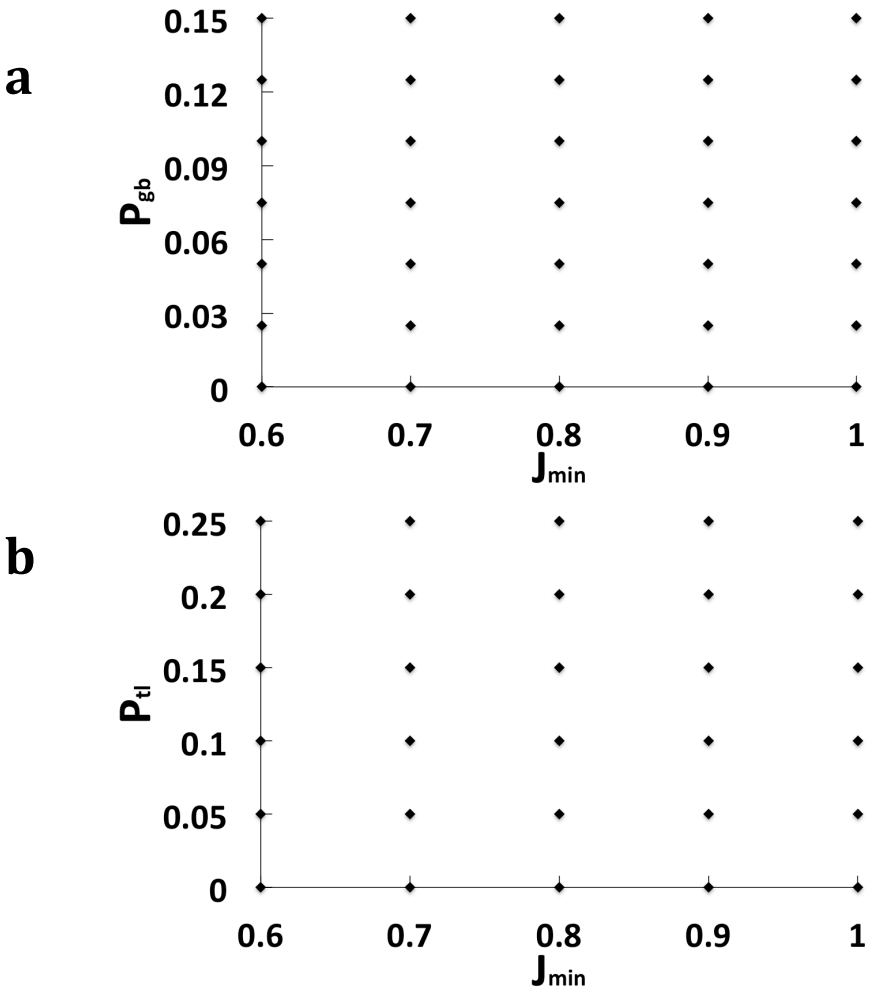

Figure 8.2: Potts Model simulations ran giving transitioned boundaries J_{min} and M = 1.0 with M_{min} = 0.01, limiting either a.) the fraction of grain boundaries that can transition to P_{gb}, or b.) the fraction of triple lines that can be crossed over to P_{tr}

8.4 Results

Results show that AGG occurs in both the triple line-limited and grain boundary-limited cases of grain boundary complexion transitions, as seen in Fig. 8.3. When a sufficiently high mobility is present, the controlling factor of whether or not AGG occurs appears to be either the fraction of triple lines that the transitioned state is allowed to spread over or the fraction of grain boundaries on which the complexion transition is allowed to occur, respectively: The most obvious result of these initial simulations is than in the cases where grain boundary transitions are limited by triple lines have more extensive abnormal grain growth than AGG in cases where grain boundary transitions are limited by the grain boundaries themselves. This can be seen in Fig 8.4, where abnormal grains clearly appear in higher volume fractions in the triple line-controlled case than in the grain boundary-controlled case. We can see in Fig. 8.5 that over the same amount of time, the transitioned boundaries spread more extensively in the grain boundary limited case. A plot of the fraction of transitioned grain boundaries in both cases reveals more complex behavior, as seen in Fig. 8.3. Early in the simulation f_t is larger in the grain boundary limited case than it is for the triple line limited case and after a long period of time the f_t becomes larger in the triple line limited case. In the former case, grain boundaries that can be spread to appear as others are eliminated, while in the latter case existing grain boundaries become open to propagation as triple lines appear and others are eliminated. These simulations show that if AGG occurs due to the propagation of high mobility complexions at the expense of a metastable complexion, then microstructures with large volume fractions of abnormal grains are likely the result

of a propagation that is at least to a significant degree triple junction limited. A microstructure with a smaller volume fraction of abnormal grains would be far more ambiguous case. Still, this apparent upper limit on the volume fraction of abnormal grains in the grain-boundary controlled case may be an effect of the rate of voxel propagation in the Potts Model.

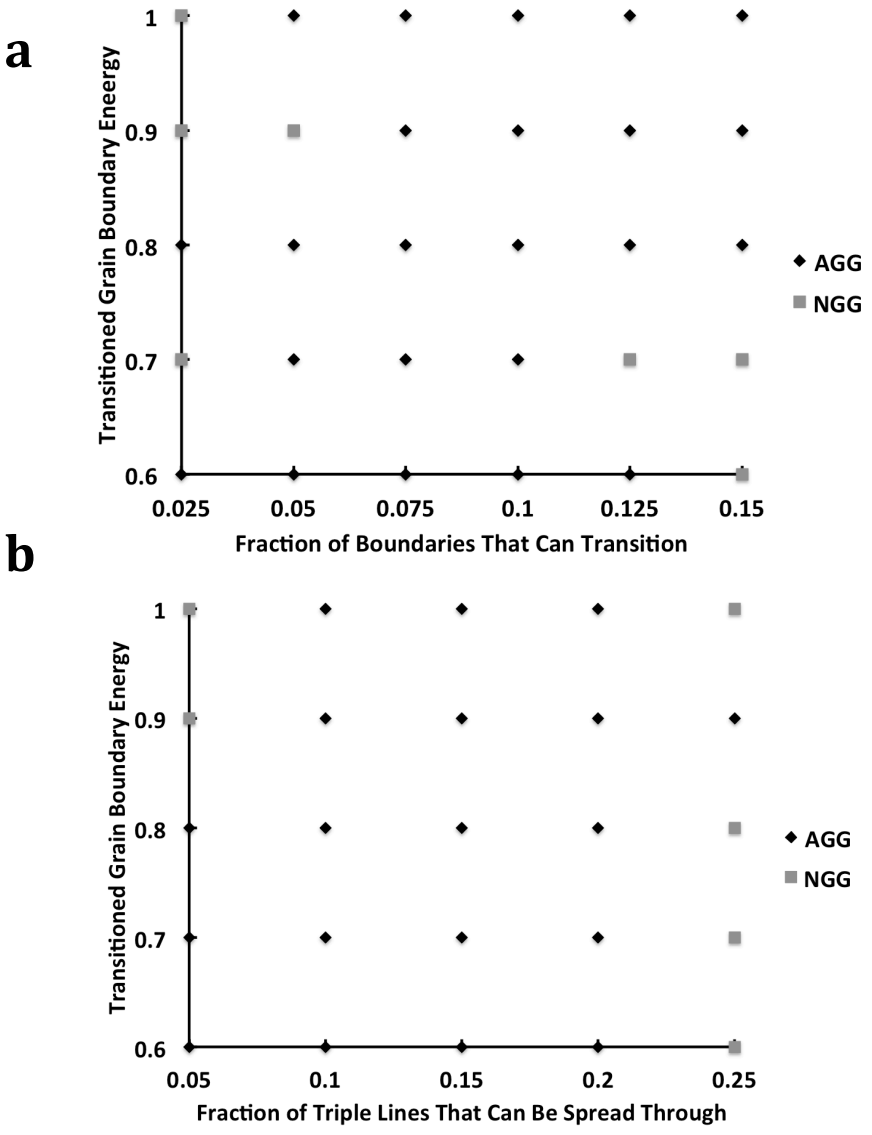

Figure 8.3: The occurrence of AGG in Potts Model simulations ran giving transitioned boundaries J_{min} and M = 1.0 with M_{min} = 0.01, limiting either a.) the fraction of grain boundaries that can transition to P_{gb}, or b.) the fraction of triple lines that can be crossed over to P_{tr}.

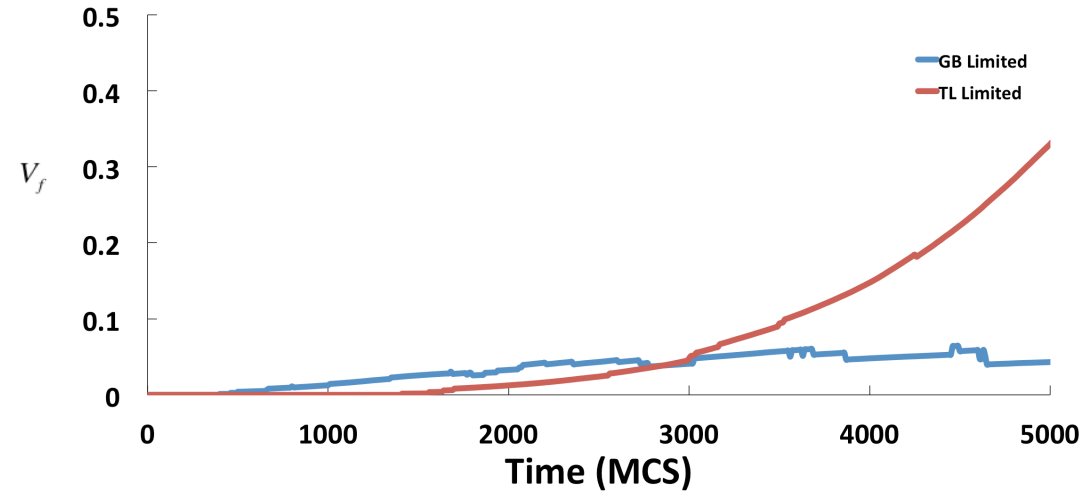

Figure 8.4: The change in the volume fraction of abnormal grains for which $V > 10V_{average}$,. These simulations gave transitioned grain boundaries the same M_{min} = 0.01 and J_{min} = 0.6, using (P_{Gb} = 0.075 and P_{Tr} = 1.0) and (P_{Gb} = 1.0 and P_{Tr} = 0.10), respectively. These simulation parameters were chosen for comparison because they yielded the highest abnormal grain volume fractions from the two respective simulation spaces. The results shown present the averages of three separate simulations performed on the same microstructure.

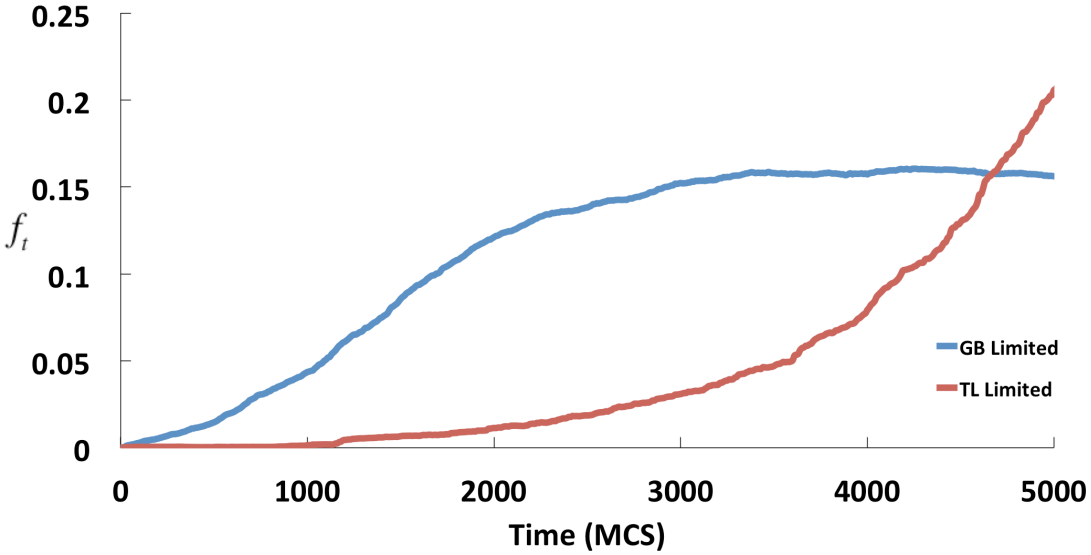

Figure 8.5: The change in the fraction of transitioned boundaries in the microstructure, f_t , over time for both of the cases.

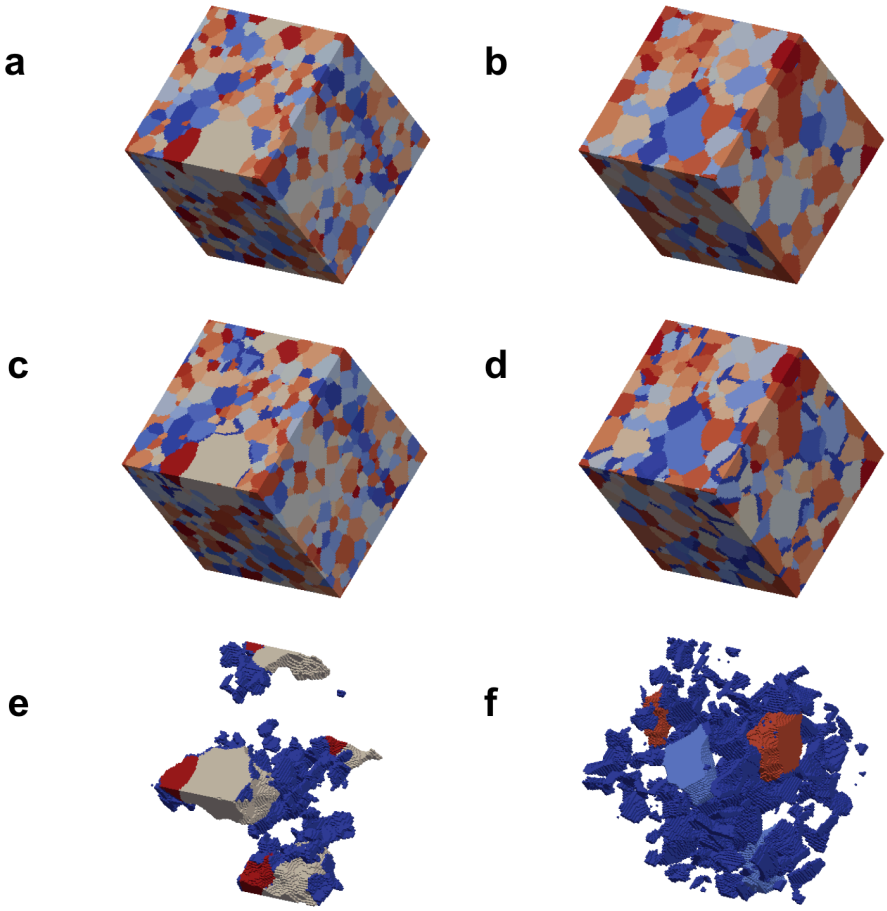

Figure 8.6: Microstructures in both the triple-line and grain boundary-limited cases of the voxel based models. Here, we can see both simulations after 3000MCS, with a) the microstructure in the triple-line controlled limited case, b) the microstructure in the grain boundary limited case, c & d) the microstructure with transitioned boundaries highlighted in blue in both cases, and e & f) cutaways of the abnormal grains and transitioned boundaries for both cases. These simulations gave transitioned grain boundaries the same M_{min} = 0.01 and J_{min} = 0.6, using (P_{Gb} = 0.075 and P_{Tr} = 1.0) and (P_{Gb} = 1.0 and P_{Tr} = 0.10), respectively. These simulation parameters were chosen for comparison because they yielded the highest abnormal grain volume fractions from the two respective simulation spaces.

The distance of each grain boundary from the nearest abnormal grain was calculated periodically during each simulation using an algorithm similar to the one used in Chapter 7. From this data, the fraction of transitioned boundaries on the abnormal grain boundaries, the nearest-neighbor grain boundaries, and the next-nearest neighbor grain boundaries to the abnormal grains was calculated. A plot of

the fraction of each of these classes of transitioned boundaries for both the grain boundary limited and triple line limited cases can be seen below in Fig 8.7:

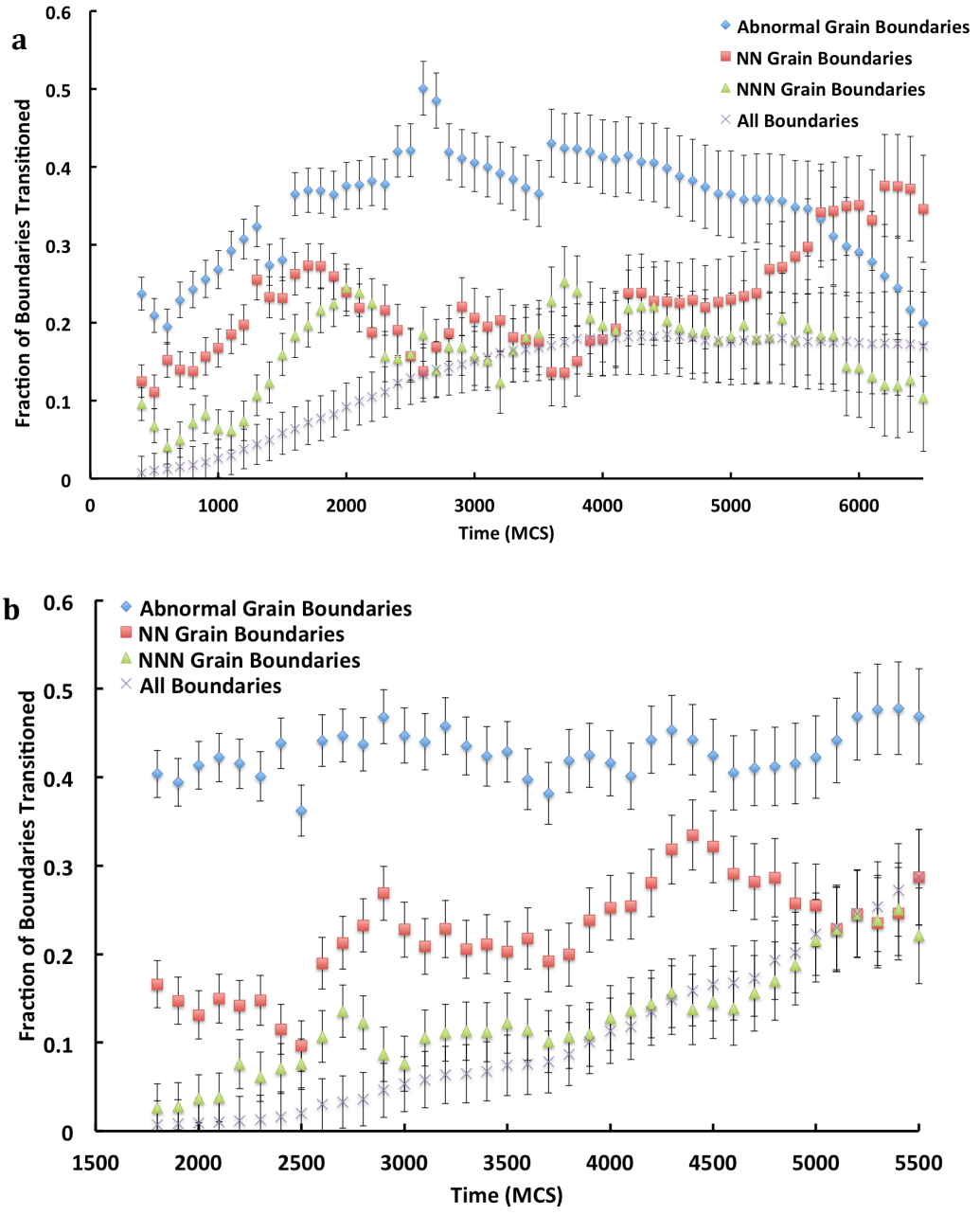

Figure 8.7: The fraction of transitioned boundaries on abnormal grain boundaries, nearest-neighbor grain boundaries, and next-nearest-neighbor grain boundaries in the grain boundary-limited case (P_{gb} = 0.075, P_{tl} = 1.0) (a) and the triple line-limited case (P_{gb} = 1.0, P_{tl} = 0.10) (b), giving transitioned voxels a 100x mobility advantage (M_{min} = 0.01) with J_{min} = 0.60.

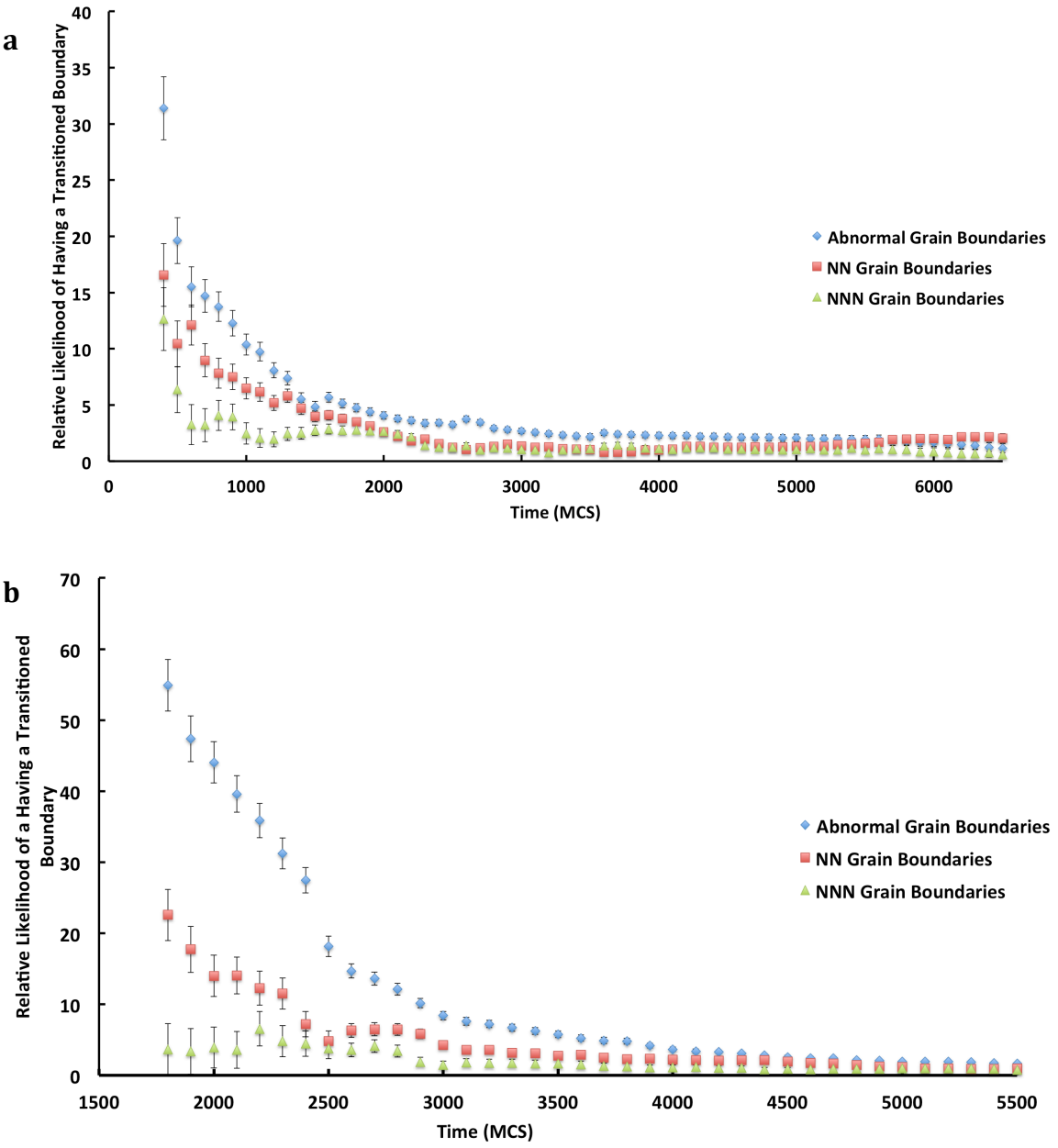

Figure 8.8: The relative likelihoods of abnormal grain boundaries, nearest-neighbor grain boundaries, and next-nearest-neighbor grain boundaries to be in the transitioned state in the grain boundary-limited case (P_{gb} = 0.075, P_{tl} = 1.0) (a) and the triple line-limited case (P_{gb} = 1.0, P_{tl} = 0.10) (b), giving transitioned voxels a 100x mobility advantage (M_{min} = 0.01) with J_{min} = 0.60.

These results appear to show the abnormal grains with higher fractions of their boundaries transitioned throughout the simulations, with the nearest and next-nearest-neighbor grain boundaries having relatively high fractions of transitioned

boundaries early in AGG, but becoming close to the average fraction of transitioned boundaries later in the simulation.

Fig 8.8 shows the relative likelihoods that the grain boundaries from the simulations in Fig 8.7 will be transitioned with respect to the fraction of boundaries in the simulation that are transitioned. It is clear from these plots that, much like cases in Chapter 7 in which the adjacency transition was used, the nearest and next-nearest neighbor grain boundaries to the abnormal grains are far more likely than random chance to be in the transitioned state at the beginning of the simulation, a difference that diminishes as the simulation continues and more grain boundaries are allowed to transition. Chapter 9 will discuss the implications of this simulation work on the inference of grain boundary transition processes in actual materials.

Chapter Nine: Discussion

The simulations in this work indicate several overarching trends in relation to grain boundary complexion transitions and abnormal grain growth. First and most simply, the occurrence of grain boundary complexion transitions must be biased in some way in order for abnormal grains to grow. The simulations described in Fig. 7.4 demonstrated this - the grain boundary complexion transitions were allowed to occur independently of each other, and no abnormal grains appeared[1].

We can eliminate several sources of possible bias. Experimental evidence indicates that the highest energy grain boundaries will be most likely to transition[2], and it is conceivable that favorably oriented grains in a textured microstructure may have boundaries far more likely to nucleate complexion transitions, causing them to grow abnormally in a manner analogous to abnormal subgrain growth. However, materials without strong texture have had AGG attributed to changes in grain boundary complexion[3]. Inhomogeneity in the distribution of solute would cause abnormal grains to form clusters, with surrounding areas experiencing noticeably more stagnant growth. While there may be other, more exotic sources of bias that cause grains to accumulate the transitioned boundaries required to grow abnormally, it is not intuitively obvious what would cause such biases. For example, is possible that somehow grain boundary complexion transitions make neighboring boundaries *less* likely to make transitions, but it is not clear how such a bias would arise, let alone how it would result in AGG.

We were therefore left with two plausible sources of bias to discriminate between with simulation – either a boundary's *adjacency* to a transitioned grain boundary increases its probability of transitioning, or a grain boundary's *motion* increases its probability of transitioning.

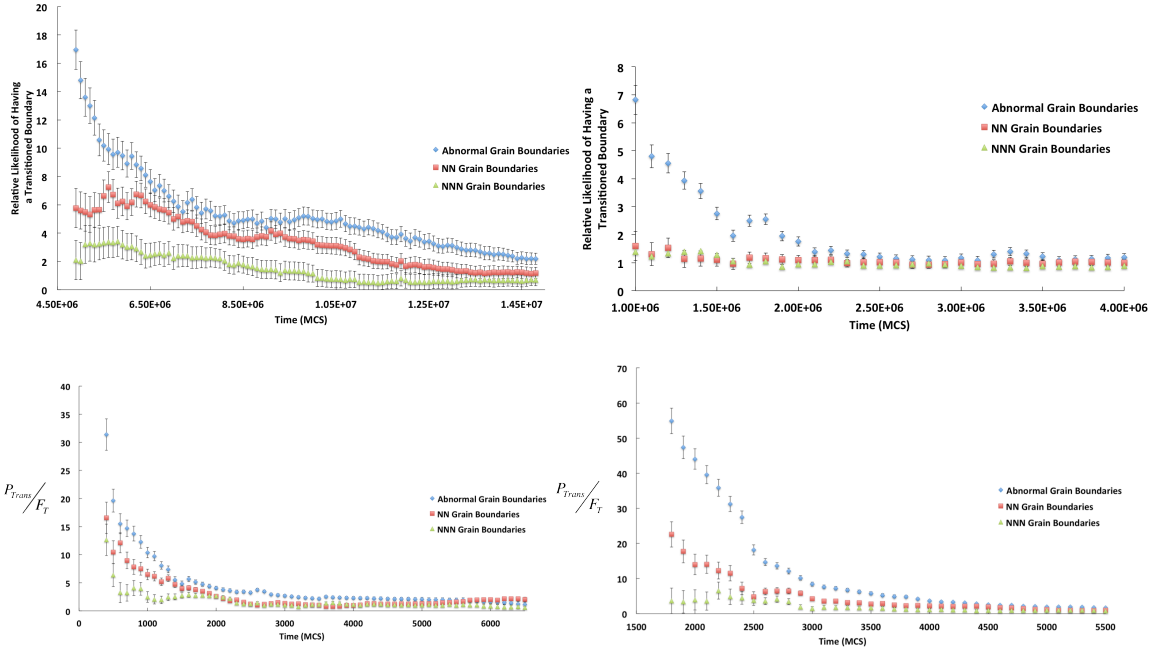

Figure 9.1: Plots of the relative likelihood of likelihoods of abnormal grain boundaries, nearest-neighbor grain boundaries, and next-nearest-neighbor grain boundaries to be in the transitioned state in the case where adjacency transitions were allowed (Fig. 7.19) (a), the case where grain boundary motion-induced transitions were allowed (Fig. 7.15) (b), the grain boundary-limited case (c), and the triple line-limited case (d).

Simulation of grain growth by introducing these biases reveals the second major trend – when grain boundary complexion transitions are dependent on adjacency to transitioned boundaries, the abnormal grains that form have nearest-neighbor grain boundaries that are significantly more likely than random chance to be transitioned as well. When grain boundary complexion transitions depend on grain boundary motion, this increased probability of nearest-neighbor grain boundaries being in the

transitioned state all but disappears. Fig 9.1 shows that this trend is consistent with simulation results:

Three separate different simulation methods in which adjacent grain boundaries were biased to be more likely to transition all resulted in abnormal growth in which the nearest-neighbor grain boundaries were several times more likely to have transitioned than random chance. The simulations in which grain boundaries were biased to transition after a threshold amount of grain boundary motion produced abnormal grains with nearest neighbor grain boundaries only about as likely as random chance to be in the transitioned state. If we accept that transitioned grain boundaries have systematically lower energies, then it should be possible to determine which of these two biases exists from an analysis of relative grain boundary energies. As previously mentioned in earlier chapters Bojarski performed these measurements in Ca-doped Yttria[3] and found that the abnormal grain boundaries had similar relative grain boundary energies in comparison to their nearest-neighbor grain boundaries, but considerably lower in comparison to the grain boundaries far away. Fig. 9.2 shows the predicted distributions of grain boundary energies that different causes of AGG should yield from the same analysis.

Bojarski's experiments showed very little difference between the relative grain boundary energies of the abnormal grains' boundaries and the nearest-neighbor grain boundaries, differences were observed by Dillon in Si-doped alumina[4]. In conjunction with our simulations, this experimental evidence gives credence to the

notion that at least in some situations, grain boundaries become more likely to change complexion when their neighbors have already transitioned.

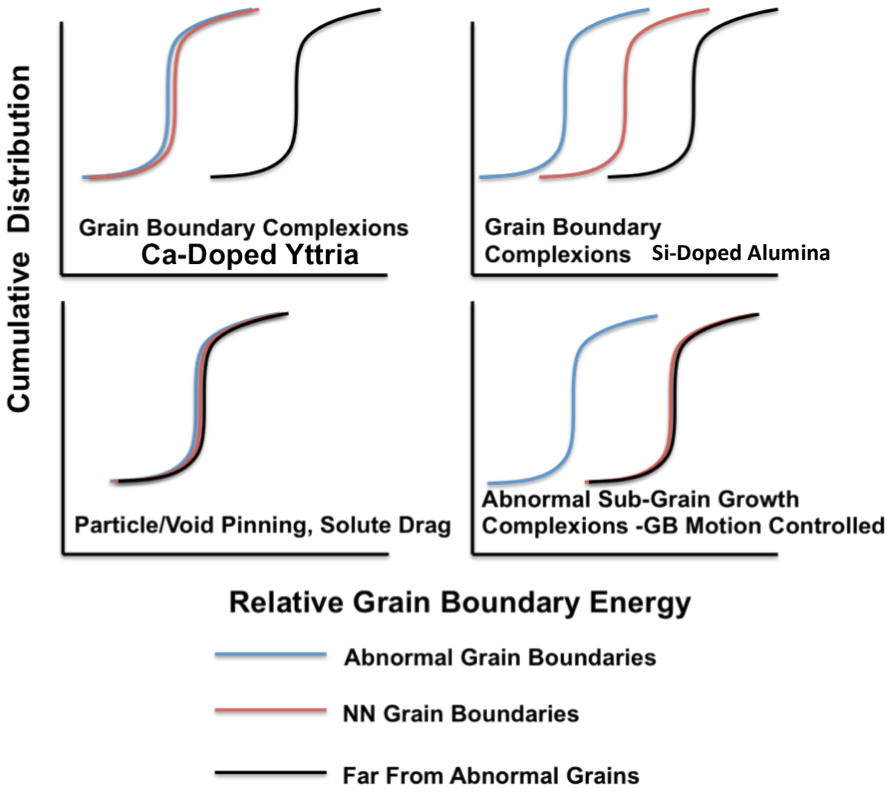

Figure 9.2: Expected cumulative relative grain boundary energy distributions for the abnormal grains boundaries, the nearest-neighbor grain boundaries, and the grain boundaries far from the abnormal grains, given the physical cause for AGG. We can see that the grain boundary energy measurements made by Bojarski in Ca-doped Yttria[3] are consistent with our simulation predictions for the occurrence of complexion transitions, most likely adjacency transitions.

While the grain growth simulations that have been performed say nothing about the intricate developments at the atomic level that result in this behavior, we can still speculate somewhat as to what occurs. For example, it was previously suggested in Chapter 7 that when a grain boundary transitions, it sometimes a preferential site

for its neighbors to transition when it grows into a grain boundary triple line. A schematic of this process is shown in Fig. 9.3.

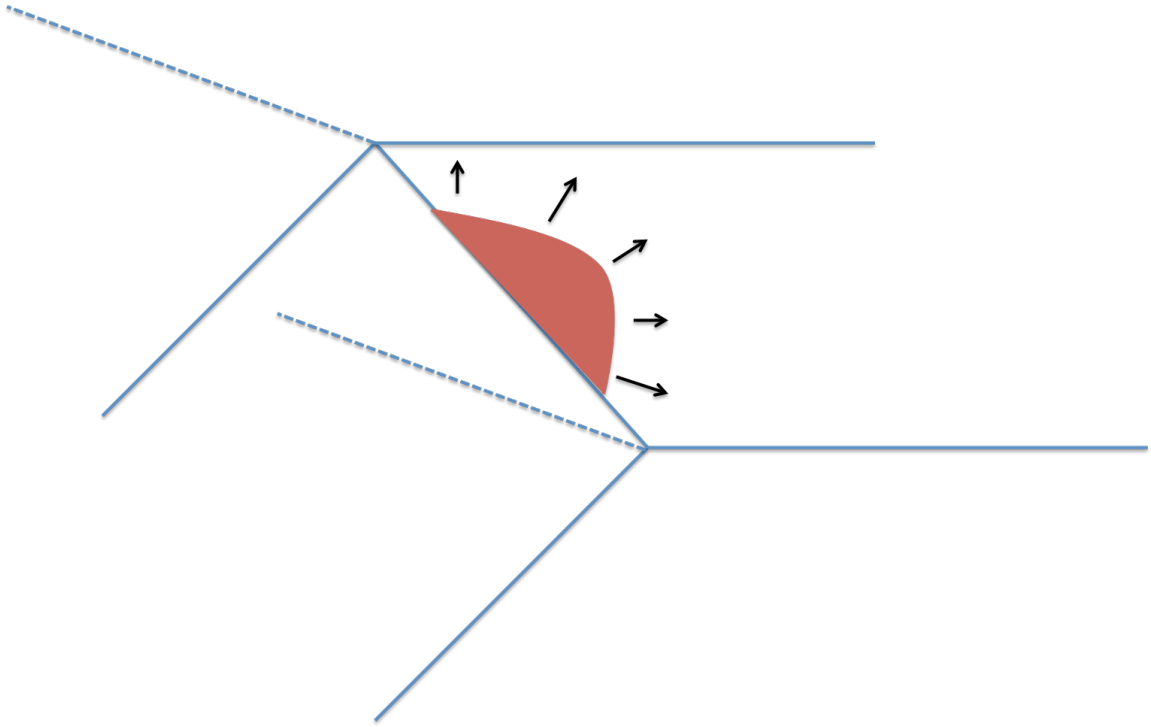

Figure 9.3: A schematic representation of a grain boundary complexion transition "nucleating" off of a grain boundary triple line.

We can roughly calculate the activation energy and critical radius of such a nucleation event happening using classical nucleation theory. This is done by simply performing analogous operations to those used to calculate the activation barrier for the nucleation of a spherical particle. In its place, the spherical particle becomes circular, the volumetric free energy becomes the calculated decrease in grain boundary per area of the complexion, and the interfacial energies become the energy associated with the complexion's edge and the energy associated with the triple line and triple line-complexion interface. The mathematical operations used for these calculations are given in Appendix D. Fig. 9.4 shows the range of critical

nucleus sizes as they depend on the complexion edge energy and the reduction in energy associated with creating a triple line-complexion interface:

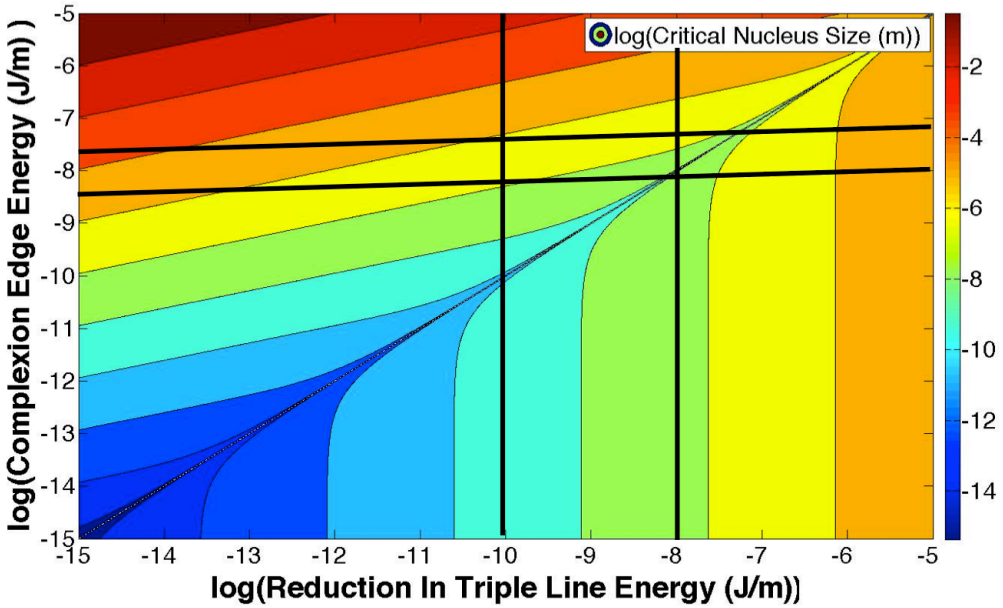

Figure 9.4: A contour plot of the predicted critical nucleus size of a grain boundary complexion transition on a grain boundary triple line, assuming that the complexion transition reduces grain boundary energy by 0.10 J/m^2. Black lines bound the region predicted by our estimations of complexion edge energy and reduction in triple line energy.

It has been previously shown[5] that grain boundary energies in alumina tend to range between 0.05 and 1.0 J/m^2, making the estimation of a reduction in grain boundary energy due to a complexion transition reasonable. The energies of grain boundary triple lines have been estimated in the past[6,7,8] to range between 10^{-7} and 10^{-10} J/m. However, there is no work, simulation or experimental, that estimates the edge energy of a transitioned section of grain boundary. If we assume that this energy is approximately the same energy as the edge length energy of a dislocation in alumina (~10^{-8} J/m), then this suggests critical a critical nuclei for transitioning

on the order of tens to hundreds of nanometers in radius. Fig. 9.5 shows the predicted activation energies for these transitions to form:

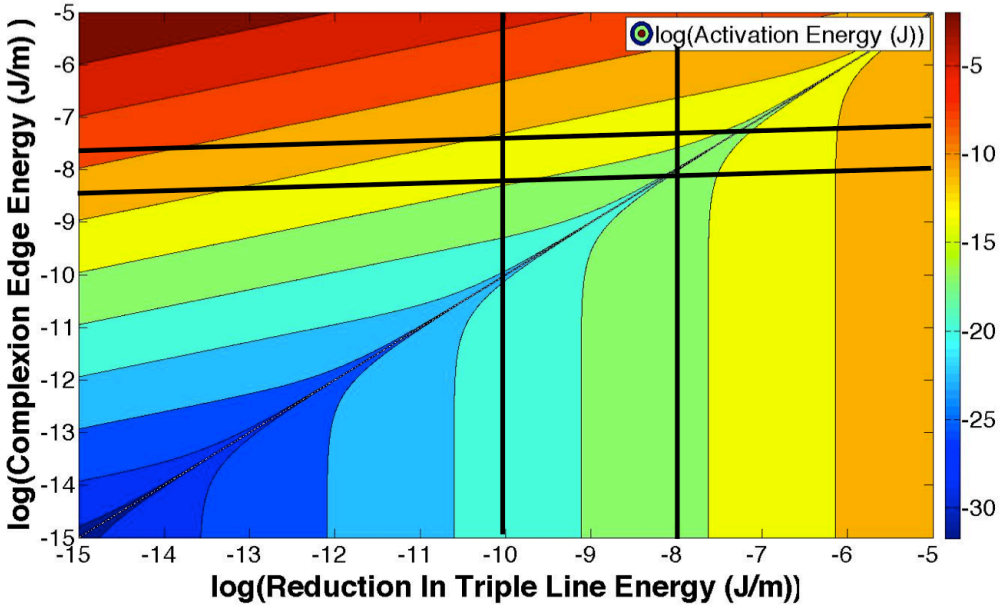

Figure 9.5: A contour plot of the predicted activation energy to form a grain boundary complexion transition on a grain boundary triple line, assuming that the complexion transition reduces grain boundary energy by 0.10 J/m^2. Black lines bound the region predicted by our estimations of complexion edge energy and reduction in triple line energy.

Optimistically, this suggests that the activation energy for the formation of a complexion transition is on the order of 10^{-17}-10^{-15} J, or approximately 100-10,000 eV. Such a high activation barrier would explain why only the highest energy grain boundaries would make the transition, and also explain why grain boundaries that change complexion do not seem to "revert". Dillon similarly discussed that this may be a reason for the tenacity of the transitioned state[2].

It is possible to estimate an approximate order of magnitude for the activation barrier using Dillon's estimate of the activation barrier for complexion transitions from analysis of abnormal grain number densities in Ca-doped alumina and Si-doped alumina. Since our simulations have produced an estimate of the minimum fraction of transitioned boundaries, F_T that are required to produce an abnormal grain (0.01%-1% of all boundaries), we can calculate the activation barrier:

$$\Delta G^*_{Trans} \sim \frac{\Delta G^*_{Ab}}{(\#GBs/Grain)*(\#Grains/mol)} * F_T * \frac{\#Atoms/Nuclei}{\#Atoms/GB} \qquad \textbf{(9.1)}$$

Dillon observed abnormal grains in microstructures with average grain sizes ranging between five and ten microns[2]. Assuming an activation energy on the order of 100 kJ/mol (From Dillon's calculation), a bond length of 1 angstrom and 6.75 grain boundaries per grain (13.5 on average dividing for double counting), we calculate an activation barrier of roughly 10^{-16} J/nuclei, where each nucleus is roughly 1 nm in radius. The estimated activation barrier should increase proportionally to the square of the radius of the stable nuclei, so a stable nucleus of 10nm requires activation energy of roughly 10^{-14} J. These calculations appear to be roughly on the same order of magnitude as our estimations using classical nucleation theory. Still, this estimation of activation energy appears to be too high for these transitions to occur over the course of a sintering treatment. We can calculate that 100kT is roughly 10^{-18} J at 1500 °C, which suggests that even making very generous assumptions, the complexion transitions should not occur. The most likely source of error in these calculation is likely the complexion edge energy, we

can calculate for nucleation without the assistance of a triple line must be several orders of magnitude lower to support a complexion transition.

These nucleation calculations show that grain boundary triple lines could lower the activation energy barrier required for complexion transitions to occur. This indicates, not surprisingly, that grain boundaries will be more likely to nucleate transitions on triple lines than not. However, in order for one transitioned grain boundary to create a "preferential site" for another transition to occur, this would mean that the triple line energy would have to decrease *twice*, once when the first transition nucleated, and second when the adjacent grain boundary transition nucleates. While it may be possible for such behavior to be possible atomistically, the process by which this would happen is not entirely clear. In contrast, it seems boundary motion-induced transitions would happen simply by sweeping up solute until, which should make the transitioned state increasingly favorable for transformation.

The notion of grain boundaries transitioning to a high velocity regime is not an entirely alien phenomenon: particle/pore pinning[9] and solute drag effects[10] are often credited for AGG in which this occurs and such grain growth behavior has been simulated in the past[11,12]. In these cases, grain boundaries must first move enough to either break away from the obstacles preventing motion, though in these cases the amount of motion is not necessarily consistent. Experiments that may be

able to discriminate between these types of AGG will be discussed in further detail in Chapter Twelve.

References

1. W. E. Frazier, G.S. Rohrer, A.D. Rollett, Abnormal Grain Growth in the Potts Model Incorporating Grain Boundary Complexion Transitions that Increase the Mobility of Individual Boundaries. Acta Mater. 2015;96:390.
2. S.J. Dillon, M.P. Harmer. Demystifying the Role of Sintering Additives with "Complexion". J. Euro. Ceram. Soc. 2008;28:1485.
3. S.A. Bojarski, S. Ma, W. Lenthe, M.P. Harmer, G.S. Rohrer. Changes in the Grain Boundary Character and Energy Distributions Resulting from a Complexion Transition in Ca-Doped Yttria. Met. and Mater. Trans. A. 2012;43:3532.
4. Dillon SJ, Harmer MP, Rohrer GS. J Am Ceram Soc 2010;93:1796.
5. T. Watanabe, H. Yoshida, Y. Ikuhara, T. Sakuma, H. Muto, M. Sakai. Grain Boundary Sliding and Atomic Structures in Alumina Bicrystals with [0001] Symmetric Tilt Boundaries. Mater. Trans. 2002;43:1561.
6. S. Sivaramakrishnan, J. Wen, M.E. Scarpelli, B.J. Pierce, J-M. Zuo. Equilibrium Shapes and Triple Line Energy of Epitaxial Gold Nanocrystals Supported on TiO_2 (110).
7. B. Zhao, J. Ch. Verhasselt, L.S. Shvindlerman, G. Gottstein. Measurement of Grain Boundary Triple Line Energy in Copper. Acta. Mater. 2010;58:5646.
8. P. Fortier, G. Palumbo, G.D. Bruce, W.A. Miller, K.T. Aust. Triple Line Energy Determination by Scanning Tunneling Microscopy.1991;25:177.
9. S-M. Na, K.M. Atwater, A.B. Flatau. Particle Pinning Force Thresholds for Promoting Abnormal Grain Growth in Magnetostrictive Fe-Ga Alloy Sheets. Scripta Mater. 2015;15:1.
10. Z. Chen, Q. Chen, F. Liu, X.Q. Yang, Y. Fan, C.H. Zhang, A.M. Liu. The Influence of Solid State Growth Mechanism on the Microstructure Evolution in Undercooled Ni – 10 at.%Fe Alloy. J. of Alloys and Compounds. 2015;622:1086.
11. C.S. Park, T.W. Na, H.K. Park, B.J. Lee, C.H. Han, N.M. Hwang. Three-dimensional Monte Carlo simulation for the effect of precipitates and sub-boundaries on abnormal grain growth. Scripta Mater. 2012;66:398.
12. S.G.Kim, Y.B. Park. Grain boundary segregation, solute drag, and abnormal grain growth. Acta. Mat. 2008;56:3739.

Chapter Ten: Hypotheses Revisited

The simulations performed in this work have allowed us to quantitatively accept or reject several hypotheses:

1. We hypothesized that abnormal grain boundaries would be more likely than random chance to be in the transitioned state for cases in which grain boundaries adjacent to transitioned boundaries were biased to be more likely to transition in the Potts Model. Analysis of the fraction of transitioned boundaries on abnormal grains in Chapters 7 and 8 shows this to consistently be true for several different variations of the bias. Abnormal grain boundaries were often more likely to be in the transitioned state than random chance by greater than a factor of ten. **We therefore ACCEPT this hypothesis.**
2. We hypothesized that abnormal grain boundaries would be more likely than random chance to be in the transitioned state when grain boundaries were allowed to transition after a preset amount of grain boundary motion in the Potts Model. Analysis of the fraction of transitioned boundaries on abnormal grains in Chapter 7 shows this to be true. **We therefore ACCEPT this hypothesis.**
3. We hypothesized that grain boundaries that are nearest-neighbors to abnormal grains would be more likely than random chance to be in the transitioned state for cases in which adjacency to transitioned grain boundaries increases the probability of a complexion transition in the Potts

Model. Analysis of the fraction of transitioned boundaries on this class of grain boundaries shows this to be consistently true for several different variations of the bias. The nearest-neighbor grain boundaries to the abnormal grains were often more likely to be in the transitioned state than random chance by greater than a factor of ten. **We therefore ACCEPT this hypothesis.**

4. We hypothesized that when grain boundaries were allowed to transition after a preset amount of grain boundary motion in the Potts Model, abnormal grains, defined as grains ten times the average grain volume, would appear at most at a frequency of one in ten thousand grains. The simulations discussed in Chapter 7 show abnormal grains appearing under these conditions with a frequency of close to one in one thousand. **We therefore REJECT this hypothesis.**
5. Finally, we hypothesized that when grain boundaries were allowed to transition after a preset amount of grain boundary motion in the Potts Model, the grain boundaries that are nearest-neighbors to abnormal grains would be more likely than random chance to be in the transitioned state. Analysis of the fraction of transitioned grain boundaries on for this grain boundary class shows that the nearest-neighbor grain boundaries are approximately just as likely to be in the transitioned state as random chance. **We therefore REJECT this hypothesis.**

Based on these experimental results, we can draw a series of conclusions and make several recommendations for future work, which we will discuss in Chapters 11 & 12.

Chapter Eleven: Conclusions

1. In addition to providing increased grain boundary mobility and reduced grain boundary energy, the occurrence of grain boundary complexion transitions in a microstructure must be systematically biased in order for some grains to grow abnormally. Potts Model simulations of grain growth have demonstrated this.
2. Potts Model simulations have shown that when the probability of making a complexion transition increases with the transitioned state of a neighbor, AGG can occur with less than one percent of grain boundaries transitioned.
3. Potts Model simulations have shown AGG can occur when the probability of making a complexion transition is dependent on how much a grain boundary moves.
4. Analysis of the fractions of transitioned boundaries on the abnormal grains' boundaries, nearest-neighbor grain boundaries, and next-nearest-neighbor grain boundaries in simulation shows that when grain boundary transitions are biased by adjacency to transitioned boundaries, the probability of the nearest-neighbor grain boundaries being in the transitioned state increases relative to the fraction of boundaries in the microstructure that are transitioned.
5. Analysis of the fractions of transitioned boundaries on the abnormal grains' boundaries, nearest-neighbor grain boundaries, and next-nearest-neighbor grain boundaries in simulation shows that when grain boundary transitions are biased by motion made by the grain boundary, the probability of the

nearest-neighbor grain boundaries being in the transitioned state is approximately the same as the fraction of boundaries in the microstructure that are transitioned.

6. Potts Model simulations indicate that tracking volumetric motion of grain boundaries can plausibly allow for discrimination between different grain boundary complexion transition mechanisms.

Chapter Twelve: Recommendations

12.1 Simulation

This chapter outlines a number of recommendations that we make based on the previously discussed simulations and their results.

We recommend further exploration of the simulation work performed here via the Potts Model. First, further simulation work in repeated trials will allow for better quantification of the probability of AGG given the number of allowed N_1 and N_0 transitions in a microstructure. This would allow contour plots of the likelihood of AGG, or perhaps the number fraction of abnormal grains in a microstructure, given the allowed number of transitioned boundaries in a microstructure.

Second, repeated trials of these simulations, perhaps on larger microstructure, would allow for a more detailed analysis of abnormal grain clustering and its relationship to the bias in the formation of complexion transitions. It is likely, for example, that abnormal grains resulting from complexion transitions that occur after grain boundary motion are roughly equally spaced, while abnormal grains resulting from adjacency transitions are not. Analysis of repeated trails of these simulations will demonstrate this difference if it exists.

We recommend investigating whether or not the adjacency bias observed in AGG is explained by solute diffusion. It is possible that excess solute returned to the lattice

as transitioned grain boundaries shrink gets redistributed to adjacent grain boundaries, making them more likely to make transitions. Simulation methods that incorporate diffusion behavior will be the most useful to investigate the physical nature and plausibility of the so-called "adjacency" transition. The Potts Model does this only in the basic sense that grain growth involves the diffusion of atoms across grain boundaries.

Therefore, we recommend implementing a phase-field model of grain growth to show that after a grain boundary reaches a threshold of excess solute and transitions to high-mobility complexion, solute tends to diffuse to the nearby grain boundaries and induce them to transition as well. With a large enough simulation, this should reproduce the AGG observed in this work and show similar relative likelihoods of neighboring grain boundaries being transitioned.

Two scenarios must be considered: that excess solute returned to the lattice as transitioned grain boundaries shrink is redistributed to adjacent grain boundaries, making it more likely for them to transition, and that transitioned grain boundaries provide preferential sites for additional transitions to occur. It may be difficult to show a transitioned boundary creating a preferential site for an adjacent boundary to transition on a triple line, however, due to the intricate atomic behavior of such a phenomenon if it were to occur. However, this may be possible to accomplish using an atomistic approach to simulating triple lines.

Therefore, we recommend implementing an atomistic kinetic Monte Carlo simulation, or a similar method, to model the complex behavior we expect to occur on the grain boundary triple lines using the following setup: have three columnar grains sharing a triple line, with the grains initially oriented so that one of the grain boundaries has a high energy and the other two have low energies. Then, add solute with interaction energies such that it will be likely to segregate to grain boundaries. It may be possible to show that solute only segregates in significant quantities to the low energy boundaries after having already diffused to the high-energy boundary, or even to calculate nucleation barriers for the complexion transitions, or the changes in the triple-line energies associated with the transitions.

12.2 Experimental

We recommend repeating Bojarski's analysis[1] of relative grain boundary energy distributions in a variety of other systems experiencing AGG. These relative grain boundary energy distributions can be derived from measurement of the dihedral angles of grain boundaries using atomic force microscopy (AFM) in conjunction with the methods described by Rohrer[2]. This will accomplish three goals: first, it will most likely show that Bojarski's experimental measurements of relative grain boundary energies in Ca-doped Yttria are common to other materials systems with a variety of dopants in ceramic materials. Second, repeating the experiments will either give credence to the occurrence of an adjacency-like transitioning process, or to a transitioning process that depends on grain boundary motion. Finally, discriminating between these two behaviors will help us to better understand grain

growth behaviors in those systems and may eventually allow for better microstructural control.

Only the processes in which complexion transitions are more likely to occur through due to the adjacency of a transitioned grain boundary should result in nearest-neighbor grain boundaries having lower relative grain boundary energy. Our simulations show that the process, which requires grain boundary motion alone to induce a complexion transition, results in abnormal grains with low relative grain boundary energies, but no such energy anisotropy for the nearest-neighbor grain boundaries. Abnormal grains formed from pinning effects in the presence of particles or voids do not require any grain boundary energy anisotropy. Similarly, solute drag effects and secondary recrystallization require no grain boundary energy anisotropy. Abnormal sub-grain growth occurs as the result of a highly misoriented grain in a textured microstructure, resulting in abnormal grains with high mobility, *high*-energy grain boundaries, as opposed to the low energy boundaries that we see in the event of grain boundary complexion transitions. The predicted relative grain boundary energies of the abnormal grain boundaries, nearest-neighbor grain boundaries, and "matrix" grain boundaries (those far away from abnormal grains) can be seen in Table 12.1, with a schematic representation in Fig. 12.1.

We recommend performing a similar analysis on a three-dimensional representation of microstructures, obtained either through destructive or

nondestructive methods. This could be done very simply by segmenting the three-dimensional dataset's grain boundaries, calculating grain boundary triple junction angles using the algorithm implemented by Lieberman[3] to calculate grain boundary normal vectors, and solving the collection of Young's equations for the relative grain boundary energies. Performing such an analysis will validate the relative grain boundary energy measurements made using AFM.

Table 12.1: Processes Responsible For Different Grain Boundary Energy Anisotropies

Grain Boundary Energies (Ranked)	Likely Mechanism(s)
Abnormal = Nearest Neighbor < Matrix	Adjacency Complexion Transitions
Abnormal < Nearest Neighbor < Matrix	Adjacency Complexion Transitions
Abnormal < Nearest Neighbor = Matrix	Motion-Induced Complexion Transitions
Matrix = Nearest Neighbor < Abnormal	Abnormal Sub-grain Growth
Abnormal = Nearest Neighbor = Matrix	Pore/Particle Pinning, Solute Drag Secondary Recrystallization

We recommend the eventual use of a nondestructive method of characterization, such as High Energy X-Ray Diffraction Microscopy (HEDM) or Diffraction Contrast Tomography (DCT), so that abnormal grains can be tracked longitudinally over multiple annealing steps. This will allow for the analysis of relative grain boundary energies in three dimensions before the beginning of AGG, with the knowledge of which grains will become abnormal. It may be possible to show, for example, that abnormal grains start the annealing process with systematically higher grain boundary energies. Analysis may also link the formation of abnormal grains to the existence of networks of high-energy grain boundaries.

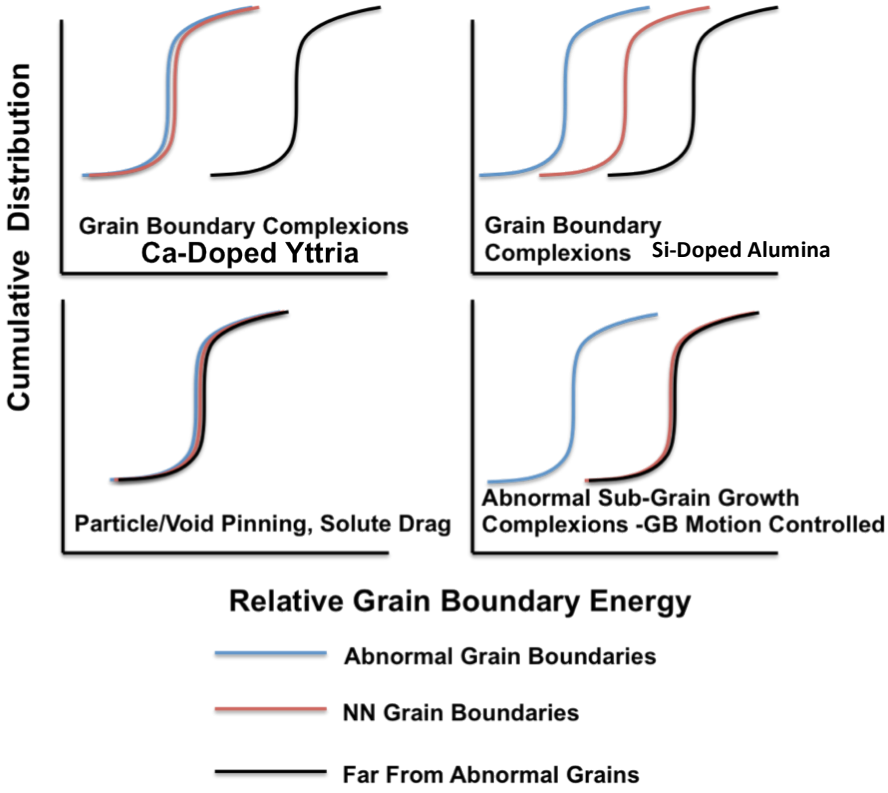

Figure 12.1: Expected cumulative relative grain boundary energy distributions for the abnormal grains boundaries, the nearest-neighbor grain boundaries, and the grain boundaries far from the abnormal grains, given the physical cause for AGG.

We recommend using these nondestructive techniques to track grain boundary motion, which can be accomplished if enough annealing steps are collected.

Like the simulation analysis shown in Chapter 7, if grain boundaries do require some amount of motion before making a transition, experimentally, a similar analysis should either confirm or reject the existence of a grain boundary motion threshold for complexion transitions to occur if one indeed exists. Further, it may be possible to relate the amount of grain boundary motion or incubation time before a transition to the relative grain boundary energy, thus revealing more complex

phenomena. For example, the first grain boundary complexion transitions may occur after a consistent amount of grain boundary motion, but later transitions may not follow this trend due to the presence of an adjacency transition-like process. Further, if we assume that complexion transitions always causes an abrupt increases in the rate of grain boundary motion, then we can measure the fraction of grain boundaries transitioned at each step even if the complexion transitions that occur do not lead to AGG. This information would allow for the inference of grain boundary complexion transition kinetics by fitting to the Johnson-Mehl-Avrami-Kolmogorov equation. Anneals performed at several temperatures would allow for the construction of time-temperature-transformation diagrams, much like the work that has been performed using Spark-Plasma Sintering experiments similar to those performed by Bojarski[4].

The limiting factor to performing the analysis discussed is experimental – non-destructive 3D techniques like HEDM and DCT are costly techniques to implement, which limits the number of time steps that can be collected. Further, the process of annealing the sample will require short dwell times and high rates of heating and cooling, which will be difficult to insure.

We recommend exploring the possibility of an analogous two-dimensional analysis in order to avoid much of this difficulty, perhaps through the use of a hot-stage scanning electron microscope. However, any such work must figure out ways to

account for the dimensionality lost, since we cannot track the motion of grain boundaries outside of the plane of view.

It is our fervent hope that these procedures we recommended provide useful insight upon the processes that cause complexion transitions and generate experimental data that will be used for other material treatments.

References

1. S.A. Bojarski, S. Ma, W. Lenthe, M.P. Harmer, G.S. Rohrer. Changes in the Grain Boundary Character and Energy Distributions Resulting from a Complexion Transition in Ca-Doped Yttria. Met. and Mater. Trans. A. 2012;43:3532.
2. G.S. Rohrer. Grain Boundary Energy Anisotropy: A Review. J. Mater. Sci. 2011;46:5881.
3. E.J. Lieberman, A.D. Rollett, R.A. Lebensohn, E.M. Kober. Calculation of Grain Boundary Normals Directly from 3D Microstructure Images. Modeling and Simulation in Materials Science and Engineering. 2015;3.
4. S.A. Bojarski, M.P. Harmer, G.S. Rohrer. Influence of Grain Boundary Energy on the Nucleation of Complexion Transitions. Scripta Mater. 2014;88:1.

Appendix A: Cellular Automata For Complexion Growth

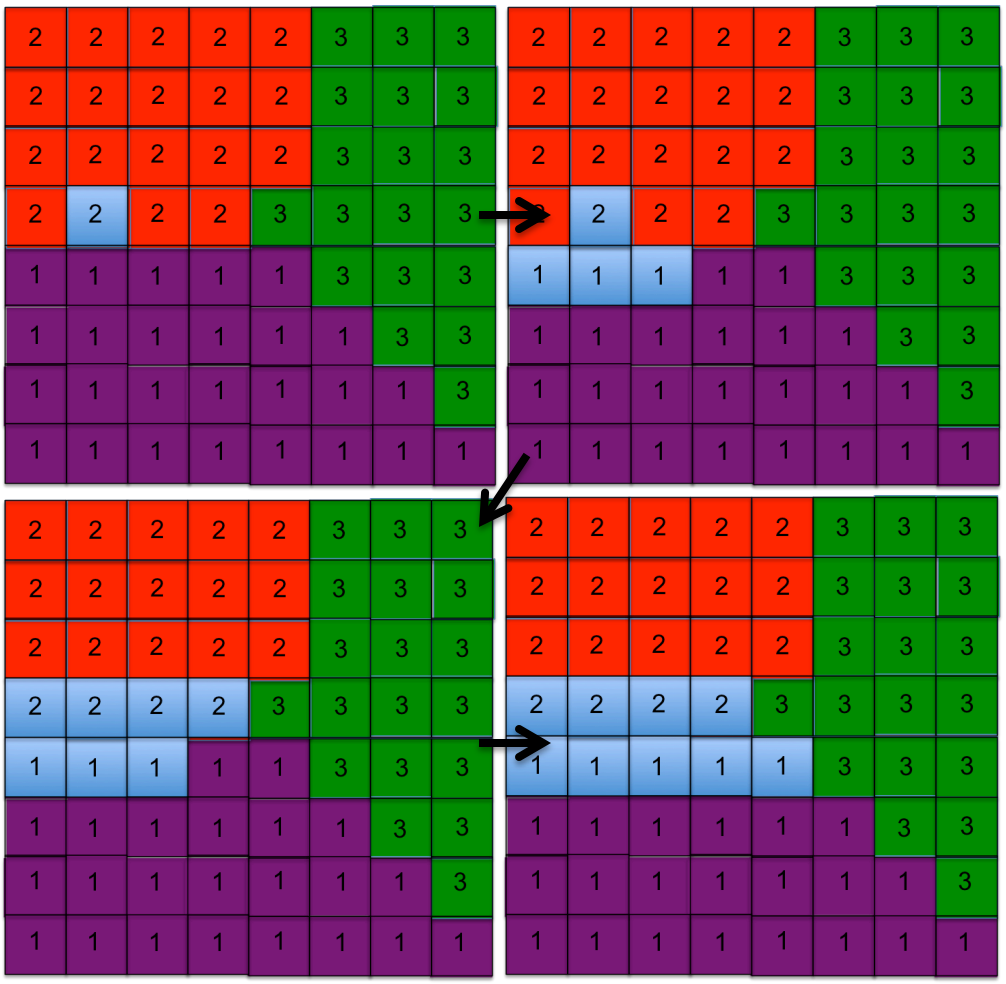

Figure A.1: Complexion growth on a grain boundary according to the cellular automata. The complexion can grow on the boundary between grains 1 and 2, as well as the boundary between grains 1 and 3. However, the complexion is not capable of spreading over this particular triple line.

Table A.1: The status of each grain boundary and triple line as "Open" or "Closed".

	1	2	3
1	N/A	Open	Open
2	Open	N/A	Closed
3	Open	Closed	N/A

TL(1,2,3) = Closed

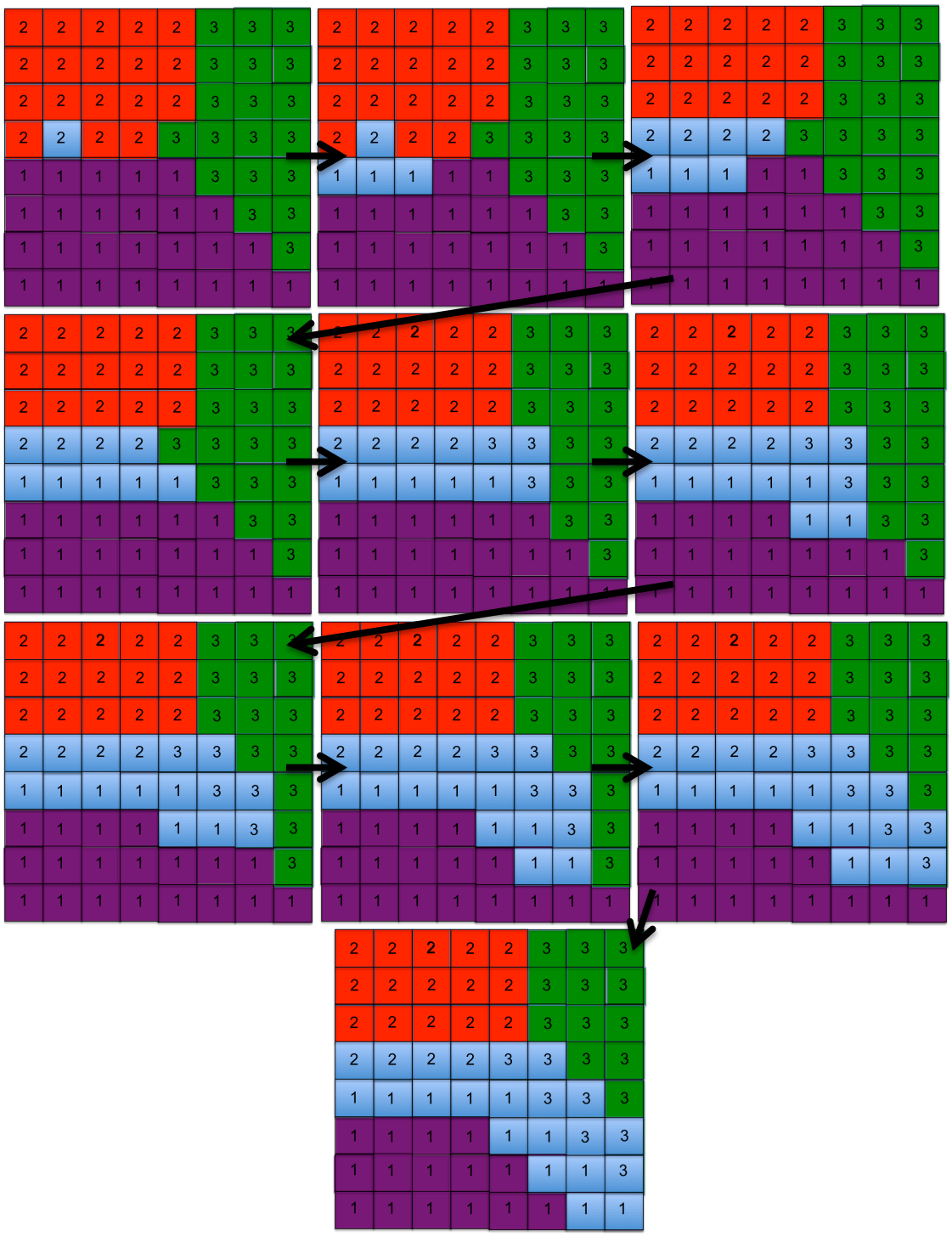

Figure A.2: Complexion growth on a grain boundary according to the cellular automata. The complexion can grow on the boundary between grains 1 and 2, as well as the boundary between grains 1 and 3. The complexion is capable of spreading over this particular triple line, so it spreads across the triple line, but not the boundary between grains 2 and 3, since it is forbidden.

Table A.2: The status of each grain boundary and triple line as "Open" or "Closed".

	1	2	3
1	N/A	Open	Open
2	Open	N/A	Closed
3	Open	Closed	N/A

TL(1,2,3) = Open

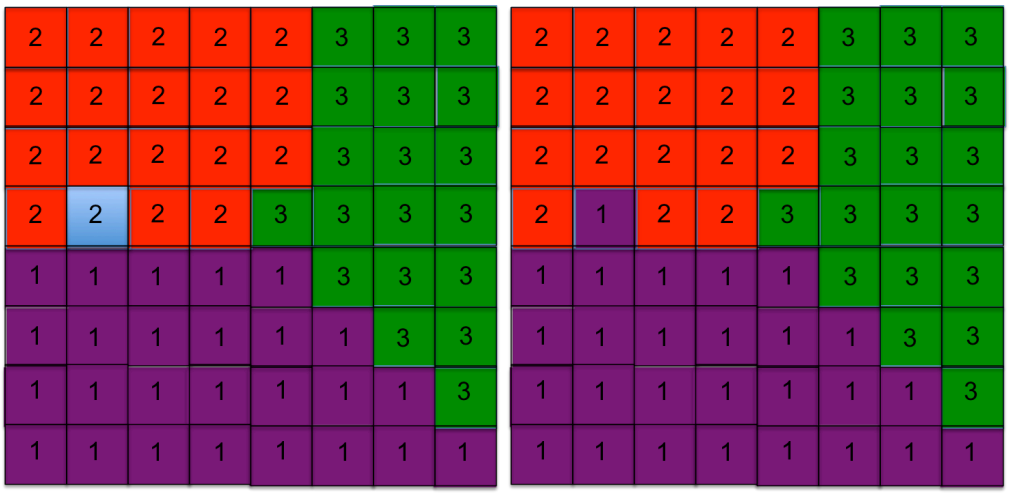

Figure A.3: A transitioned voxel "reverts" when it reorients to the ID of a neighboring untransitioned voxel.

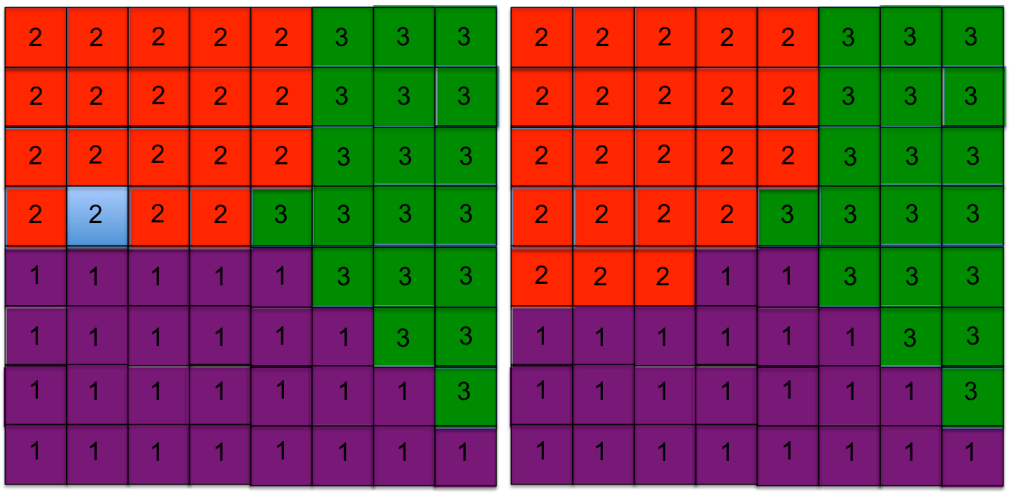

Figure A.4: A transitioned voxel "reverts" when it no longer lies on a grain boundary.

Appendix B: Analysis of Change in Simulation Results with Size of Microstructure

Simulations were performed in which P_{Gb} = 0.075 and P_{Tl} = 1.0 using microstructures of size 64x64x64, 100x100x100, 150x150x150, and 200x200x200. The fractions of transitioned boundaries on the abnormal grains that appeared in the simulations were collected, as well as the fractions of transitioned boundaries on the nearest neighbor grain boundaries. We can see that the results of the simulations are relatively consistent – the grain boundaries are considerably more likely than random chance to be transitioned for both the abnormal grain boundaries and the nearest-neighbor grain boundaries in Figs B.1 and B.2:

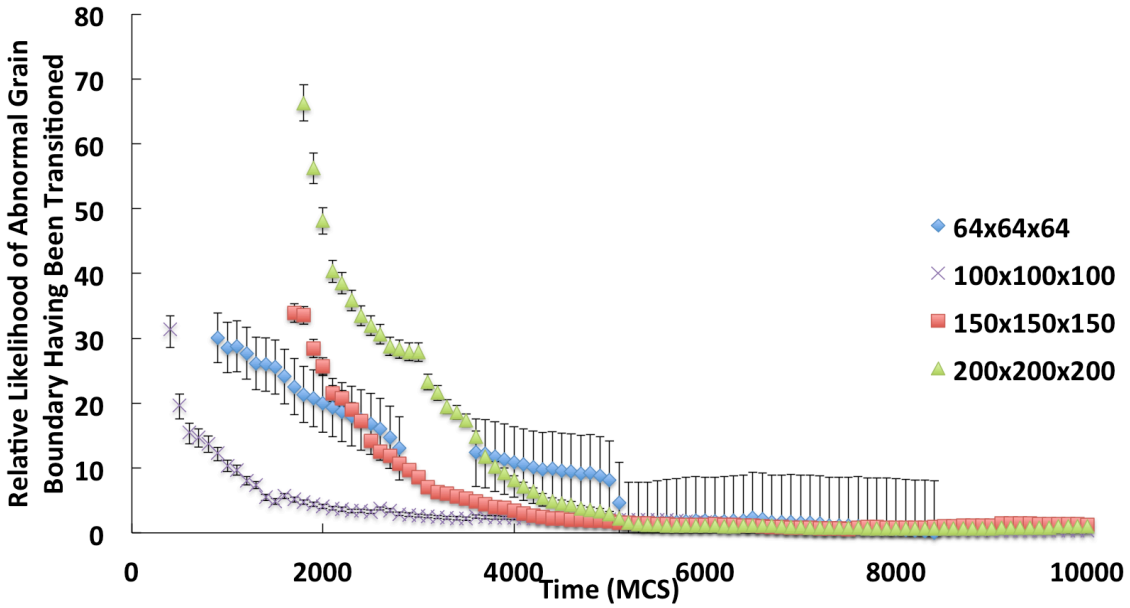

Figure B.1: The relative likelihood of abnormal grains' boundaries to be in the transitioned state in comparison to random chance for different simulation sizes. Simulations employed the voxel-based transition model and ran for 10,000 MCS, with P_{Gb} = 0.075 and P_{Tl} = 1.0.

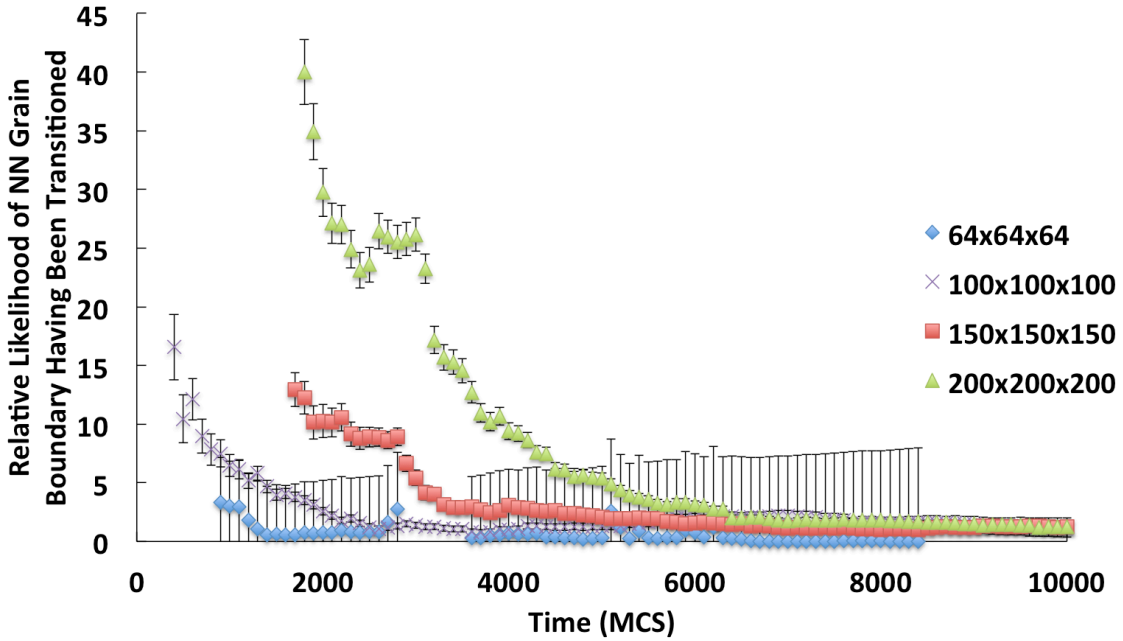

Figure B.2: The relative likelihood of nearest-neighbor grain boundaries to be in the transitioned state in comparison to random chance for different simulation sizes. Simulations employed the voxel-based transition model and ran for 10,000 MCS, with P_{Gb} = 0.075 and P_{Tl} = 1.0.

Appendix C: Plots of Relative Likelihood of Having Transitions for AGG With Grain Boundary Motion-Induced Complexion Transitions

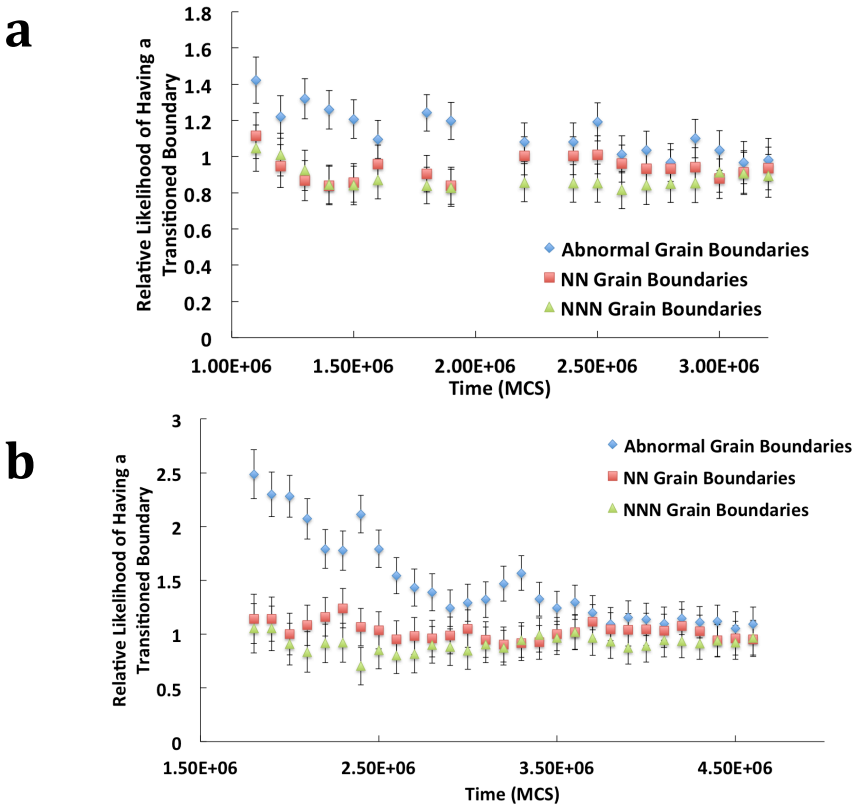

Figure C.1: Plots of the relative likelihood of different classes of grain boundaries having transitioned boundaries when the transitioned grain boundary mobility is ten times the default mobility (M_{min} = 0.10) and when the threshold for making a transition is C = 25 (a), and C = 50 voxels (b).

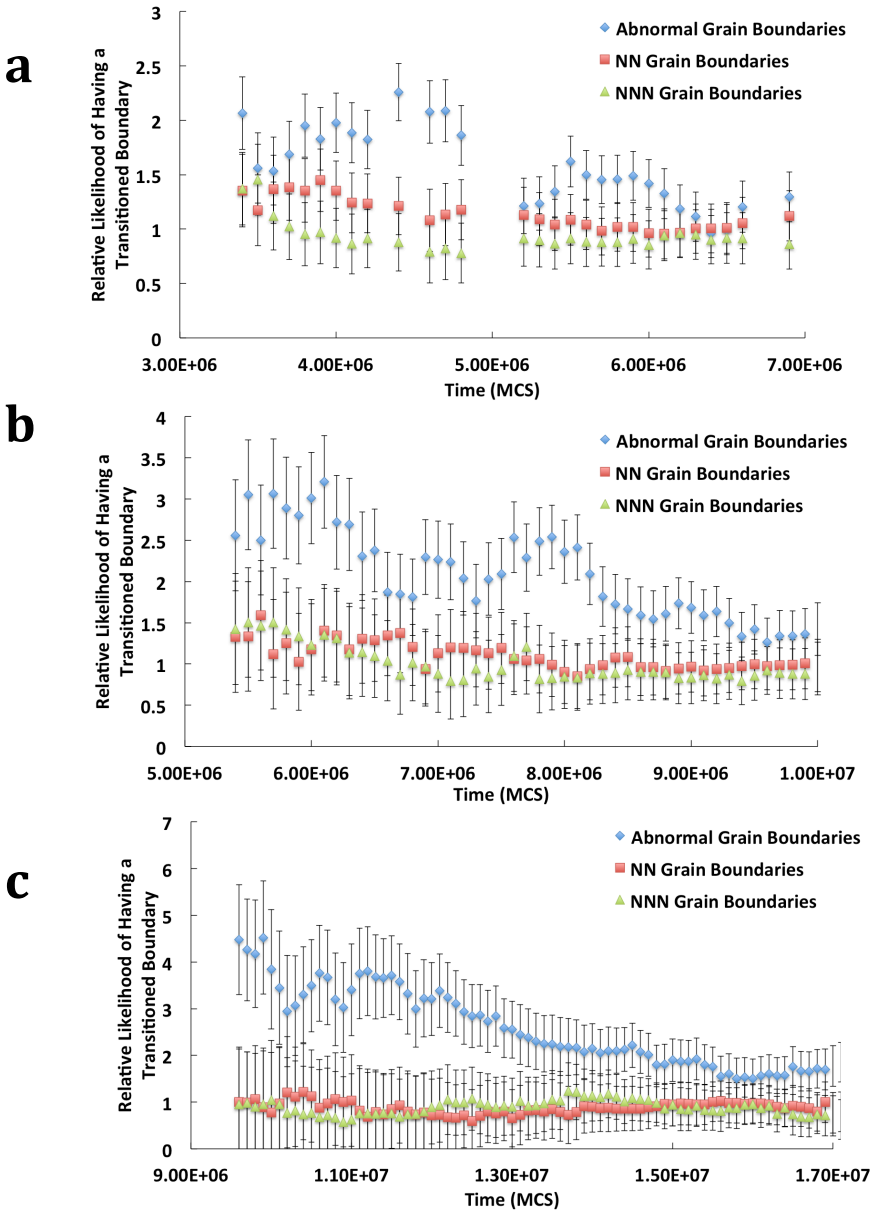

Figure C.2: Plots of the relative likelihood of different classes of grain boundaries having transitioned boundaries when the transitioned grain boundary mobility is ten times the default mobility (M_{min} = 0.10) and when the threshold for making a transition is C = 100 (a), C = 200 (b), and C = 400 voxels (c).

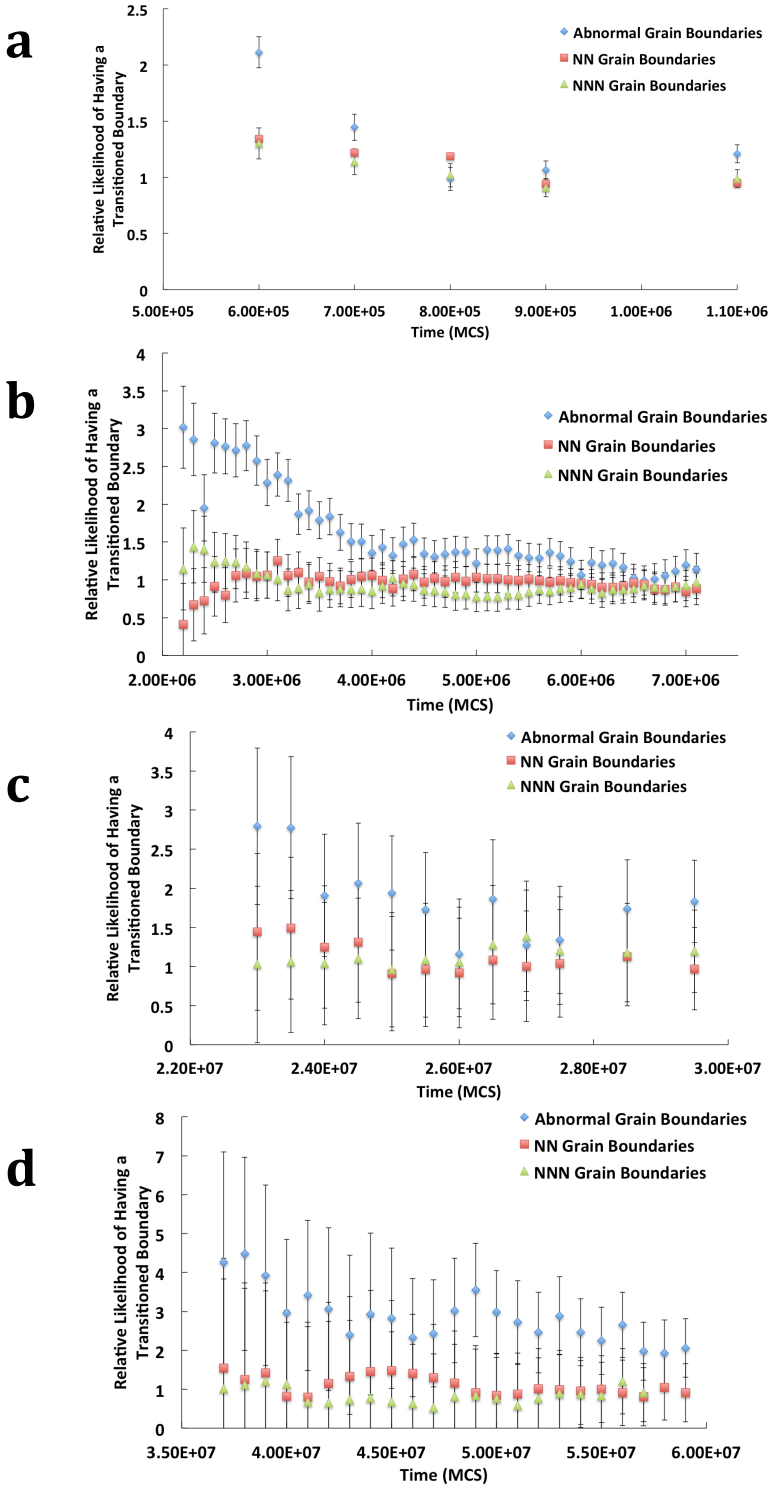

Figure C.3: Plots of the relative likelihood of different classes of grain boundaries having transitioned boundaries when the transitioned grain boundary mobility is twenty times the default mobility (M_{min} = 0.05) and when the threshold for making a transition is C = 10 (a), C = 50 (b), C = 400 (c), and C = 1000 voxels (d).

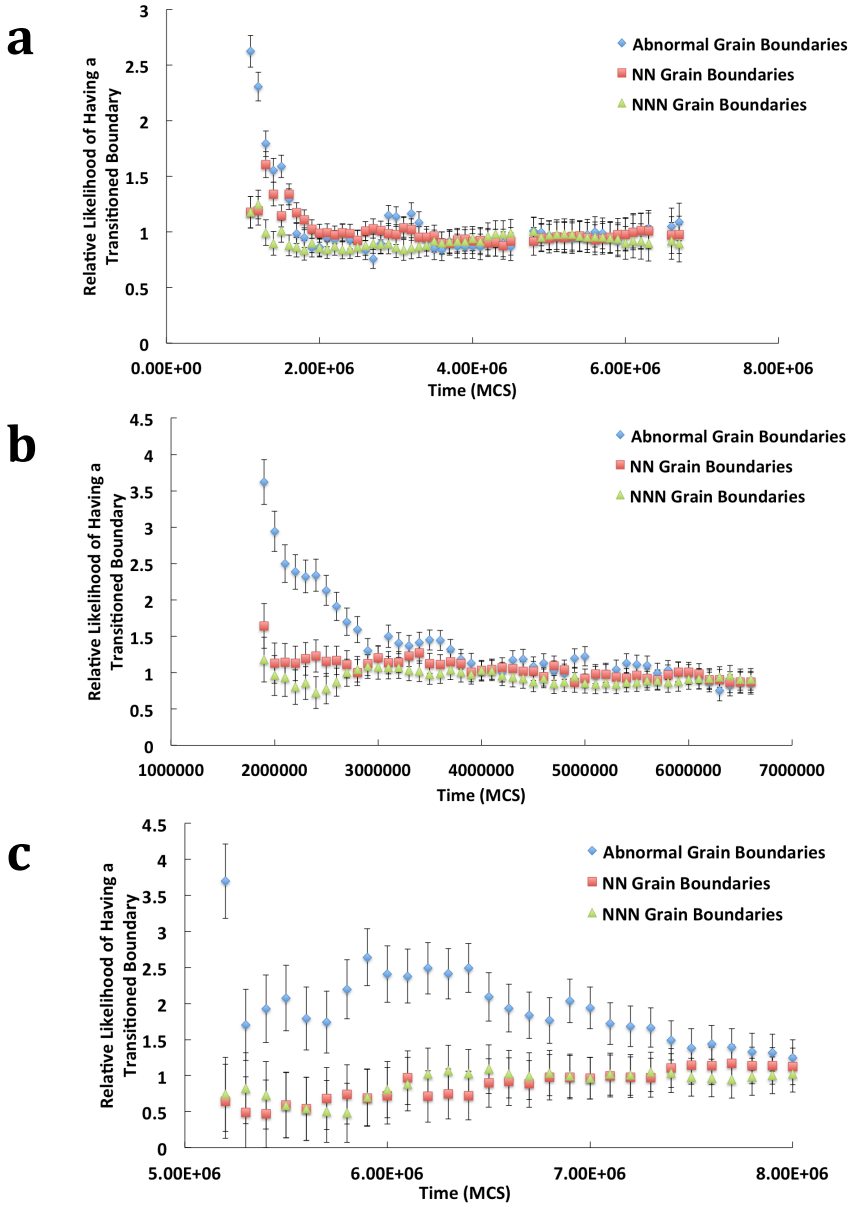

Figure C.4: Plots of the relative likelihood of different classes of grain boundaries having transitioned boundaries when the transitioned grain boundary mobility is one hundred times the default mobility (M_{min} = 0.01) and when the threshold for making a transition is C = 5 (a), C = 10 (b), and C = 25 voxels.

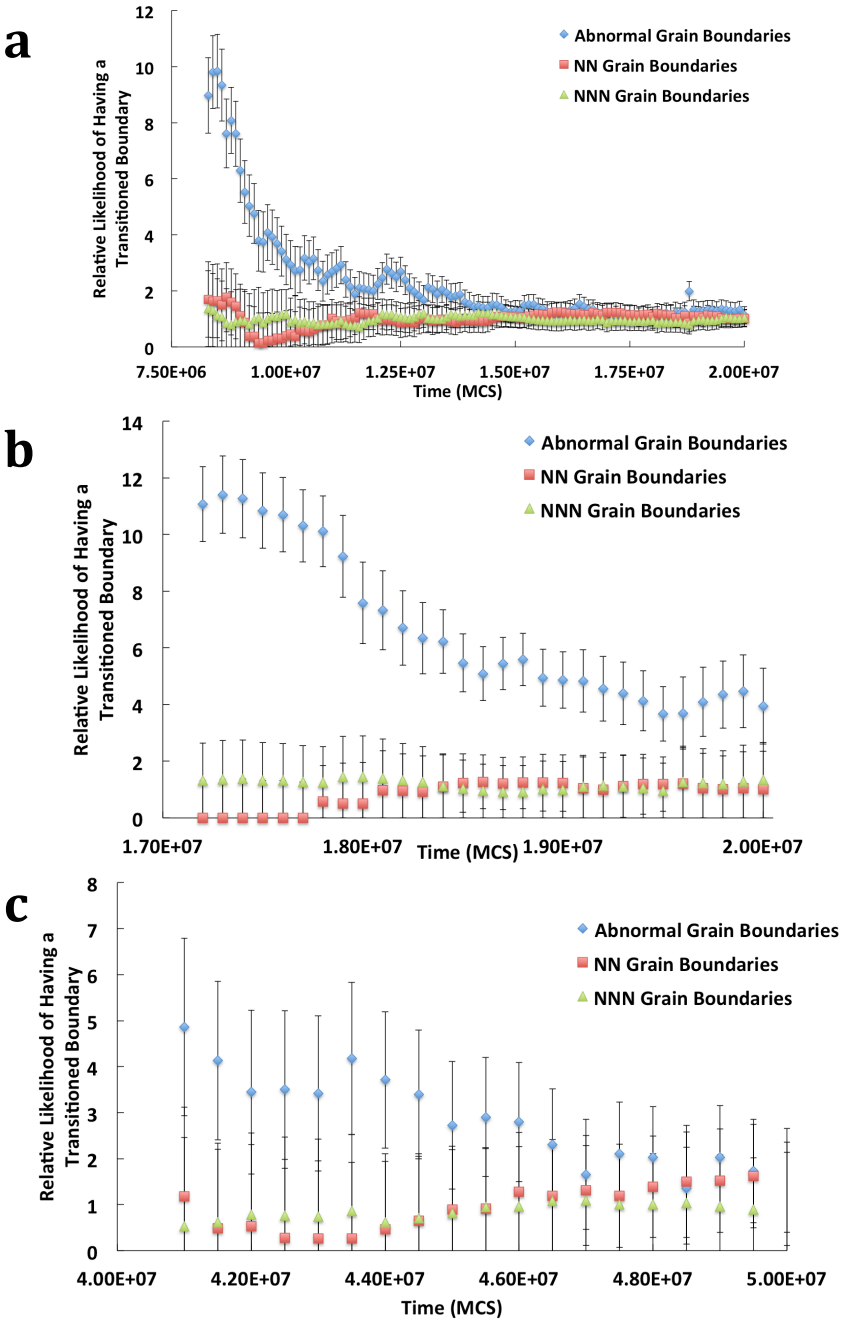

Figure C.5: Plots of the relative likelihood of different classes of grain boundaries having transitioned boundaries when the transitioned grain boundary mobility is one hundred times the default mobility (M_{min} = 0.01) and when the threshold for making a transition is C = 50 (a), C = 100 (b), and C = 200 voxels (c).

Appendix D: Complexion Nucleation Barrier Calculations

We can represent the nucleus of the complexion transition with a radius of curvature *r* and a contact angle θ, as shown in Fig D.1:

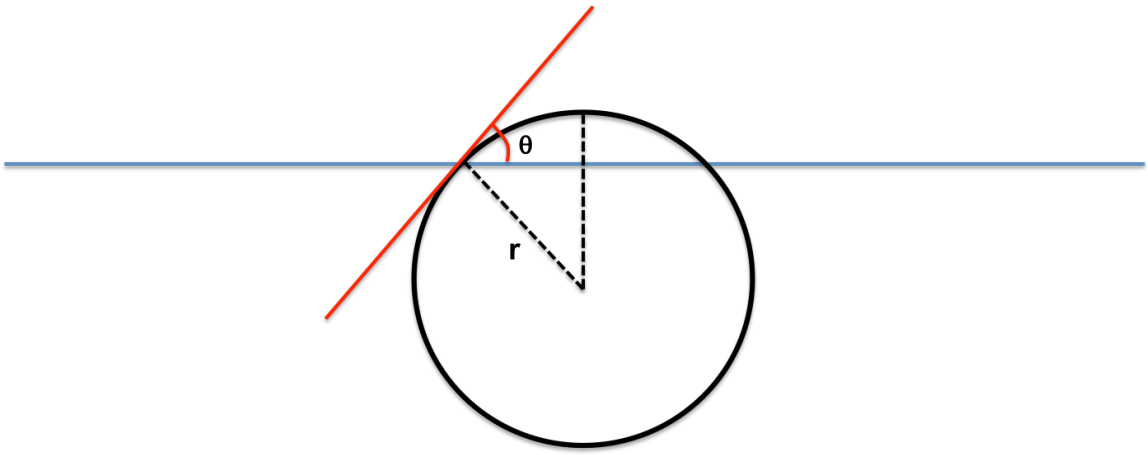

Figure D.1: A schematic representation of the transitioned nucleus.

We then define the following terms:

- $\Delta\gamma$: The change in grain boundary energy associated with the complexion transition.
- σ_{Cp} : The energy associated with the edge length of the transitioned boundary.
- σ_{Tl} : The triple line energy per unit length.
- σ_{CpTl} :The triple line energy per unit length after the complexion transition.

We will assume that the both the triple line and the section of grain boundary being transitioned are both flat.

The change in free energy associated with the nucleation of the complexion transition is:

$$\Delta G = A\Delta\gamma + P\sigma_{Cp} + l_{Tl}(\sigma_{CpTl} - \sigma_{Tl}) \qquad \textbf{(D.1)}$$

In addition, we can expect the edge energies to follow an analogous relationship to bulk precipitates:

$$\sigma_{Tl} - \sigma_{CpTl} = \sigma_{Cp}\cos(\theta) \qquad \textbf{(D.2)}$$

The area of the complexion can be obtained by integrating the over the chord length over θ:

$$A = \int_0^{\theta} r\sin(\varepsilon) \bullet r\, d\varepsilon = r^2(1-\cos(\theta)) \quad \textbf{(D.3)}$$

Further, we can easily calculate *P* and l_{Tl}:

$$P = 2\theta r \quad \textbf{(D.4)}$$

$$l_{Tl} = 2r\sin(\theta) \quad \textbf{(D.5)}$$

Substitution of D.2, D.3, D.4, and D.5 into D.1 yields:

$$\Delta G = r^2(1-\cos(\theta))\Delta\gamma + 2\theta r\sigma_{Cp} - 2r\sigma_{Cp}\sin(\theta)\cos(\theta) = r^2(1-\cos(\theta)) + 2r\sigma_{Cp}(\theta - \sin(\theta)\cos(\theta)) \quad \textbf{(D.6)}$$

Since $d\Delta G/dr = 0$ at equilibrium, we can solve for the critical radius of curvature, r*, and the activation energy, ΔG*:

$$r^* = -\sigma_{Cp}\frac{(\theta - \sin(\theta)\cos(\theta))}{(1-\cos(\theta))\Delta\gamma} \quad \textbf{(D.7)}$$

$$\Delta G^* = -\sigma_{Cp}^2\frac{(\theta - \sin(\theta)\cos(\theta))^2}{(1-\cos(\theta))\Delta\gamma} \quad \textbf{(D.8)}$$

We can convert the critical radius of curvature to the area using equation D.3 and taking the square root yields the equivalent "radius":

$$r^*_{Equivalent} = \sqrt{\left(r^*\right)^2(1-\cos(\theta)} = -\sigma_{Cp}\frac{\theta - \sin(\theta)\cos(\theta)}{\Delta\gamma\sqrt{(1-\cos(\theta))}} \quad \textbf{(D.9)}$$

Therefore, with the inputs of Δγ, σ_{Cp}, σ_{Tl}, and σ_{CpTl} we can estimate the expected critical grain radius. Figs. D.2 and D.3 show the critical radii of the nucleating complexion given different values of Δγ. Fig. D.4 Shows the variation in both values for a constant $\sigma_{Cp} = 10^{-8}$ J/m.

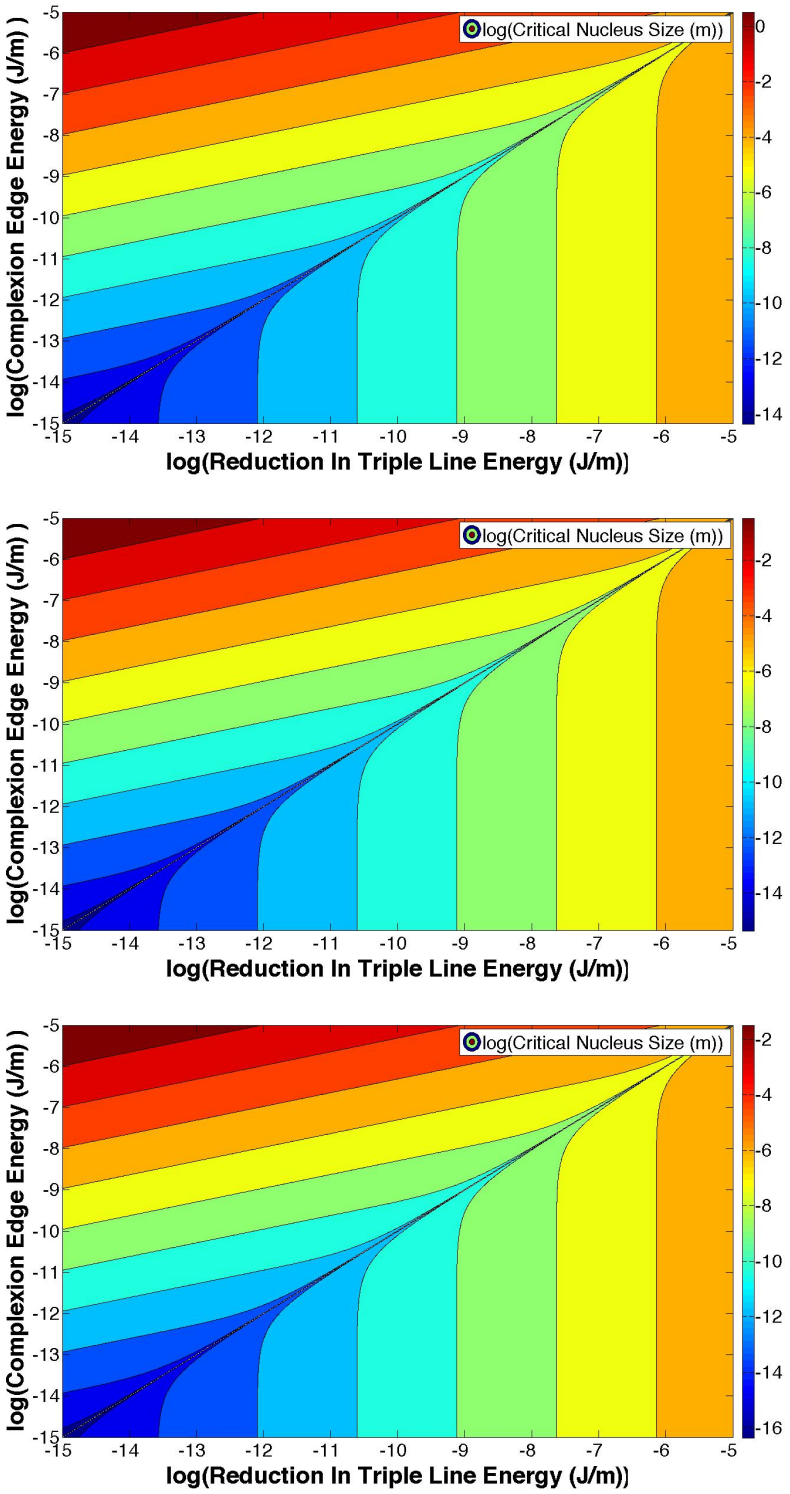

Fig D.2: Contour plots of the effective critical radius given a $\Delta\gamma$ of 0.01 J/m^2 (a), 0.10 J/m^2 (b), and 1.0 J/m^2 (c).

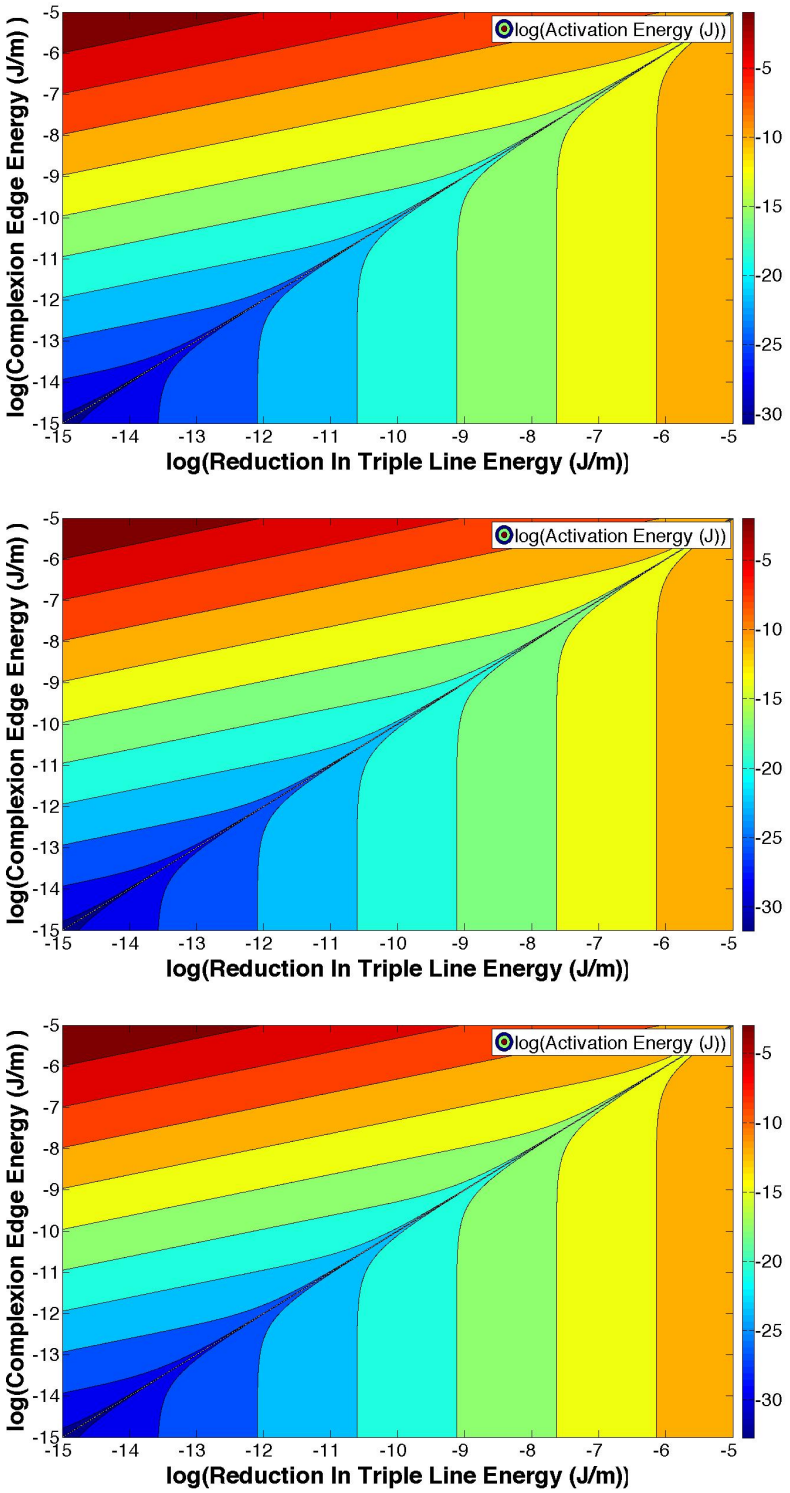

Fig D.3: Contour plots of the effective critical radius given a $\Delta\gamma$ of 0.01 J/m^2 (a), 0.10 J/m^2 (b), and 1.0 J/m^2 (c).

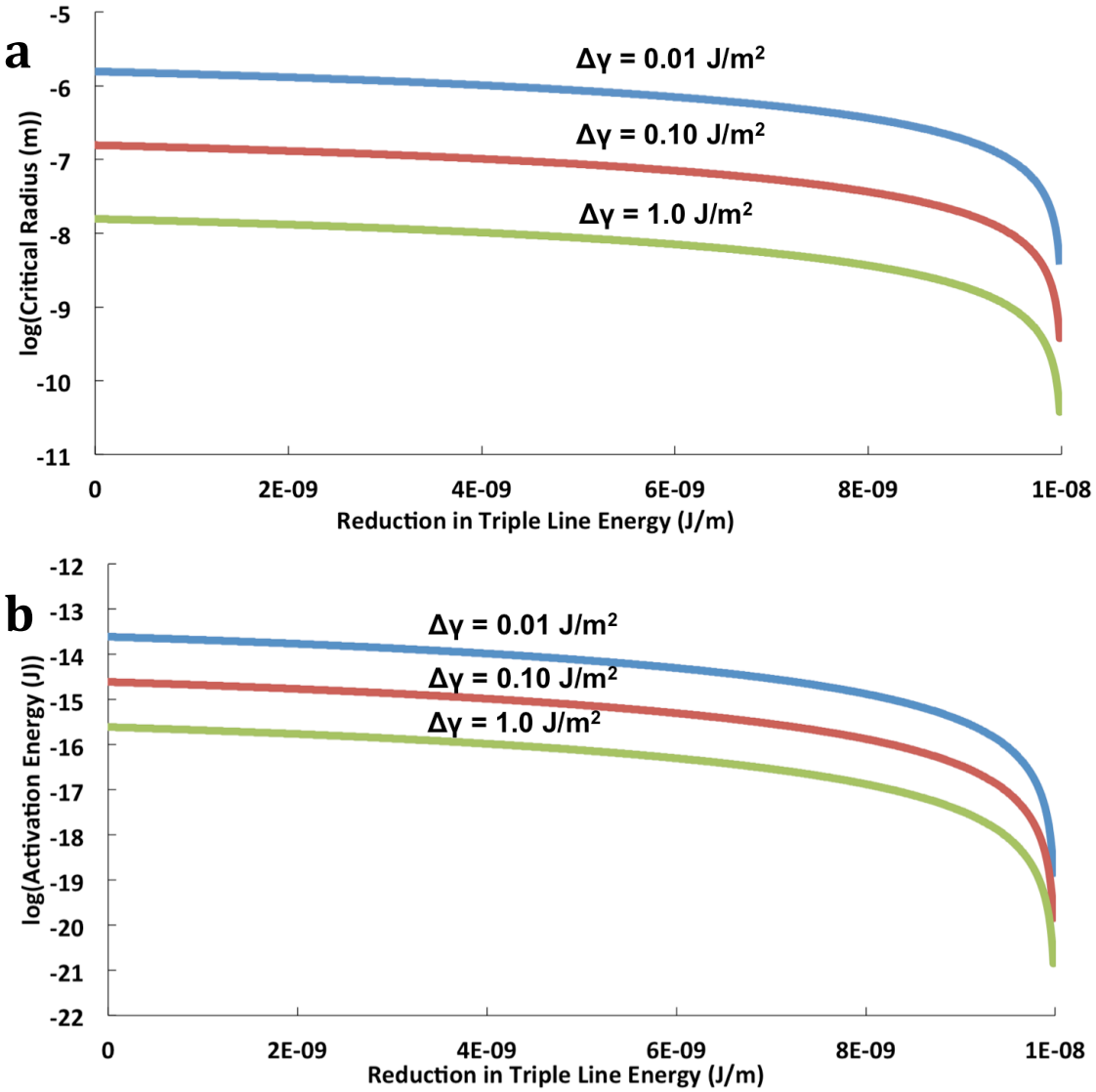

Figure D.4: The estimated critical radii and activation energies for nucleation of a complexion transition on a triple line given the associated reduction in triple line energy and $\sigma_{Cp} = 10^{-8}$ J/m for different values of $\Delta\gamma$.